UNIVERSITY OF SOUTHAMPTON

FACULTY OF ENGINEERING AND APPLIED SCIENCE

INSTITUTE OF SOUND AND VIBRATION RESEARCH

Doctor of Philosophy

ULTRASONIC PROPAGATION IN CANCELLOUS BONE : SOME THEORETICAL MODELS

by Elinor Ruth Hubbuck

April 2000

UNIVERSITY OF SOUTHAMPTON

ABSTRACT

FACULTY OF ENGINEERING AND APPLIED SCIENCE

INSTITUTE OF SOUND AND VIBRATION RESEARCH

Doctor of Philosophy

ULTRASONIC PROPAGATION IN CANCELLOUS BONE : SOME THEORETICAL MODELS

by Elinor Ruth Hubbuck

The theoretical modelling of ultrasonic propagation in cancellous bone is pertinent to the improvement of ultrasonic techniques for diagnosing the bone disease osteoporosis. For such techniques to be confidently used in the clinical management of osteoporosis, fundamental research is required to establish an understanding of how ultrasonic waves travel in porous, or cancellous, bone. This thesis concerns investigations into various theoretical models of propagation in porous media. These studies are supported by *in vitro* experiments on bovine cancellous bone around 1 MHz.

Previous applications to bone of established theories, such as Biot's theory for fluid-saturated porous media, have enjoyed limited success. This thesis begins by considering Biot's theory in more detail than previously reported in the literature. Biot's theory predicts that two longitudinal waves travel in cancellous bone in response to insonation with a single wave. The existence of two waves, known as fast and slow waves, is confirmed, which had not been reported in the literature prior to the start of this work. The importance of the presence of marrow in the pores on these waves is investigated.

The phase velocities of fast and slow waves are observed to be strongly dependent on direction, relative to the internal cancellous structure. However, the isotropic form of Biot is not appropriate for modelling this response. Therefore, a second approach is proposed, which uses Schoenberg's theory to model propagation in a parallel-plate model of cancellous bone. Direction dependent measured velocities are observed to give qualitative agreement with the predictions of the Schoenberg model. The two theoretical approaches are compared when anisotropic mechanical and fluid motion effects are introduced into Biot's theory.

Finally the findings of this research are discussed with respect to current clinical ultrasonic measurements of bone. Recommendations are made for the development of a future model-based system for bone assessment.

Contents

List of Illustrations

List of Tables

Preface

In recent years, research into the bone disease osteoporosis has escalated. Simultaneously, the diagnostics industry has embraced the introduction of the technique Broadband Ultrasonic Attenuation, based on the potential of the technique to become a cheaper option than x-rays and ideal for use in screening programmes. However, after fifteen years, BUA has not delivered on those initial expectations, and it is widely acknowledged that further research is required before it may be confidently used in the clinical management of osteoporosis. If the technology and the industry are to be sustained, basic work into the physics of the application is required to improve the technology's reputation for reliability and to yield maximum clinical information.

This thesis sets out to describe investigations into the theoretical modelling of the propagation of ultrasonic waves in porous cancellous bone, with the aim of advancing understanding and contributing to the development of ultrasonic bone diagnostics. The work is presented in seven chapters, beginning with introductions to the fields of osteoporosis, the modelling of propagation in porous media and ultrasonics. The development of two theoretical models is described, and results from experimental investigations are presented.

It is hoped that this thesis will in some way contribute to the improvement of existing ultrasonic techniques, or to aid the development of novel uses of ultrasound to render a better clinical tool than currently exists.

Acknowledgements

This work was carried out on a full time PhD studentship funded by the Faculty of Engineering and Applied Science of the University of Southampton.

During the past four years, I have been fortunate to have been influenced by physicists, acousticians and mathematicians; medics, vets and patients, alike. I acknowledge the guidance of my supervisors, Professor Leighton, Dr White and Dr Petley. Each brought a different approach to supervision necessary for this multidisciplined work, and I was fortunate to have such a varied input. Since the project grew from modest objectives, they acted as the sounding boards for many of my pet theories in the early stages. In particular, I express my gratitude to Tim Leighton for academic guidance, approachable support and for having an inspiring confidence in me. I thank Paul White for his considered criticism and encouragement, and Graham Petley for keeping practical objectives to the forefront.

I also acknowledge Joanne Edwards, for the use of her unpublished experimental results and extend my gratitude to the ISVR Ultralab researchers past and present (Ruthven Evans, Andy Phelps, Niven Brown and Jim Clarke). Thanks to Sue Brindle for her assistance and female perspective. I am extremely grateful for the help of Emeritus Professor Robert Chivers, and for the genuine encouragement of Emeritus Professor Peter Davies. Thank you to Andreas Rassau for proof reading my first submission, and to Professor Robert Allen for reading the revised version.

Thank you to my parents, Professor and Mrs John Hubbuck, for supporting my studying engineering, and for sharing their insights into academia, which helped me through the re-examination period. I thank Scott for his understanding and support through the rewriting, and before our marriage.

Finally, I was motivated by a group of people whose encouragement was the most sincere of any I received. They are Mrs Diana Cozens and the ladies and gents of the National Osteoporosis Society Local Southampton Group. I hope this work does justice to their enthusiastic support.

Definition of Symbols and Abbreviations

A	generalised elastic (Lame) coefficient
AF Biot	anisotropic fluid Biot
a	diameter of pore, tube or discontinuity (m)
a_o	amplitude of echo in reverberant signal
a_p	radius of piston transducer (m)
BMD	bone mineral density
BUA	Broadband Ultrasonic Attenuation (dB / MHz as gradient)
b	absorption parameter = $\eta\beta^2 / k$
C	elastic coefficient of transverse isotropy
C_D	coefficient of diffusion
CT	computed (computerised) tomography
CV, %CV	coefficient of variance
c	wave speed = ω / q (m/s)
c_{bar}	bar velocity = $\sqrt{E / \rho}$ (m/s)
D_i	coefficient of TI Biot theory (Table 6.3)
DXA, DEXA	Dual Energy X-Ray Absorptiometry
d	target thickness (m)
d_s	viscous skin depth (m)
d_{tr}	trabecular thickness (m)
E	Young's modulus (GPa)
E_b	Young's modulus of frame (GPa)
E_s	Young's modulus of solid material (GPa)
e_{ij}	component of solid strain in ij-plane
F	elastic coefficient of transverse isotropy
$F(\gamma)$	function of viscous deviation from Poiseuille flow
f	frequency (Hz)
f_{scat}	scattering frequency (Hz)
$f_{viscous}$	viscous frequency (Hz)
G	coefficient of Cardano's method
g	term in phase velocity compensating for refraction
H	period in array of parallel plates
$H_i(f)$	amplitude of FFT of a signal, i
HRT	Hormone Replacement Therapy
$h(x)$	cost function in optimisation
I	time-averaged intensity (W/m^2)
$I(t)$	instantaneous intensity (W/m^2)
IL	intensity level (dB)
$Im(\omega)$	imaginary part of FFT
I_o, I_{ref}	maximum, reference intensity (W/m^2)
I_z	intensity at position on z axis (W/m^2)
K_b	bulk modulus of the solid frame(GPa)
K_f	bulk modulus of the fluid (GPa)
K_s	bulk modulus of the solid material (GPa)
k	permeability (m^2)
k_o	d.c. permeability (m^2)
L	elastic coefficient of transverse isotropy
L_c	time-compensation length (m)
$\mathbf{l}$	coefficient of anisotropy
M	elastic coefficient of transverse isotropy

MTPS	mean trabecular plate separation
MTPT	mean trabecular plate thickness
m	coefficient of anisotropy
N	shear modulus of solid (GPa)
N_b	shear modulus of frame (GPa)
NOS	National Osteoporosis Society
n	indice for relating moduli in porous medium
P	generalised elastic coefficient
P_o	peak pressure
PSM	Phase Spectrum Method
PVDF	polyvinyldenfluoride
PZT	lead zirconate titanate
p	complex pressure
Q	generalised elastic coefficient
QCT	Quantitative Computer Tomography
QUS	Quantitative Ultrasound
q	wavenumber of harmonic wave = $2\pi/\lambda = c / \omega$
q_{fast}	wavenumber of fast wave = V_{fast} / ω
q_{shear}	wavenumber of shear wave = V_{shear} / ω
q_{slow}	wavenumber of slow wave = V_{slow} / ω
q	complex wavenumber = $q + j\alpha_a$
R	pressure reflection coefficient
R	generalised elastic coefficient
$Re(\omega)$	real part of FFT
r	pore radius (m)
S	structure factor
SD, std	standard deviation
SERMS	Selective Estrogen Receptor Modulators
SOS	speed of sound
SPA	Single Photon Absorptiometry
SXA	Single X-Ray Absorptiometry
s	slowness vector = (s_1, s_2, s_3)
T_{ij}	coefficients of TI Biot method (Table 6.3)
TI Biot	transversely isotropic Biot
TIAF Biot	transversely-isotropic anisotropic fluid Biot
t	time (seconds)
t_c	thickness compensating time term (seconds)
U	displacement of the solid (m)
u	displacement of the fluid (m)
$\dot{u}$	velocity of fluid (m/s)
$\dot{u}_{\max}$	maximum velocity of fluid (m/s)
V_{fast}	velocity of fast wave (m/s)
$V_p(\omega)$	phase velocity (m/s)
V_{pl}	velocity of plate mode (m/s)
V_s	velocity of compresssional wave in solid (m/s)
V_{shear}	velocity of shear wave (m/s)
V_{slow}	velocity of slow wave (m/s)
V_w	speed of sound in water (m/s)
v, $v(t)$	particle velocity (m/s)
w	shear strain in fluid
$X(f)$, $S(f)$	FFT of signals x(t), s(t)

$x(t)$, $s(t)$	arbitrary functions of time
Y	lateral shift in y axis (m)

Greek Letters

α, α_∞	geometric, real tortuosity
$\alpha(\omega)$	JKD frequency-dependent tortuosity
α_a	amplitude attenuation coefficient (NP/m)
$\alpha(\theta)$	angle dependent tortuosity
β	interconnected porosity (often as %)
Δ	Biot coefficient defined in equation (2.11)
ε	vector of fluid strain
$\phi(\omega)$	phase spectrum
ϕ_{ref}	phase spectrum of reference signal
ϕ_{target}	phase spectrum of signal through target
η	shear viscosity of fluid (Pa.s)
λ	wavelength (m)
ν_b	Poisson's ratio of porous frame
ν_s	Poisson's ratio of solid material
θ	angle (rads or °)
θ_g	angle of refraction of group velocity (rads or °)
θ_i	angle of incidence (rads or °)
θ_{ia}	apparent angle of incidence (rads or °)
θ_r	angle of refraction of phase velocity (rads or °)
ρ	isotropic, macroscopic density (kg/m^3)
ρ_o	ambient density (kg/m^3)
ρ_{ij}	mass densities of Biot's theory : $i, j = 1, 2$
ρ_s	solid density (kg/m^3)
ρ_f	fluid density (kg/m^3)
$\langle\rho\rangle$	volume averaged density (kg/m^3)
σ	fluid stress vector
σ_{ij}	component of stress in the solid in ij plane
υ_{cuboid}	volume of cuboid (m^3)
υ_{sample}	volume of column of water containing sample (m^3)
υ_{solid}	volume of solid (m^3)
υ_{water}	volume of column of water (m^3)
Ω	shear strain in solid
ω	angular frequency (rads / sec)
ω_{scat}	scattering frequency (rads / sec)
$\omega_{viscous}$	viscous frequency (rads / sec)
ω_{crit}	critical frequency (rads / sec)
ξ	normal mode component
ζ	JKD constant = 0.01

Where observation is concerned,

chance favours only the prepared mind.

Louis Pasteur

Chapter One

Introduction to Ultrasonic Bone Assessment

1.1 General Introduction

Throughout the development of medical practice, scientists have been intrigued by methods for examining the human body without the need for invasive surgery. The development of X-Ray technology in the early twentieth century marked a vast step forward in this field, and modern tools such as computed tomography, MRI and virtual reality have given physicians new means of examining patients.

Non-invasive and non-ionising ultrasonic testing has been used to great effect in biomedical diagnostics, in applications such as foetal imaging and Doppler techniques for monitoring blood flow. The compressions and rarefractions in pressure that accompany acoustic propagation mean that wave characteristics closely relate to the mechanical properties of the host medium. Such a dependence had previously been exploited in the non-destructive testing of mechanical and structural integrity, and the development of diagnostics was grounded in the application of ultrasound in engineering environments.

This thesis is principally concerned with the application of ultrasound to the testing of skeletal integrity *in vivo*, and in the understanding of propagation in porous bone, for the diagnosis of the bone disease, osteoporosis.

1.2 Osteoporosis

Osteoporosis is a skeletal disease characterised by low bone mass and microarchitecture deterioration of bone tissue, leading to increased fragility and fracture risk (Consensus Development Conference 1993). In the UK, around 30 % of women and around 8 % of men over 50 years of age are affected by osteoporosis (National Osteoporosis Society (NOS) 1998a). Women are exposed to a higher risk owing to rapidly declining oestrogen levels after the menopause, whilst the occurrence of the disease in men is linked to a lack of testosterone. The use of corticosteroids, and lifestyle factors such as smoking or lack of exercise, also affect its occurrence, which is increasing by 10 % per year (NOS 1998a).

Osteoporosis contributes to causing 200,000 fractures in the UK annually (NOS 1998a). Around 60,000 of these are hip fractures, which often lead to prolonged convalescence and disability. Fractures of the spine and forearm are also common. Many patients do not recover sufficiently to allow a return to their previous lifestyle, and many die within one year of a hip fracture. Not only does the occurrence of fractures significantly affect the quality of life of individual sufferers, but it also places a financial burden on public health resources close to £1 billion (NOS 1998a). In contrast to risk factors such as the trauma of a fall or impaired mobility through other disease, the lack of bone strength constitutes a quantifiable and treatable risk factor.

1.3 The Configuration and Strength of Bone Material

1.3.1 The Configuration of Bone

The skeleton provides a rigid framework for the support and protection of the anatomy of vertebrates. The bones of the skeleton have adapted in form and configuration to give optimal weight bearing capacity with a given amount of calcified tissue. Most bones contain two types of calcified tissue: *cortical* and *cancellous* bone. Cortical bone is dense and compact, with density around 2000 kg/m^3 (Duck 1990). Cancellous bone is a porous cellular network of bony strands

called *trabeculae* (figure 1.1), filled with fatty bone marrow with macroscopic density close to 1100 kg/m^3 (Duck 1990).

Long bones, such as the femur pictured in figure 1.2, consist of a hollow *medullary* cavity, with two extremities known as *epiphyses*. The medullary shaft is made of cortical bone, while cancellous bone forms a lining of increasing thickness at the ends of the cavity. Marrow fills the medullary cavity and the pores of the spongy tissue of cancellous bone. Bone is also highly vascular, with long arteries running the length of the femur, and numerous fine vessels and nerve fibres.

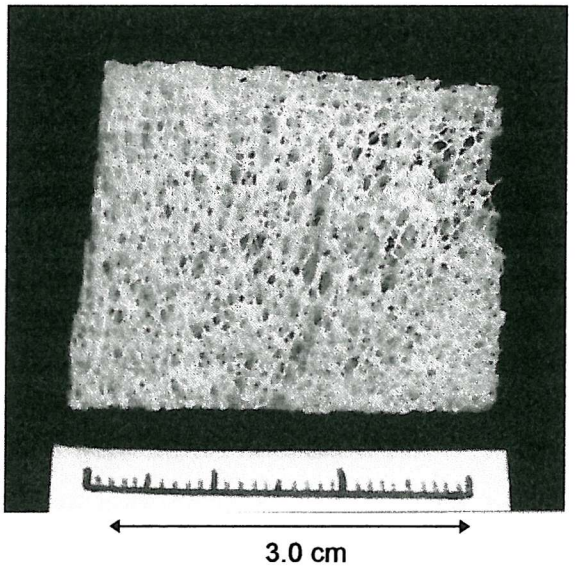

Figure 1.1 - Cancellous bone from the bovine femur.

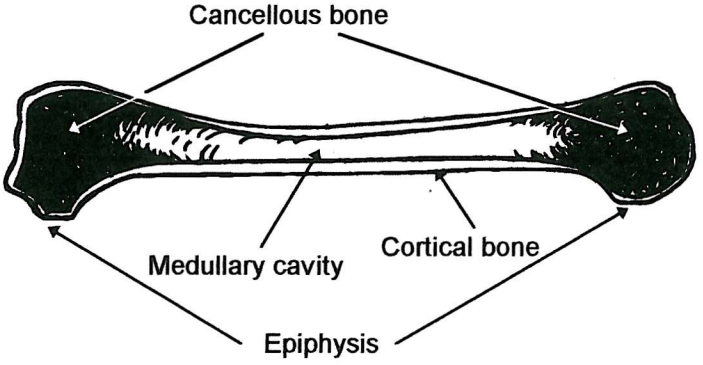

Figure 1.2 - The configuration of bone tissue in the femur.

1.3.2 Mechanical Strength of Bone Tissue

Bone strength is predominantly determined by two factors: bone density and the spatial distribution of calcified tissue.

(a) Bone Mass

Research on fractures in humans shows that those in the population who have less bone, on average sustain more fractures than those with higher mass (Smith *et al.* 1975). Women achieve a lower peak bone mass than men, and the period of accelerated bone loss following the menopause is coincident with an exponential increase in hip fractures in women around this age (Cooper 1989).

The breaking stress of bone is a function of the density and Young's modulus (Gibson 1985). (Density here relates to the macroscopic or volume density of cancellous bone, rather than the density of an individual trabecula.) *In vitro* mechanical loading tests established that the compressive strength of cancellous bone varies with the square of density (Carter and Hayes 1977). This is discussed further in Chapter 2.

(b) Bone Structure

The distribution of calcified tissue is determined by its role at a certain site. Cortical bone, being denser than cancellous, is found at sites exposed to the greatest strain.

The strength of cancellous bone is determined by the structure of the trabeculae network. The trabecular arrangement of cancellous bone is optimally adapted to provide a large load-bearing area, while minimising the weight of tissue. This enables it to withstand the variety of stresses to which it may be subjected. Bone material generates an electric potential under stress, which may be either a semiconductor or a piezoelectric effect (Lang 1970). This behaviour may induce growth along the principal stress trajectories in cancellous bone (Gibson and Ashby 1988).

Furthermore, the density and symmetry of the cancellous architecture depend on the magnitude and direction of the loads it withstands in a particular location (Gibson and Ashby 1988). Rod-like structures occur in regions of low stress, while plate-like arrangements are seen in areas subject to higher stress. In bones where loading is uniaxial, trabeculae are often arranged in a dominant orientation with cylindrical symmetry (Currey 1984). If the stress pattern on the skeletal site is complex, then the trabecular structure is elaborate and may be asymmetric. The same mass of bone is more biomechanically competent when arranged in numerous, highly connected thin plates rather than thicker, fewer and less connected plates (Kleerekoper *et al.* 1985). The classification and mathematical description of the cancellous fabric will be discussed in further in sections 2.3.2 and 5.2.

At a finer level of structure, cortical bone is composed of a fibrous organic matrix (largely collagen) and inorganic calcium compounds. These compounds include crystalline hydroxyapatite, whose fibres are partially aligned along the length of long bones, providing higher stiffness in certain directions. Highly oriented cancellous bone displays relatively high stiffness and compressive strength in the direction of trabecular alignment, with the stiffness in transverse direction being as much as ten times lower, for example, in the human tibia (Williams and Lewis 1982).

1.3.3 Bone Growth and Osteoporosis

Osteoporosis is associated with an imbalance in the regeneration cycle of bone tissue. Bone is constantly being laid down by cells known as osteoblasts and resorbed by those called osteoclasts (McFadyean 1953). In healthy humans, these processes are balanced, such that there is no overall gain or loss of bone. The regeneration cycle is severely disrupted in post-menopausal women as a result of a lack of oestrogen, which results in accelerated bone loss. Additional diseases, such as liver or thyroid problems, or certain treatments for unrelated illnesses, such as corticosteroids for asthma, may also contribute to causing osteoporosis and bone loss (Cooper 1989).

The large surface area of cancellous bone enables more effective metabolism than in cortical bone. Hence, the result from imbalances in the regeneration cycle may be observed first in cancellous bone. In particular, osteoporosis significantly affects the structure of cancellous bone. The pores become larger and the structure becomes more open. Image processing has shown that aged or osteoporotic bone has significantly fewer trabeculae, while those that remain are reduced in thickness (Mellish *et al.* 1989, Croucher *et al.* 1994).

Changes in the trabecular architecture contribute to changes in bone strength (Kleerekoper *et al.* 1985). The deterioration of the cancellous structure has been correlated with fracture incidence in humans. Patients who sustained osteoporotic-related fractures had a significantly lower trabecular plate density, thickness and connectivity of trabecular elements than control subjects (Kleerekoper *et al.* 1985, Croucher *et al.* 1994). Therefore, although fractures occur in sites containing both bone types, most clinical techniques assess cancellous, rather than cortical, bone for early signs of degeneration.

1.4 Clinical Bone Assessment

1.4.1 The Targeting of Treatment

The ultimate aim of current research programmes is to reduce the risk of age-related hip fractures and the financial burden they incur. Although factors such as the risk of falling and poor diet also contribute to fracture risk, drug treatments are available that resist bone loss. The early administration of treatments such as Hormone Replacement Therapy (HRT), Calcium and Vitamin D have been shown to be effective at reducing fracture risk (NOS 1998a). However, although HRT also has cardiovascular benefits, it has been shown to increase the risk of cancer. Recently developed synthetic hormones, called Selective Estrogen Receptor Modulators (SERMS), reduce fracture risk and heart disease, but do not increase cancer rise (NOS 1998a).

Tackling low bone mass by the prescription of such drugs as HRT or SERMS, requires identification of those in the population requiring treatment.

One approach is to treat the entire population, ensuring that everyone who required treatment received it, and reducing a great number of fractures. However, in addition to this being an extremely expensive approach, patients would be unaware of their true bone status or response to treatment, and may be reluctant to comply with such a course.

An alternative strategy is to target those in the population with low bone mass who are at highest risk of fracture. Treatment could then be administered where required, providing incentives for patient and doctor to continue treatment and monitor its progress. However, for such an approach to be effective, those at risk must be identified as early as possible. Identification requires population screening using reliable and precise clinical bone assessment techniques.

1.4.2 The Assessment of Bone Condition

Bone assessment systems may be designed with two roles: first, the early identification of those at highest risk of fracture, and, second, the monitoring of bone status during treatment. Achieving these aims relies on techniques satisfying various prerequisites. First, the system should provide information about fracture risk from a characterising index or parameter that can be measured non-invasively and *in vivo*. Second, that parameter should either significantly alter with the disease over time, or should be of a quantitative level to establish bone condition from one measurement. Such requirements are strongly dependent on the performance of an individual technique, and define its clinical utility.

General experimental practice says that, for a result to be meaningful, the measurement error should be less than the random variability of the parameter being investigated. The role of a clinical assessment technique is dependent on its precision[1], usually quoted as a coefficient of variance (CV or, as a percentage, %CV), with respect to the variation in the population (95 % confidence limits, or two standard deviations). Figure 1.3 shows the comparison between the variation of bone mineral density in the normal population (mean ± standard deviation) and

[1] The word 'precision' has varying usage. In engineering it refers to the resolution (decimal places, scale gradations) to which a measurement may be made. In clinical research, it is often taken as a technique's reproducibility, as mean ± std. The latter definition is used in this thesis.

the error (± 95 % confidence limits), for various coefficients of variance in bone densitometry of the lumbar region. Coefficients of 1 and 2 % are small compared with the distribution, whilst 5 % covers a significant proportion of the range. This suggests a system with a %CV of 1 % would have strong discriminatory capabilities, whilst that with a %CV of 5 % would not be as beneficial. To be useful in unique screening measurements, the %CV of a bone assessment system should be better than 2 % (Reid and Stewart 1998).

If the system is being used to detect a change in a parameter, the measurement uncertainty must be significantly less than any difference it is trying to distinguish. The magnitude of a change in bone density between two measurements depends on the rate of bone loss and the duration of the interval between tests. However, to be confident of detecting a change with the technique, the percentage loss must also be significantly greater than the precision. A certain amount of bone must be lost for a change to be detected, and the delay between measurements until this occurs can be very long if the system has poor precision. This is clearly unsatisfactory for the patient requiring urgent treatment. Therefore, for monitoring the response to treatment, bone densitometers should have precision around 1 % (Reid and Stewart 1998).

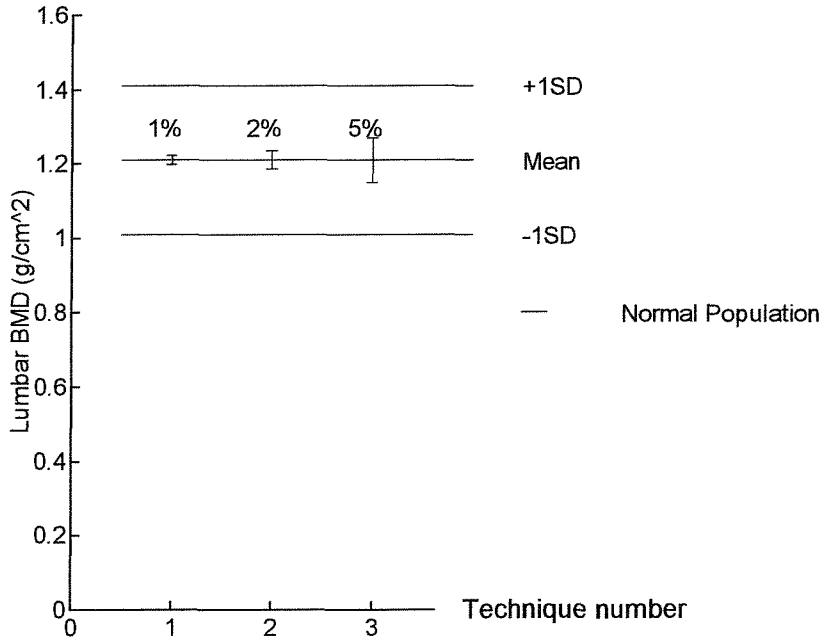

Figure 1.3 - Possible precision values of bone densitometry, with coefficients of variance as vertical bars and mean and standard deviation of normal population as dashed lines (Petley1994).

1.4.3 Current Diagnostic Techniques

Dual Energy X-Ray Absorptiometry (DXA or DEXA) of the lumbar spine is currently the preferred method for identifying fracture risk and monitoring response to treatment of osteoporosis (NOS 1998b). An x-ray beam containing two energies is passed through the body. Since the interaction of x-rays with bone differs from that with soft tissue, it is possible to compensate for the absorption from soft tissue and isolate that from the bone. DXA provides high resolution images and has a precision better than 1 %.

Generally used to assess sites such as the lumbar vertebrae, DXA replaced Single Photon Absorptiometry, which was applied to peripheral sites. Quantitative Computer Tomography was adapted for bone assessment, but is expensive (Consensus Development Conference 1993). Although the DXA method is seen as being the gold standard in densitometry (Miller *et al.* 1996), it is relatively expensive and not widely available in the UK in comparison to the rest of Europe (European Foundation for Osteoporosis and Bone Disease 1998). A national screening programme for osteoporosis was recently rejected on the basis that its cost could not be justified (Royal College of Physicians 1999).

Techniques such as DXA examine bone for one indication of osteoporosis: reduced mass. However, as stated in section 1.3.2, bone strength also depends on its internal microstructure. Therefore, assessment that also evaluates architectural changes, may be a better determinant of fracture risk than DXA alone. Deterioration of the bone microstructure may potentially be assessed *in vivo* by ultrasonic techniques.

Quantitative Ultrasound (QUS) has been available since the mid-1980s and has experienced rapid development in recent years. It has attracted considerable interest since it involves no ionising radiation and can be provided by easily portable and inexpensive machines. The development of such systems, and the role and performance of clinical QUS are described in the following section.

1.5 Ultrasonic Studies of Bone

1.5.1 Historical Studies

Ultrasound has been used to characterise the mechanical properties of bone in attempts to predict bone strength and resistance to fracture. Studies were first reported in 1949 (Theismann and Pfander), and most early work focused on cortical bone (for example, Anast *et al.* 1958, Yoon and Katz 1976). The first studies on cancellous bone reported in the late 1970s (Fry and Barger 1978, Smith *et al.* 1979).

Bone is generally tested at frequencies below 1 MHz, but studies have been performed using frequencies up to 15 MHz (Lakes *et al.* 1983). A wide variety of spatial dimensions and organisational levels have been probed, which range from the ultrastructural level (dimension < 10 μm, such as collagen (Yoon and Katz 1976)); to the microstructural level (dimension > 10 μm, such as trabeculae (Evans and Tavakoli 1990)); to the whole organ (Antich 1993).

The measurement of ultrasonic velocity and frequency-dependent attenuation have been most extensively studied. Further factors that have been studied include resonance (Selle and Jurist 1966) and a combination of velocity and frequency-dependent attenuation, named *stiffness* (Lees and Stevenson 1993), but whose physical significance is not well defined. This parameter is not considered further here, but the measurement of velocity and attenuation in bone is considered below.

1.5.2 Measurement of Ultrasonic Velocity

Two distinct velocities of wave propagation may be defined; group and phase velocity. For a plane harmonic wave of angular frequency, ω, and wavenumber, q (= $2\pi/\lambda$, for wavelength, λ), the *phase velocity* is $c = \omega/q$. The phase velocity equals the propagation speed if the ratio ω/q is constant with frequency. If the phase velocity is a function of frequency, the propagation is dispersive (Kinsler *et al.* 1982), which may arise from sources such as scattering,

the frequency dependence of material constants, or the dissipation of wave energy into heat. The energy of the wave travels at the group velocity, defined as the derivative of angular frequency with respect to wavenumber, q (which may be complex), $d\omega/dq$.

Group velocity is evaluated from the time taken for a pulse to travel through a specimen of known thickness. In a dispersive media, such measurements are subject to the definition of pulse arrival time. A principal feature of dispersion is that a pulse may not retain its original shape as it propagates through a dispersive medium (Sachse and Pao 1978). The group velocity in cortical bone has been measured on many occasions (e.g. Abendschein and Hyatt 1970, Ashman *et al.* 1984, Hunt *et al.* 1998). It has also been measured through cancellous bone (e.g. Rich *et al.* 1966, Ashman and Rho 1988, Nicholson *et al.* 1994). It is also forms an assessment in clinical QUS, where it is known as Speed of Sound, or SOS. Studies in cancellous bone have shown that group velocity, calculated from a given waveform, varied by 6 %, depending on the choice of zero-crossing point (Strelitzki *et al.* 1996), owing to the presence of frequency dependent dispersion.

The measurement of phase velocity in cancellous bone has received less attention. There is evidence that the phase velocity decreases with frequency, that is, it experiences negative dispersion (Nicholson *et al.* 1994), although later research shows evidence of positive dispersion (Strelitzki and Evans 1998).

1.5.3 Young's Modulus

The measurement of ultrasonic velocity has generated much interest owing to the relation between velocity and Young's modulus. The velocity, c_{bar}, of a longitudinal wave travelling along a thin rod may be expressed as

$$c_{bar} = \sqrt{E/\rho}\,, \tag{1.1}$$

for density, ρ, and Young's modulus, E.

The Young's modulus of bone indicates its potential breaking stress (Gibson 1985), traditionally found by static loading tests. Such tests permanently

alter the specimen and assume a linear relationship between stress and strain, which may not exist owing to the visco-elastic nature of bone (Gibson & Ashby 1988). Ultrasound offers a non-destructive measurement of Young's modulus.

Equation (1.1) is valid for longitudinal disturbances in a bar, the lateral dimensions of which are small compared with its length. In such cases, the displacement of particles is parallel to its axis and each cross-sectional plane of the bar may be considered to move as a unit (Kinsler *et al.* 1982). In practice, this condition may be satisfied by choosing a suitable frequency. Propagation in a sample of finite size is dependent on the ratio of the wavelength to some characteristic length of the sample. In homogeneous media, this effect is known as geometric dispersion (Thurston 1978, Ashman *et al.* 1984). Bar propagation occurs if the ratio of the characteristic size to the wavelength is much less than unity. If this ratio is much greater than unity bulk propagation occurs.

Equation (1.1) has been used on numerous occasions to evaluate the Young's modulus of cortical bone from measurements of ultrasonic velocity (for example, Lang 1970, Carter and Hayes 1977). Since cortical bone is relatively homogeneous at the millimetre scale, measurements at frequencies around 2 - 5 MHz, where the wavelength is of the order of 1 mm, satisfy the bar assumption. Ultrasonically derived Young's modulus correlates well with that derived from loading tests (Abendschien and Hyatt 1970).

For studies of inhomogeneous cancellous bone, experimenters have sought to satisfy the conditions for bar propagation in two distinct ways. The mode of propagation in a cancellous sample depends on the ratio of the wavelength to, either, the size of the discontinuity (pore or trabecular width); or, the specimen size. Therefore, two possible scenarios emerge: propagation along individual trabecula, or propagation through a whole cancellous sample.

In the first case, Rho (1998) took the trabecular width as the characteristic length, and assumed that waves travel along each trabecula. Tests were performed at 2.25 MHz, where the wavelength in water is 667 μm, which, for the bar equation to be applicable, should be considerably less than the trabecular width. However, typically trabeculae are 500 μm in width (Mellish *et al.* 1989), so the assumption is not strictly valid. Furthermore, this approach neglects the

contribution of the marrow in propagation, and the possibility of bulk wave propagation at these frequencies.

The second approach has considered propagation through a whole cancellous specimen, typically a few centimetres in width, at lower frequencies. Strelitzki *et al.* (1997a) used pulses of centre frequency 37 kHz (wavelength around 4 cm), to ensure the wavelength was greater than the macroscopic dimensions of the specimen. The resulting time-of-flight velocity values were significantly lower than those observed at higher ultrasonic frequencies, and it was suggested that bar propagation was occurring at this frequency.

Ashman *et al.* (1984) suggested that bar propagation in cancellous bone may transform into bulk propagation as the frequency increases by a geometric dispersion effect. The method by which this mode conversion may occur had not been thoroughly investigated, nor explained with theory.

1.5.4 Broadband Ultrasonic Attenuation

As ultrasonic waves travel through bone, energy is lost. In a lossy medium, a plane harmonic wave, of peak amplitude, P_o, may be represented as $\mathbf{p}(x, t) = P_o.exp(j\omega t - \boldsymbol{q}x)$, where the wavenumber is complex, $\boldsymbol{q} = q - j\alpha_a$, and where α_a is the absorption coefficient (Kinsler *et al.* 1982).

Attenuation of ultrasonic waves in bone was first reported by Fry and Barger (1978) and Smith *et al.* (1979) for the measurements of the skull. In 1984, Langton *et al.* generated much interest in the measurement of ultrasonic attenuation for bone health assessment. The subsequent technique has come to be known as Broadband Ultrasonic Attenuation (BUA) and is the parameter most commonly measured in clinical ultrasonic bone assessment today.

Broadband Ultrasonic Attenuation measurements are taken by passing signal with a bandwidth 200 - 600 kHz through the os calcis (the heel bone), often performed in a water bath. The os calcis is used because it contains a high proportion of cancellous bone, its sides are approximately parallel, and it is easily accessible for testing.

The assumption is made that when attenuation, is plotted on a decibel scale as a function of frequency, *f*, the plot is linear in the bandwidth 200 - 600 kHz, that is,

$$atten(f) = (gradient \times frequency) + constant \qquad (1.2)$$

where the *gradient* is also called the BUA value, in dB per MHz. The BUA value is the gradient of the attenuation spectrum in figure 1.4, evaluated by linear regression.

In a relatively small study of sixty women, Langton found that the BUA gradient was significantly higher in young healthy women than in those who had sustained fractures of the femoral neck. Subsequent studies showing similar results, became the basis for BUA as a parameter of clinical utility.

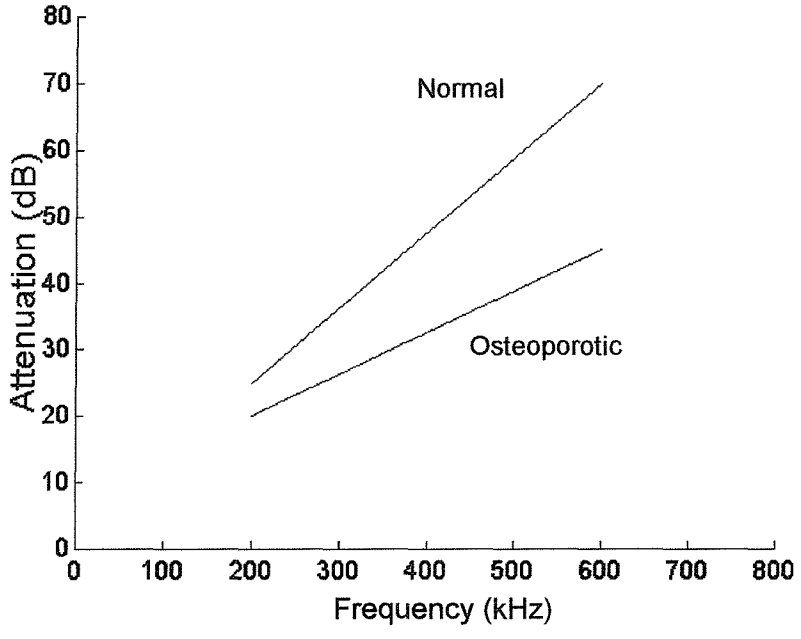

Figure 1.4 Linear relationship between attenuation & frequency which is assumed for BUA.

1.5.5 The Role of QUS in Bone Assessment

Quantitative ultrasound of the heel bone has attracted considerable interest as a potential tool in the clinical management of osteoporosis. There are currently a number of commercial QUS systems, using either a contact method (McCue CUBA, Hologic Sahara, Metra QUS-2), or a water bath technique (Lunar Achilles). It is a portable, quick and inexpensive method of bone assessment. However, its acceptance as a reliable tool has taken some time, owing to a number of uncertainties regarding its performance.

The potential role of QUS techniques in the management of osteoporosis is determined by its clinical precision. The static instrument precision of Broadband Ultrasonic Attenuation has been reported as 2 - 3 %, although for repositioning, a coefficient of up to 9 % has been measured (Greenspan *et al.* 1997, Stewart and Reid 1998). For Speed of Sound, the %CV has been quoted as being in the range 0.5 - 0.8 % (Greenspan *et al.* 1997). Comparing with normal population ranges for BUA and SOS of 4.3 % and 1.4 %, respectively (Truscott *et al.* 1996), both techniques do not perform as well as established DXA.

However, clinical trials have shown QUS is able to predict hip fracture risk in the elderly, with and without supporting DXA data (Hans *et al.* 1996), and, alone, it may be a stronger predictor of low bone mass than when combined with other factors (Langton *et al.* 1997). As a result, the National Osteoporosis Society recommended that QUS may be used to assess hip fracture risk in elderly women, with patients with low results being referred for DXA assessment (NOS 1998b). However, its relatively poor precision, combined with the low rate of change in BUA and SOS over time, means that the technique cannot currently be used to assess response to therapy over a period of time (NOS 1998b).

Research has aimed to establish which physical factors of bone influence QUS measurements. BUA is correlated with bone mineral density, as measured by DXA (Petley *et al.* 1987), although not sufficiently strong to suggest that BUA is only affected by density. Indeed, BUA is affected more by the structure of cancellous bone than by the density (Tavakoli and Evans 1992).

Factors affecting the precision of BUA measurement have undergone investigation. No industrial standards exist, and a large variation in BUA between

different makes of commercial system has been reported (Evans *et al.* 1996). The assumed linear relationship between attenuation and frequency, typified in figure 1.4, has undergone scrutiny, since the attenuation slope varies in different frequency ranges (Strelitzki and Evans 1996), or it may be a function of receiver size (Edwards 1998). The effect of foot positioning was researched by Petley (1994) who proposed a Region of Interest on which to calibrate measurements. Laugier *et al.* (1994) proposed a BUA imaging system to overcome positioning problems.

Bone-mimicking materials have been developed by some commercial manufacturers, and by researchers, for testing the precision BUA systems. Such materials have been made of a mixture of epoxy resin and gelatin (Clarke *et al.* 1994) to simulate the acoustic properties of real bone. The performance of these phantoms will be discussed further in section 4.2.6.

Therefore, although QUS technology may offer complementary information about bone condition to radiological data, further research into underlying influences is required before it may be used in longitudinal studies. In particular, the interaction between ultrasound and cancellous bone is poorly understood, and the identities of those parameters that may be optimal for assessing bone condition, are not known.

1.6 Presentation of Research

1.6.1 Contributions

The definition of osteoporosis refers to the deterioration of the architecture of cancellous bone. Ultrasonic waves are influenced by this structure, and may help to indicate the strength of bone and fracture risk. Since the interaction between ultrasound and cancellous bone is not fully understood, examination of an accurate theoretical model is vital if ultrasound is to be applied in an optimal way. It is the aim of this thesis to further the understanding of ultrasonic propagation in cancellous bone, and the contributions to the field may be summarised as follows:

- Biot's theory for propagation in fluid-saturated porous media, previously investigated by other authors, is considered here in greater detail, where the importance of the pore fluid dynamics is highlighted.
- The existence of two compressional waves, which are predicted by Biot's theory in cancellous bone and which had not been reported in the literature prior to the start of this work, is confirmed. Wave velocities are observed to depend on trabecular orientation, which Biot's theory is unable to model.
- A second model is introduced here, which uses Schoenberg's theory for propagation in parallel-plates to gain qualitative agreement to experimental data.
- The theories of Biot and Schoenberg are compared. This involves the introduction of transverse isotropy and anisotropic fluid effects into Biot's theory.

Throughout the thesis, a number of issue are tackled, including:

- Can a useful theoretical model be found to describe propagation?
- How does frequency affect propagation?
- What physical factors of the composition and configuration of cancellous bone affect the propagation of ultrasonic waves?
- Can any suggestions be made regarding the improvement of current clinical systems ?

1.6.2 Outline

The research is presented as follows:

Chapter 2 Biot's theory is discussed in detail, the mechanisms of the propagation of two compressional waves are addressed, and the theory is used to predict wave properties for a model of cancellous bone.

Chapter 3 An experimental plan was designed to investigate the propagation of two compressional waves in bovine cancellous bone *in vitro*. The principles of ultrasonic measurement are described, and the methods for evaluating wave properties, the experimental immersion system used here and the extraction of bone specimens are discussed.

Chapter 4 Experimental results are presented and discussed. The fast and slow compressional waves of Biot's theory are observed and measured wave properties are compared with theory. Wave properties are observed to be affected by the inclusion of marrow in the pores and to vary with angle to the trabecular orientation.

Chapter 5 An alternative propagation model for to Biot's theory is presented here which accounts for the direction dependence of observed wave properties. Schoenberg's theory for propagation in periodically alternating fluid-solid layers is applied to a stratified model of cancellous bone. Experimental results are compared with predictions from this second approach.

Chapter 6 The Biot and Schoenberg theories for modelling ultrasound in cancellous bone are compared. Anisotropic fluid and frame effects are introduced into Biot's theory, to enable the theory to account for wave properties that change with angle. These predictions are compared with the available experimental results.

Chapter 7 The implications of the experimental and theoretical findings of the previous chapters for clinical bone assessment is discussed. Various suggestions are made regarding areas for future work in both theoretical modelling and clinical studies.

Chapter Two

The Application of Biot's Theory to Ultrasonic Propagation in Cancellous Bone

2.1 Introduction

Whilst many experimental studies of ultrasonic propagation in cancellous bone have been undertaken by previous authors, relatively little research has been carried out into its theoretical modelling. A thorough theoretical understanding of the problem may lead to the most appropriate use of ultrasound in diagnostic systems. Theoretical modelling also identifies relationships that allow factors indicating bone strength to be inferred from measurable parameters.

This chapter reviews Biot's theory and discusses its application to ultrasound in cancellous bone. The derivation of Biot's theory is described, and the main influences on propagation are discussed, including important practical details.

2.2 Biot's Theory for Acoustic Propagation in Porous Media

2.2.1 Acoustics of Porous Media

Several approaches for modelling acoustic wave propagation in porous media have been proposed. One group is known as Rigid Frame models[1] (Zwikker and Kosten 1949, Attenborough 1983, Allard *et al.* 1992). These consider media where the porous solid component (the *matrix* or *frame*) has a high density or elastic moduli and its movement can be neglected. Rigid Frame models have been used to model acoustic wave propagation in the audio range through air-saturated foams for noise control applications (Champoux and Stinson 1992). However, for media where the movement of the solid frame is elastic and contributes to wave propagation, a more comprehensive theory is necessary.

Biot's theory is widely acknowledged as the most general theory for propagation in fluid-solid composite systems. *Fluid* relates to both liquid and gas. The theory has been able to model a broad group of physical problems. These include fluid diffusion through a porous matrix (Chandler and Johnson 1981); dispersion and attenuation due to relative fluid-solid motion (Stoll and Bryan 1970); and the experimental observation of two compressional waves in water-saturated porous solids (Plona and Johnson 1980). It has been used extensively in the geophysical world for seismic prospecting of oil saturated rocks (Bourbie *et al.* 1987) and in sediments (Stoll and Bryan 1970). Furthermore, it has been shown that predictions for Rigid Frame media and Biot's theory are equivalent under certain conditions (Geertsma and Smit 1961, Attenborough 1983).

The following sections outline the derivation of the theory and discuss the main results of Biot's theory. Equations for wave propagation are given, which are used in sections 2.4 and 4.4.2 to predict wave properties in cancellous bone.

[1] A Rigid Frame medium occurs when the bulk modulus of the frame, K_b, is much greater than that of the fluid, K_f; and the bulk modulus of the solid material, K_s is greater than its shear modulus, N.

2.2.2 Derivation of Biot's Theory

Biot's theory (1956a, b) considers acoustic wave propagation in porous elastic media, saturated with a viscous fluid. The average motions of solid and fluid are considered separately, creating two *effective media*. The theory predicts that three waves propagate simultaneously: two compressional waves (called waves of the first and second kind, or *fast* and *slow* waves), and a shear wave. The fast wave is a bulk wave, where the fluid and solid are locked together and move in phase. It usually exhibits negligible dispersion. The slow wave corresponds to an out-of-phase motion between fluid and solid and is usually highly attenuated.

A *saturated* porous medium occurs when both fluid and solid phases are continuous. Compressional and shear modes propagate in an isotropic elastic solid, whilst only one compressional wave may propagate in a fluid. Therefore, it appears logical that three waves will propagate in a fluid saturated porous solid if the fluid and solid are continuous. This is a useful, but crude image, since the theory relies on the motion of fluid and solid being coupled. This will be discussed in sections 2.2.3 and 2.2.4.

The theory assumes that the saturating fluid is compressible and viscous, whilst the solid is perfectly elastic (that is, it obeys Hooke's law) and impervious to the fluid. Fluid and solid displacements are assumed to be small, allowing the linearisation of the equations of motion. The theory is valid for frequencies where the wavelength is large relative to the size of the discontinuities, to allow the medium to be considered as a homogeneous and isotropic continuum. This criterion is common to most continuum porous media theories (for example, see Schoenberg's theory of Chapter 5), and is called the *long wavelength* regime. This regime should not be confused with the *Low* and *High* frequency regions of Biot's theory, introduced in section 2.2.3, the length-scale of which is defined with respect to the dynamics of the pore fluid rather than the discontinuity size.

An abridged derivation of the theory is presented here to demonstrate the physical significance and importance of particular terms, and is also useful for understanding the modifications to the theory presented in Chapter 6.

Maurice A. Biot derived his theory of porous media in four stages. In the first stage, the static deformation of a porous medium containing a fluid is considered. Using the fundamental assumption of the theory of elasticity, where strain and stresss are proportional (Jaeger 1964), relationships between stresses in the solid, σ_{ij}, and fluid, σ; and strains in the solid, e_{ij}, and fluid, ε, are found to be,

$$\sigma_{xx} = 2Ne_{xx} + A(e_{xx} + e_{yy} + e_{zz}) + Q\varepsilon,$$
$$\sigma_{yy} = 2Ne_{yy} + A(e_{xx} + e_{yy} + e_{zz}) + Q\varepsilon,$$
$$\sigma_{zz} = 2Ne_{zz} + A(e_{xx} + e_{yy} + e_{zz}) + Q\varepsilon,$$
$$\sigma_{yz} = Ne_{yz}, \quad \sigma_{zx} = Ne_{zx}, \quad \sigma_{xy} = Ne_{xy} \qquad \sigma = Qe + R\varepsilon. \quad (2.1)$$

with the co-ordinate system shown in figure 2.1. The terms N, A, Q and R are known as generalised elastic coefficients. Constants A and N correspond to the Lame coefficients in the theory of elasticity (Jaeger 1964), with the latter being the shear modulus. Equations (2.1) are for an isotropic porous medium, that is, one whose properties do not vary with direction.

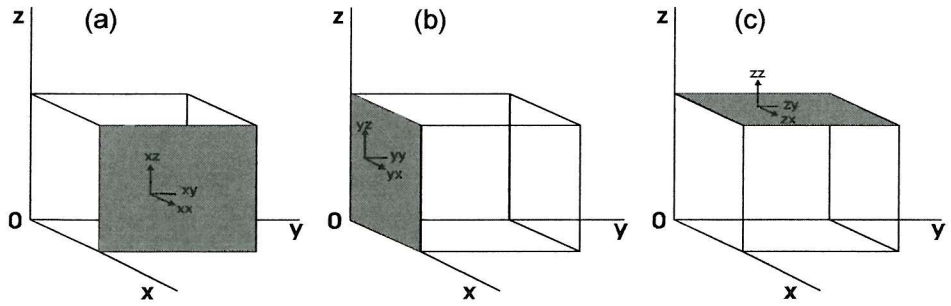

Figure 2.1 - Co-ordinates for subscripts in eqn (2.1) (a) *zy*-; (b) *xz*-; and (c) *xy*-planes, such that stresses over the *ij*-plane lead to lateral or shear strain in an orthogonal plane.

Expressions for A, Q, and R are derived in terms of measurable parameters (Biot 1962). These parameters can be determined by "jacketed" and "unjacketed" compressibility tests. In the former, the specimen is enclosed in an impermeable jacket and subjected to an external pressure. The pressure

of the fluid is transmitted to the internal pore walls, and analysis of the response yields an expression for the bulk modulus of the solid frame, K_b. The unjacketed compressibility test involves immersing a specimen in a pressurised fluid. The dilatation of the specimen is measured once the fluid has penetrated the pores, and an analysis of compressibility yields relations between the bulk modulus of the solid material, K_s, and the fluid bulk modulus, K_f. Using these results, the following expressions for A, Q and R may be found,

$$A = \frac{\beta\left(K_s / K_f - 1\right)K_b + \beta^2 K_s + \left(1-2\beta\right)\left(K_s - K_b\right)}{1-\beta - K_b / K_s + \beta K_s / K_f} - \frac{2N}{3}, \quad (2.2)$$

$$Q = \frac{\left(1-\beta - K_b / K_s\right).\beta K_s}{1-\beta - K_b / K_s + \beta K_s / K_f}, \quad (2.3)$$

$$R = \frac{K_s \beta^2}{1-\beta - K_b / K_s + \beta K_s / K_f}, \quad (2.4)$$

In the second stage of the derivation, Biot considers the dynamics of the porous medium. Using the displacement of the solid, $\boldsymbol{U}$, and the fluid, $\boldsymbol{u}$, the acceleration of the solid and the fluid are related to strain forces and mass densities in Lagranian terms. By introducing the operators, *div* $\boldsymbol{U} = e$, *div* $\boldsymbol{u} = \varepsilon$, *curl* $\boldsymbol{U} = w$, and *curl* $\boldsymbol{u} = \Omega$, for compressional strains in fluid and solid (ε and e, respectively) and shear strains in fluid and solid (w and Ω, respectively), dynamic relationships are used to obtain equations of the propagation of elastic waves. This results in two sets of coupled wave equations,

$$\left\{\begin{aligned} \nabla^2\left(Pe + Q\varepsilon\right) &= \frac{\partial^2}{\partial t^2}\left(\rho_{11}e + \rho_{12}\varepsilon\right) \\ \nabla^2\left(Qe + R\varepsilon\right) &= \frac{\partial^2}{\partial t^2}\left(\rho_{12}e + \rho_{22}\varepsilon\right) \end{aligned}\right\}, \quad (2.5)$$

$$\left\{\begin{aligned} N\nabla^2 w &= \frac{\partial^2}{\partial t^2}\left(\rho_{11}w + \rho_{12}\Omega\right) \\ 0 &= \frac{\partial^2}{\partial t^2}\left(\rho_{12}w + \rho_{22}\Omega\right) \end{aligned}\right\}, \quad (2.6)$$

where equation (2.5) represents compressional propagation, whilst equation (2.6) represents shear propagation. In the first set, the term $P = A + 2N$, and mass densities, ρ_{ij}, are defined as

$$\rho_{11} + \rho_{12} = (1-\beta)\rho_s, \quad \text{and} \quad \rho_{12} + \rho_{22} = \beta\rho_f, \tag{2.7}$$

$$\rho_{12} = (1-\alpha)\beta\rho_f, \tag{2.8}$$

for fluid density ρ_f; solid density, ρ_s, and interconnected porosity, β. The term ρ_{12} is the cross-mass density, which describes the inertial drag that the fluid exerts on the solid as the one is accelerated relative to the other. The term, α, is the tortuosity and is a crucial parameter in Biot's theory. The significance of the cross-mass density and the tortuosity will be discussed in section 2.2.4.

Finally, equations (2.5) and (2.6) may be solved by assuming a harmonic pressure wave, to yield expressions for the complex velocities as,

$$V_{fast,\,slow} = \sqrt{\frac{\Delta \pm \left[\Delta^2 - 4\left(PR - Q^2\right)\left(\rho_{11}\rho_{22} - \rho_{12}^2\right)\right]^{1/2}}{2\left(\rho_{11}\rho_{22} - \rho_{12}^2\right)}}, \tag{2.9}$$

$$V_{shear} = \sqrt{N / \left[(1-\beta)\rho_s + (1-1/\alpha)\rho_f\right]}, \tag{2.10}$$

where $$\Delta = P\rho_{22} + R\rho_{11} - 2Q\rho_{12}. \tag{2.11}$$

Equation (2.9) governs the propagation of two compressional waves, known as *waves of the first and second kind*, or *fast* and *slow* waves, respectively. Equation (2.10) describes shear wave propagation. The real part of the root of equations (2.9) and (2.10) provides the phase velocity in metres per second. Absorption, in Nepers per metre, due to viscous damping at the fluid-solid interface, is found from the imaginary part of the wavenumber, $q_{fast,\,slow,\,shear} = \omega / V_{fast,\,slow,\,shear}$. Viscous drag causes a phase lag between fluid and solid, hence an imaginary term, $j\omega t$.

It is often useful to consider that the wave of the first kind propagates predominantly in the solid frame. Similarly, it may be imagined that the wave

of second kind propagates mainly in the pore fluid, and is influenced by factors associated with fluid dynamics in a pore or tube. This approximation is generally true of Rigid Frame media, such as air-saturated foam, where the densities and moduli of fluid and solid differ by a few orders of magnitude. The properties of bone and marrow, however, are of the same order of magnitude (shown in Table 2.1, later), but the Rigid Frame propagation approximation is still a useful one. The following sections discuss additional factors important to propagation.

2.2.3 Fluid Flow in Porous Media

During propagation of the compressional wave of the first kind, fluid and solid are locked together and move in-phase. This locking arises through two dynamic coupling forces: viscous and inertial. The extent of the relative motion required for the propagation of the wave of the second kind depends on the ability of the fluid to move freely within the pores, and on the frequency of the incident wave. Biot's theory assumes for low frequencies, that the motion of the pore fluid, relative to the solid, follows Poiseuille flow.

Poiseuille flow describes the motion of a viscous fluid in a tube,of radius, r, and is characterised by a parabolic velocity gradient, as in figure 2.2 for flow between parallel plates (Daily and Harleman 1966). Macroscopic fluid particles move in imaginary layers in the x-direction. Each layer has a different velocity, from zero at the boundary, to a maximum at the centre.

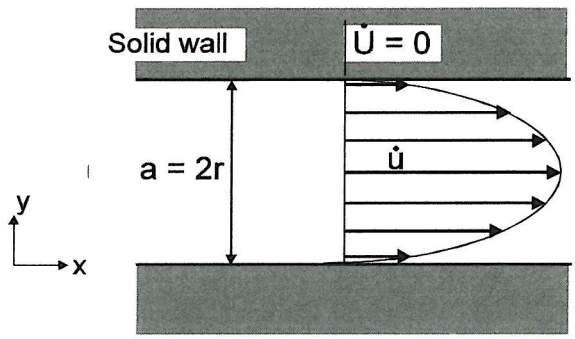

Figure 2.2 - Poiseuille flow in a tube, radius r, of parallel sides; with fluid velocity, $\dot{u}$, and solid velocity, $\dot{U}$.

If the wall oscillates harmonically with $exp(j\omega t)$, a disturbance will be set up in the fluid. In general, at a distance perpendicular from the wall, y, the velocity parallel to wall, $\dot{u}$, can be expressed as,

$$\dot{u} = \dot{u}_{\max} \exp\left[j\omega t - (1+j)\left(\frac{\omega\rho_f}{2\eta}\right)^{1/2} y \right], \tag{2.12}$$

for maximum velocity, $\dot{u}_{\max}$; shear viscosity, η; fluid density, ρ_f; and angular frequency, ω (Biot 1956a). Equation (2.12) describes the relationship between the flow in adjacent imaginary layers, depicted in figure 2.2, in the y-direction. Such behaviour has previously been interpreted as a harmonic wave in the y-direction, the amplitude of which is subject to exponentially decreasing damping with increasing distance from the wall. For different profiles of viscous flow, boundary layers are often defined by various criteria, such as that distance within which the velocity does not exceed a certain percentage of its maximum value (Sherman 1990). For the case of Poiseuille flow in a porous medium, the characterising boundary layer is known as the viscous skin depth, d_s, and is expressed[2] as,

$$d_s = (2\eta / \omega\rho_f)^{1/2}. \tag{2.13}$$

Equation (2.13) shows that the viscous skin depth is dependent on frequency. Indeed, Poiseuille flow only occurs for frequencies where the viscous skin depth, d_s, is greater than the pore radius, r. The parabolic velocity profile breaks down where $d_s = r$, which occurs at the critical frequency, ω_{crit},

$$\omega_{crit} = 2\eta / \rho_f r^2. \tag{2.14}$$

Therefore, the viscous skin depth may be used as a yardstick for acoustic propagation porous media, and its influence on predicted absorption

[2] Strictly, d_s is the distance over which the *vorticity* decays to zero. Vorticity is a vector field describing the rotation of fluid particles, relating the flow of adjacent layers (Sherman 1990).

is discussed in section 2.2.4. The critical frequency will be lower for a medium with large pores, than one of smaller pores, for the same pore fluid. Furthermore, the critical frequency divides propagation into two frequency regimes: *Low* and *High*.

(a) Low Frequency Range: $d_s > r;\ \omega < \omega_{crit}$

Poiseuille flow occurs at frequencies below the critical frequency, where the viscous skin depth is large compared with the pore radius, r. The viscosity of the fluid causes the fluid motion to lock on to the solid motion, enabling the fast wave to propagate. However, since the slow wave involves a relative motion of fluid and solid, it becomes over damped, and is described by a diffusion equation, rather than a wave equation (Biot 1956a)[3]:

$$C_D \nabla^2 \xi = \frac{\partial \xi}{\partial t}\ , \tag{2.15}$$

where ξ is a normal mode co-ordinate (of pressure, particle velocity) and C_D is the diffusion constant (Johnson and Plona 1982). This means the slow wave will not propagate below the critical frequency.

(a) High Frequency Range : $d_s < r;\ \omega > \omega_{crit}$

Above the critical frequency, Poiseuille flow breaks down where the viscous skin depth is smaller than the pore size. Consequently, relative motion of fluid and solid is not impeded by viscous drag, which enables the slow wave to propagate. Inertial coupling dominates viscous coupling, and enables locking between fluid and solid for fast wave propagation. Hence, at frequencies above the critical frequency, both fast and slow compressional waves propagate and may be observed. Figure 2.3 summarises the frequency regions.

[3] During diffusion, fluid particles filter from high pressure to low, owing to a pressure gradient.

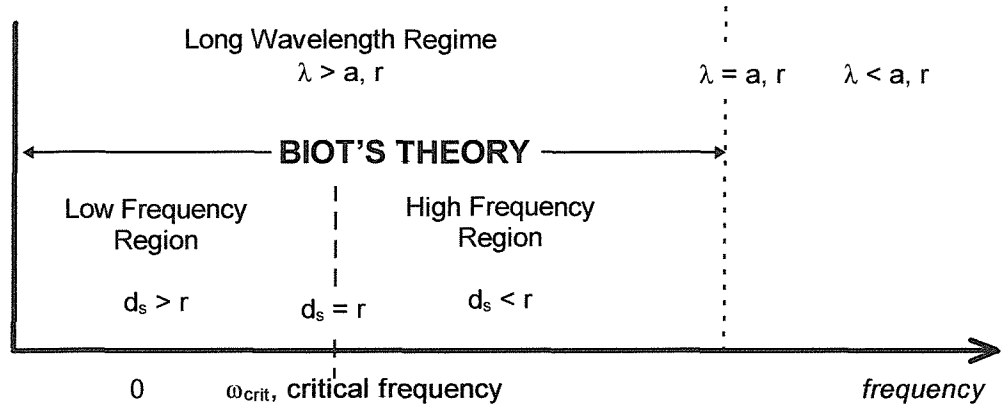

Figure 2.3 - Conditions determining the theoretical frequency regions of Biot's theory.

2.2.4 Inertial Coupling and Tortuosity

Inertial coupling, or mass coupling, dominates viscous effects at high frequencies, and may be regarded in the following way. When a solid body accelerates in a fluid, it drags its own mass plus an additional mass of surrounding fluid (Daily and Harleman 1966). The extent of this coupled mass will depend on the shape and size of the solid body; or, in a porous solid, on the porosity and surface area of the solid matrix. In Biot's theory, the effect is represented by the cross mass density, ρ_{12} and the tortuosity, α.

The tortuosity, α, is a critical parameter in the theory. It is strictly defined as the ratio of the length of the winding path through the pores, to the length of the path if it were straight. It therefore represents the fractional deviation from a straight path, and is always greater than unity. Various expressions have been derived for its evaluation in practice, many of which relate to the geometry of the matrix. However, other factors may cause a deviation in the path of fluid flow through the pores, and hence some expressions include factors of fluid motion.

If the dynamics of the fluid are contained in the definition, they may add a frequency-dependent term. Thus, the cross-mass density of equation (2.8), may be rewritten as being dependent on frequency,

$$\rho_{12}(\omega) = -(\alpha(\omega) - 1)\beta\rho_f, \tag{2.16}$$

where $\alpha(\omega)$, the frequency-dependent tortuosity, defines the entire dynamics of the pore fluid, incorporating inertial and viscous effects. Such effects may be analysed by considering fluid motion in a Rigid Frame porous solid.

For a harmonic pressure gradient, $\nabla P_o e^{-j\omega t}$ (constant, P_o), applied to a porous medium, the linear (small amplitude) equation of motion of fluid in the pores is,

$$-\nabla P_o = \alpha(\omega)\rho_f \frac{\partial \dot{u}}{\partial t}, \tag{2.17}$$

where $\dot{u}$ is fluid velocity, β is porosity, ρ_f is fluid density, and $\alpha(\omega)$ is the frequency-dependent tortuosity. The product, $\alpha(\omega)\rho_f$, represents the added fluid mass, coupled by inertial effects. Darcy's law states that the rate of flow through a porous medium is proportional to the pressure gradient causing that flow,

$$\beta\dot{u} = -\frac{k}{\eta}\nabla P_o, \tag{2.18}$$

where η is viscosity and k is the permeability (in m^2), which characterises the rate of fluid flow. The permeability is related to the tortuosity by

$$\alpha(\omega) = \frac{j\eta\beta}{k\omega\rho_f}, \tag{2.19}$$

which may be alternatively expressed as,

$$\alpha(\omega) = \alpha_\infty + \frac{jbF(\lambda)}{\omega\beta\rho_f}, \tag{2.20}$$

where α_∞ is tortuosity at the limit of infinite frequency, that is, it only relates to geometry. The product, $bF(\gamma)$, governs attenuation, where $b = \eta\beta^2/k$. The

function, $F(\gamma)$, measures the deviation from Poiseuille flow as a function of frequency, and accounts for changes in damping when the skin depth becomes less than the pore radius. Its definition also describes the geometry of the medium, whilst γ depends on the ratio of the pore size to skin depth (Attenborough 1987), defined elsewhere. Johnson *et al.* (1987) evaluated equation (2.20) in terms of measurable parameters,

$$\alpha(\omega) = \alpha_\infty + j\eta\beta\left(1 - \frac{4j\alpha_\infty^2 k_0^2 \rho_f \omega}{\beta^2 a^2}\right) / \omega\rho_f k_0, \qquad (2.21)$$

where a is the pore diameter; k_o is the *d.c. permeability* (for static conditions without a fluid pressure gradient). Equation (2.21) is also known as the JKD-tortuosity. Berryman (1980) derived a purely geometric tortuosity for a matrix of fused spheres, independent of density, and related to a structure factor, S,

$$\alpha = 1 - S(1 - 1/\beta) \equiv \alpha_\infty. \qquad (2.22)$$

Equation (2.22) has often been used as the first evaluation of tortuosity in the application of Biot's theory (for example, for cancellous bone, Williams 1992). An alternative definition of tortuosity for a layered structure, is discussed in section 6.3.1.

In practice, the critical frequency is a transitional bandwidth. Johnson and Plona proposed a rule-of-thumb for a *viscous frequency*, $\omega_{viscous}$, above which the slow wave may be experimentally observed (Johnson and Plona 1982). This occurs at frequencies where the viscous skin depth, d_s, is much less than the pore radius, r,

$$\omega_{viscous} = \frac{2\eta}{\rho_f r^2 \zeta^2}, \qquad (2.23)$$

for the scaling constant, $\zeta \approx 0.01$ (Johnson and Plona 1982). The viscous frequency is therefore a number of orders of magnitude higher than the critical frequency.

2.2.5 Conditions for Slow Wave Propagation

Biot's theory introduces the propagation phenomenon of the wave of the second kind, or slow wave. This wave propagates mainly in the pore fluid, and is therefore dependent on those factors relating to fluid flow. The previous section showed that the ratio between pore radius and viscous skin depth is a crucial factor. The conditions for effective slow wave propagation are:

- the continuity of fluid and solid phases and a high permeability;
- a high frequency content of incident wave;
- a large pore size;
- a low fluid viscosity.

2.3 A Biot Model for Cancellous Bone

2.3.1 Historical Studies

McKelvie and Palmer first applied Biot's theory to ultrasound in cancellous bone in 1987. Since then, a number of researchers have investigated its ability to predict wave properties (McKelvie and Palmer 1991, Williams 1992, Lauriks *et al.* 1994, Williams *et al.* 1996, Hosokawa and Otani 1997). Results show that velocity may be correctly predicted when input parameters are independently evaluated (Williams 1992, Lauriks *et al.* 1994, Williams *et al.* 1996, Hosokawa and Otani 1997). However, a discrepancy between measured attenuation and predicted absorption has been reported on more than one occasion (Williams *et al.* 1996, Hosokawa and Otani 1997). The reasons behind this inconsistency will be discussed at length in section 3.3. Biot's theory predicted qualitative changes in attenuation gradient with porosity (McKelvie and Palmer 1991), but quantitative agreement was poor.

Lakes *et al.* (1983) reported observing the two compressional waves in cortical bone, although this result has not since been independently verified. At the outset of this work, the slow wave had not been observed in cancellous bone. This marked a significant omission to the evidence supporting the applicability of Biot's theory. Observations detailed in following chapters confirm the existence of the slow wave for certain trabecular geometries. First, this section describes the estimation of wave properties using a Biot model for cancellous bone.

2.3.2 Model Input Parameters

The input parameters of a theoretical model generally relate physical properties of the system to quantifiable parameters, which allow the practical interpretation of experimental data. If these variables are accurately known, a straightforward comparison between experiment and theory may be made. However, in many circumstances, input variables may be undetermined, or

determined to an insufficient degree, and the behaviour of the model must be estimated. One method for estimating the predictions of Biot's theory is described in section 2.3.3, whilst the evaluation of the input parameters is considered here.

Accurate prediction of the Biot wave speeds and absorption for cancellous bone requires knowledge of the properties of the constituents and the porous architecture. The values of fourteen parameters must be known. The version of Biot's theory applied here uses the JKD tortuosity term of equation (2.21), which requires more knowledge of the structure and fluid properties than the purely geometric term of equation (2.22), used by previous authors (Williams 1992, Hosokawa and Otani 1997).

(a) Material and Mechanical Properties of Cancellous Bone

The material properties of cancellous bone have not been as widely investigated as those of cortical bone. However, the composition of both types is approximately the same at the collagen level, and, therefore, it is widely accepted that the properties of individual trabecula are the same as those of compact bone (Gibson and Ashby 1988).

The density of human cortical bone is 1800 - 2000 kg/m^3, whilst that of individual trabecula average 1820 kg/m^3 (from summaries by Gibson and Ashby 1988; Duck 1990). A value of 1960 kg/m^3 for bovine bone has been used in previous Biot models (Williams 1992, Hosokawa and Otani 1997).

Understanding the relationship between density, microstructure and strength in cancellous bone is beneficial, first, for fracture risk assessment; second, for prosthetic design; and, finally, for determining how stress across joints cause damage during osteoarthritis. Furthermore, an appreciation of the mechanical behaviour of cancellous bone is useful for predicting its response to acoustic waves. Both cortical and cancellous bone are mechanically anisotropic, that is, their behaviour under tension and compression varies with direction. Anisotropy in cortical bone arises from the alignment of hydroxyapatite fibres at the ultra-structural level, whereas in cancellous bone, it is mainly due to the trabecular structure. The Young's modulus of human

cortical bone along the longitudinal axes is 18.1 - 22.6 GPa, and perpendicular to this, is 10.2 - 11.5 GPa (Gibson and Ashby 1988, Duck 1990).

A problem arises in modelling propagation, because Biot's theory assumes cancellous bone to be isotropic, where realistically, it is not. Previous authors have tackled this problem by modelling wave propagation only in the direction in which the solid Young's modulus, E_s, and the Poisson's ratio, ν_s, are evaluated. The problem of modelling waves in anisotropic media will be discussed further in Chapter 5 and 6.

The mechanical behaviour of cancellous bone is typical of a cellular material and was investigated by Gibson (1985). Cell deformation under stress depends on three factors: the openness of the cells; the porosity; and the properties of the cell walls. Standard techniques for the analysis of synthetic foams and honeycombs, have been employed to investigate the mechanics of cancellous bone. Gibson showed the relative density of cancellous bone was proportional to its relative Young's modulus;

$$E / E_S = C(\rho / \rho_S)^n, \tag{2.24}$$

for Young's Moduli, E and E_s, of the total medium and solid component, respectively; densities ρ and ρ_s of the total medium and solid components, respectively; and constant, C. The index, n, takes the value 2 for open cells, and 3 for closed cells, and has been evaluated as 1.23 for cancellous bone (Williams 1992). The ratio of densities, (ρ/ρ_s), is equivalent to the volume fraction of the solid, or $(1-\beta)$, for porosity, β. The Young's modulus of the cancellous frame, E_b, can therefore be found from equation (2.24) as,

$$E_b = E_s(1-\beta)^n. \tag{2.25}$$

Equation (2.25) may be used to evaluate the bulk modulus of the solid, K_s (i.e. the material of individual trabecula, taken to resemble cortical bone), and the bulk and shear moduli of the cancellous frame, as K_b and N_b, respectively, from standard expressions for an isotropic medium (Jaeger 1964), as,

$$K_s = E_s / 3(1-2\nu_s), \tag{2.26}$$

$$K_b = E_b / 3(1-2\nu_b), \tag{2.27}$$

$$N_b = E_b / 2(1+2\nu_b), \tag{2.28}$$

where ν_s and ν_b are the Poisson's ratio of the solid material and frame, respectively. Poisson's ratio is the quotient of lateral contraction to longitudinal extension under lateral stress (Jaeger 1964), and is therefore direction dependent. Along the long axis of in bovine cortical bone its value is 0.32 - 0.36, whilst it is 0.4 - 0.5 perpendicular to this (Duck 1990).

(b) Properties of Bone Marrow

Bone marrow is classified as either red or yellow. Yellow marrow fills the shafts of cortical bones and is composed principally of fat cells, supported by a delicate vascular connective tissue (McFaydean 1953). Its density is 923 - 1027 kg/m^3 and its amount increases with age. Highly vascularised red marrow, containing fewer fat cells, fills the trabecular cavities and its density lies in the range 992 - 1047 kg/m^3. Its bulk modulus was previously estimated as being similar to that of fat at 2.0 GPa (McKelvie and Palmer 1991).

Little is known of the mechanical properties of bone marrow or its response to ultrasound[4]. The viscosity of marrow from bovine radii is dependent on temperature (Bryant *et al.* 1989), and its value can vary from 0.25 at 20°C to 0.05 Pa.s at 37°C.

(c) Structural Parameters

Defining the structure of cancellous bone is a complex task. The field of biomechanics has proposed several geometric models, some of which will be discussed in section 5.2, in addition to a measure of local anisotropy, known as the fabric ellipsoid (Turner and Cowin 1987). By contrast, acoustic propagation models such as Biot's theory require knowledge of parameters

[4] Hrazdira (1965) found that ultrasound corrupted marrow cell suspensions by mechanical effects and the production of free radicals. An ultrasonic response of this sort is not considered here.

unique to dynamics, such as tortuosity and permeability. However, parameters such as the porosity and pore size are common for analysis in both fields, and, in practice, the assessment of the trabecular microstructure has been performed using image processing and topological classification (Mellish *et al.* 1989, Croucher *et al.* 1994). Such methods evaluate mean trabecular plate thickness (*MTPT*) and separation (*MTPS*), as well as information regarding connectivity.

The porosity of young healthy human cancellous bone has been estimated as around 77 %, rising to around 88 % in older, osteoporotic bone (Mellish *et al.* 1989). It should be noted that it is the pore radius, not diameter or plate separation which is considered by Biot's theory, and data on the MTPS (that is, pore diameter, a), suggests the pore radius in normal human bone may be estimated as 285 ± 50 μm, whilst that of osteoporotic bone may be taken as 455 ± 130 μm.

Williams *et al.* (1996) established empirical expressions for the tortuosity and static permeability of cancellous bone. The authors measured the tortuosity of cancellous bone from the electrical conductivity after marrow removal. The ratio of conductivity of saline alone to the conductivity of the sample saturated with saline, provides a geometrical factor which is proportional to the tortuosity, α_∞. The authors measured the permeability using Darcy's law (equation (2.18)) and a gravity-fed permeability chamber. Such analysis yielded the expressions,

$$\alpha_\infty = 1{\cdot}2 + (72{\cdot}6 \times 10^{-6}.MTPS), \tag{2.29}$$

$$k_o = 44{\cdot}9.\beta^7, \tag{2.30}$$

where *MTPS* is the mean trabecular plate separation in microns.

Evaluating all model parameters for a specific sample of cancellous bone, for the purposes of comparing theory with experimental results, is problematic. Therefore, established values from literature are used and, since many of the parameters in Table 2.1 may take a value within a given range, the extreme limits of the behaviour of the model are estimated. The following section discusses how the uncertainty in the prediction may be evaluated.

Table 2.1 - Input parameters for Biot's theory for a model of propagation in marrow-saturated healthy and osteoporotic cancellous bone at 20°C.

Parameter	Value	Source and Detail
Independent & Variable		
Density of solid (cortical), ρ_s	1800- 2000 kg/m^3	Gibson & Ashby (1988)
Density of fluid (marrow), ρ_f	992 - 1047 kg/m^3	Duck(1990); unknown species
Young's modulus of solid, E_s	18.1 - 22.6 GPa	Duck(1990) trabecular axis
porosity, β	(a) 0.77 ± 0.05 (b) 0.88 ± 0.03	female 19-40 yrs " 61-90 yrs, Mellish 1989
pore radius, r	(a) 285 ± 50 μm (b) 455 ± 130 μm	female 19-40 yrs " 61-90 yrs, Mellish 1989
Independent & Fixed		
Bulk modulus of fluid, K_f	2.2 GPa	McKelvie (1991); as water
Viscosity of fluid, η	0.15 Pa.s	Bryant (1989); bovine at 20°C
Index of power law, n	1.23	Williams (1992); bovine tibia
Poisson's ratio of solid, ν_s	0.32	Gibson (1988); bovine
Dependent		
Shear modulus of bone, N_b	found from equation (2.28)	
Poisson's ratio of frame, ν_b	equivalent to ν_s	
tortuosity, α_∞	found from equation (2.22)	
permeability, k_o	found from equation (2.30)	

2.3.3 Dealing with Uncertainties in Predictions

If values of the input parameters to a model are all known, subject to some error, the simplest method for establishing the uncertainty in the prediction is to find the upper and lower bounds that the model can take. These extreme values may be found by determining the appropriate combination of input values, which may be a complex task if performed by hand. In practice, the use of optimisation algorithms simplifies this task.

Optimisation is part of almost every simulation or modelling situation in engineering. It implies either minimising or maximising. Since the maximum of a function, $h(x)$, occurs at the same place as the minimum of $-h(x)$, however, it is possible to consider only minimisation. In finding the maximum and minimum bounds of a theoretical prediction, the function $h(x)$ being optimised is the output of the model itself.

Numerical methods that perform optimisation may use the principle that derivatives of the function are zero at the minimum, or they may look for the steepest gradient of descent towards the minimum (Kincaid and Cheney 1990). Classic methods, such as Newton's method (Kincaid and Cheney 1990), adjust one variable at a time. However, they are slow for complex problems. Faster and more sophisticated methods, such as genetic algorithms (Kirkpatrick 1983), allow many variables to change at once, and may allow the input values to be subject certain constraints.

There are established methods and computer algorithms for those problems where both the function and input constraints are linear. One example is the Simplex method (Kincaid and Cheney 1990), which is discussed further in Appendix A.III. In practice, multivariable optimisation problems can be solved using software that represents data as matrices, such as MatLab. This method has been programmed in the software package MatLab using standard commands.

Optimisation may be used to evaluate the upper and lower bounds of wave properties predicted by Biot's theory. Although there are over a dozen parameters in the Biot model, not all of those listed in Table 2.1 will contribute to determining the value of the bounds. Only those which can vary

within a given range are taken as input parameters. The optimisation searches iteratively by varying the inputs and monitoring that the value of the model decreases, until the minimum bound is found.

Parameters headed *Variable* in Table 2.1, are independent with respect to other variables in the theory, and may take a value within the range given. These are the fluid and solid densities, ρ_f and ρ_s, respectively; the Young's modulus of the solid, E_s; the porosity, β, and the pore radius, r. These parameters are those which may be varied during optimisation. For those parameters listed as *Fixed*, there is only one value they can take, generally because their value is estimated or is the only one quoted in the literature. These include the fluid bulk modulus, the viscosity, and the index, n. The Poisson's ratio of the frame is assumed that same as that of the solid, and so is fixed. Those parameters listed as *Dependent* may be evaluated from empirical or theoretical equations. In this model, solid and frame moduli and the shear modulus are be found from equations (2.25 - 2.28) and the tortuosity and permeability are be found from equations (2.22) and (2.30), respectively. Therefore, of the original fourteen parameters, only five may be varied within the given range to find the bounds of theory. These are fluid and solid densities, ρ_f and ρ_s, respectively; Young's modulus of the solid, E_s; porosity, β; and pore radius, r.

To use the Simplex method to find the bounds of the predictions, it is necessary to establish that the function (the equations of Biot's theory) and the constraints (input variable limits) are linear. Linearity was established for Biot's theory and the method used to establish this is outlined in Appendix A.III. Once linearity was established, the Simplex method was used to find the bounds of the Biot's theory, allowing the *Variable* parameters in Table 2.1 to alter within the given ranges.

2.4 Prediction of Wave Properties for Cancellous Bone

2.4.1 Viscous Skin Depth and Critical Frequency

Before predictions for wave properties are presented, it is useful to consider Biot's defining frequency limits for a model of cancellous bone. In particular, it is valuable to calculate the critical frequency, ω_{crit}. (the intercept of Low and High frequency regions in Biot's theory), since this parameter represents the frequency above which two compressional waves will propagate in that medium. The critical frequency is the frequency where the viscous skin depth equals the pore radius, r. In addition, the presence of a pore size distribution in real bone will yield a critical *bandwidth*.

Figure 2.4 shows the viscous skin depth, d_s, of equation (2.13), versus frequency for pore fluids of marrow at 20 and 37°C (for viscosity, η as 0.15 and 0.05 Pa.s, respectively), and for water at 20°C (η = 0.001 Pa.s). The fluid density was 1000 kg/m^3 for all cases. Figure 2.4 also shows the mean pore radii for normal and osteoporotic bone, as given in Table 2.1, with pore size distribution given by the error bars. The critical bandwidths and their mean values for the three fluid conditions were evaluated from Figure 2.4, and are summarised in Table 2.2.

Clearly, the greater the fluid viscosity, the higher the critical frequency, and the greater the critical bandwidth. Osteoporotic bone yields lower critical frequencies for the same fluid conditions than healthy bone, although the larger pore size distribution in the former does not necessarily give a larger critical bandwidth, owing to the curvature of the graphs. Consequently, these results provide the frequency limits below which two compressional waves will theoretically propagate in cancellous bone with these fluid conditions. It may be concluded that the two compressional slow waves will propagate at all ultrasonic frequencies (defined as above 20 kHz) in cancellous bone with pore radius equal to, or greater than 0.285 mm. It should be noted that, according to Johnson's rule of thumb (equation (2.23)), the frequency above which the slow wave will be easily observed in practice, will be a few orders of magnitude higher than this.

Table 2.2 - Summary of critical frequencies for propagation through normal and osteoporotic human cancellous bone saturated with various fluids.

	Critical Bandwidth (and Mean) in Hertz	
	Normal	**Osteoporotic**
Water at 20°C	3.3 - 6.9 (4.5)	0.1 - 2.9 (1.4)
Marrow at 37°C	156 - 341 (224)	48 - 148 (76)
Marrow at 20°C	490 - 1042 (705)	143 - 451 (231)

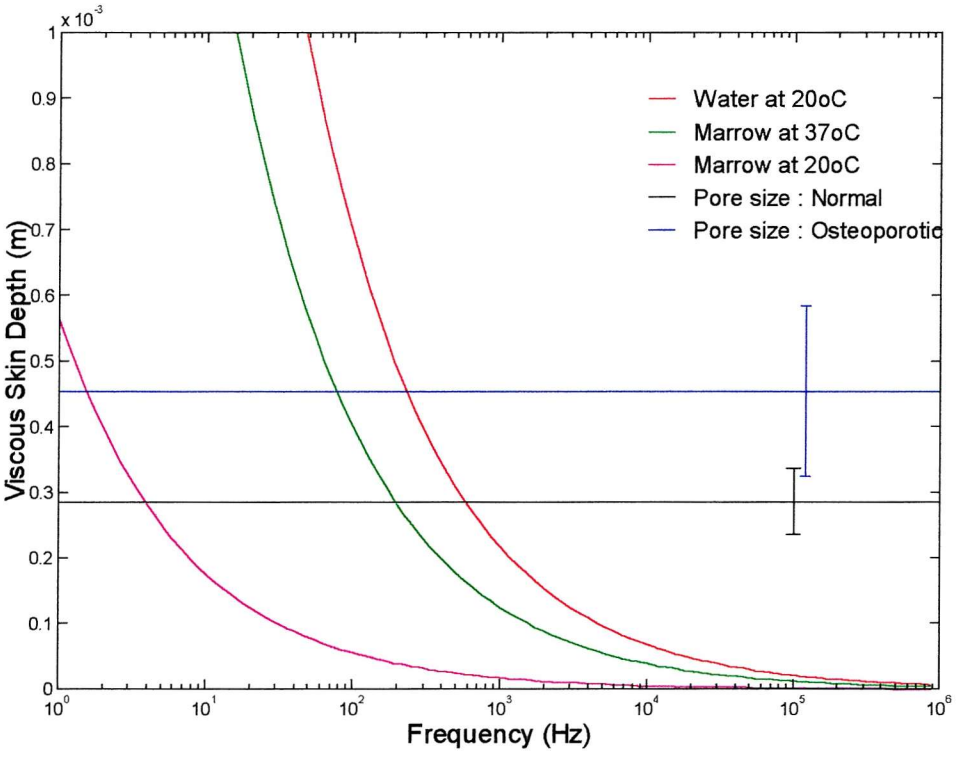

Figure 2.4 - Viscous skin depth versus frequency for marrow at 20°C & 37°C, and water at 20°C, with mean pore radii for normal and osteoporotic bone.

2.4.2 Phase Velocities and Attenuation

Phase velocities and absorption of fast and slow waves were predicted using the values in Table 2.1 and equations (2.2 - 2.4), (2.7), (2.9 - 2.11), (2.16), (2.21 - 2.22), and (2.25 - 2.28). The model was evaluated for marrow-saturated cancellous bone at 20°C. Figure 2.5 shows the phase velocities of fast and slow waves and Figure 2.6 shows attenuation plotted over a wide frequency range.

The effect of the critical frequency, ω_{crit}, may be seen in figures 2.5 (a) and (b) and figures 2.6 (a) and (b), which clearly show a bi-phasic response over the frequency range. These phase velocity and attenuation curves both show a *knee* between low and high frequency regions. This juncture corresponds to the critical frequency, or, rather, to a critical bandwidth.

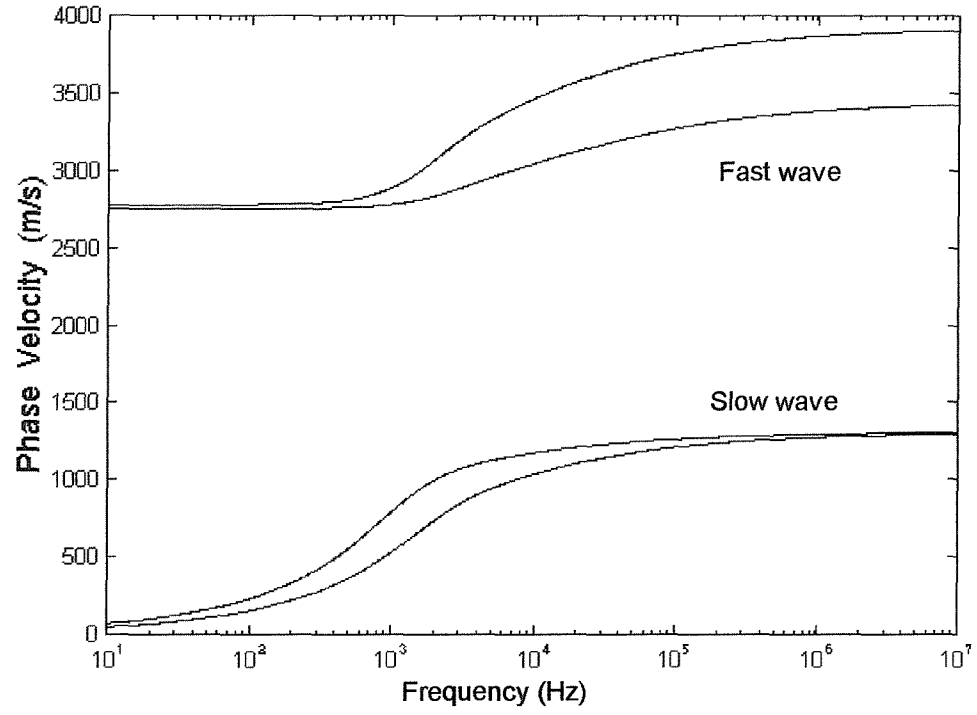

Figure 2.5 - Maximum and minimum phase velocities of fast and slow waves, predicted by Biot for marrow-filled cancellous bone at 20°C.

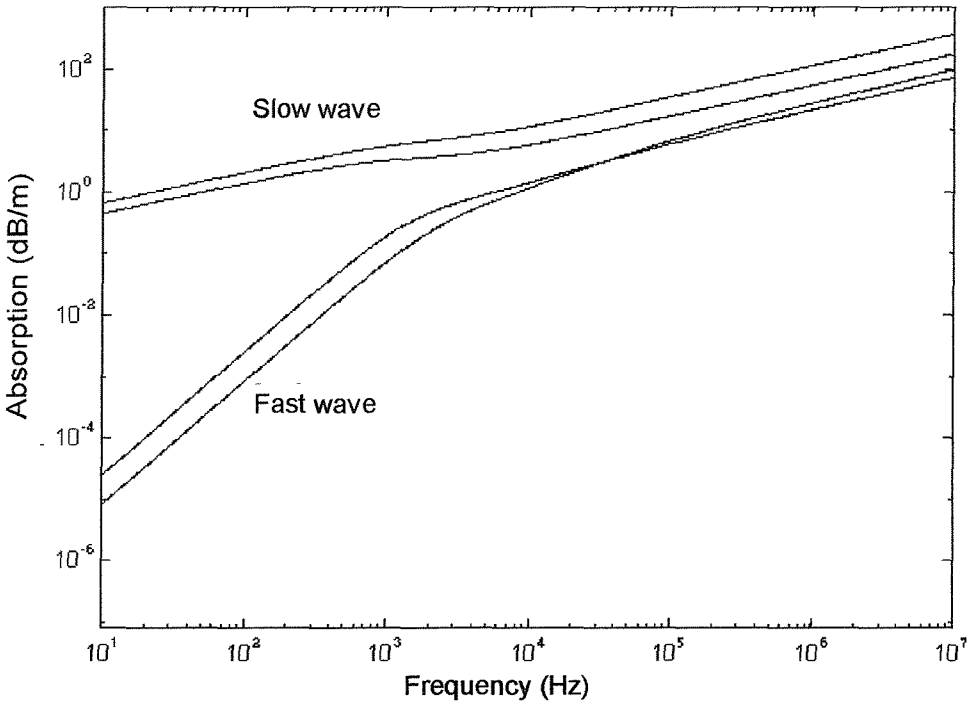

Figure 2.6 - Maximum and minimum absorption of fast and slow waves, predicted by Biot for marrow-filled cancellous bone at 20°C.

2.5 Summary and Conclusions

This chapter has presented a detailed discussion of the application of Biot's theory to ultrasonic propagation in cancellous bone. The equations of Biot's theory were presented, and the evaluation of input parameters for a model of cancellous bone was described. The effects of frequency, structure and mechanical properties on propagation were discussed, and the phase velocity and absorption of the two compressional modes were predicted over a large frequency range.

This analysis has lead to the following conclusions regarding the practical observation of two compressional waves in cancellous bone at ultrasonic frequencies.

- Theoretically, both fast and slow compressional waves will propagate at ultrasonic frequencies in marrow-saturated cancellous bone.
- The open and permeable structure of cancellous bone will aid slow wave propagation at ultrasonic frequencies.

During the course of the research for this thesis, Hosokawa and Otani (1997) reported observing two compressional waves in cancellous bone for propagation in the direction of the trabeculae. Their experiments were similar to those being carried out for this study at the same time, the experimental methods of which are detailed in the next chapter.

Chapter Three

Procedures for the Measurement of Ultrasonic Properties in Cancellous Samples

3.1 Introduction to Experimental Methods

Whilst the theoretical understanding of ultrasonic propagation has much in common with that of acoustic propagation at frequencies below 20 kHz, the practical investigation of the phenomenon has a number of distinctive characteristics. Ultrasonic transducers utilise materials capable of oscillating at high frequencies, and measurements are often performed under water, or using a coupling medium.

Chapter 4 will later present the results of a series of experiments, designed to investigate ultrasonic waves in cancellous bone *in vitro*. This study aims to examine the correlation of measured wave properties with predictions from Biot's theory, introduced in the previous chapter. A number of established experimental and analytical techniques are utilised in the research.

This chapter first describes the principles of ultrasonic measurement, including the generation and reception of high frequency waves, and the causes of deviation from ideal acoustic behaviour. The evaluation and interpretation of measured attenuation is considered in some detail. Next, attention is turned to the evaluation of phase velocity from experimental data using spectral processing. The apparatus used in the experimental studies is described, the performance of which is characterised in various tests. The chapter concludes by describing the preparation and classification of specimens of bovine bone.

3.2 Principles of Ultrasonic Measurement

3.2.1 Piezoelectric Transducers

Ultrasonic waves are most commonly generated by the conversion of a fluctuating electrical signal to mechanical oscillations by a transmitting transducer. The process is reversed in the measurement of ultrasound by a receiving transducer. Such conversion is often achieved using semiconductor materials that exhibit the piezoelectric phenomenon.

The piezoelectric effect occurs in materials where the application of an electric potential causes a mechanical distortion. The phenomenon is reversible, such that, if pressure is applied to a sample of such a material, an electrical potential arises between its opposing faces. Transducers containing piezoelectric elements are widely used to generate and detect ultrasonic waves, being composed of materials such as lead zirconate titanate (PZT) and polyvinylidenefluoride (PVDF). Applying an oscillating voltage to the faces of such a material produces mechanical fluctuations, which, when coupled to a propagation medium, cause acoustic waves to be generated.

The practical performance of piston-type piezoelectric transducers, of the type used in these studies, is now discussed.

3.2.2 Ultrasonic Generation

In general, acoustic waves in air spread out spherically from a point source. However, the sound field from a plane piston oscillator is more complex, and has been investigated using Huygen's principle (Leighton 1994). Huygen's principle treats each wavefront (the surface connecting points of the same phase) as an array of point sources, which radiate secondary spherical wavelets. The position of the wavefront at some time later, is the envelope of these secondary wavelets.

If the size of oscillating source is small compared to the wavelength, the sound field is uniform. In practice, however, ultrasonic sources generate fields with wavelengths comparable with the source dimensions, and so the acoustic field is far more complex. The circular surface of a piston-type transducer can be imagined to be an array of point sources, and, from Huygen's principle, the wavelets emerging from these distributed sources interfere, producing diffraction.

Hence, piston transducers project a field that varies spatially, the variation of which depends on the transducer geometry and the excitation. For a piston transducer in the *xy*-plane, the intensity, I_z, of a continuous wave field at a position, z, in the on-axis z-direction, relative to the maximum intensity, I_0, is,

$$\frac{I_z}{I_0} = \sin^2 \frac{\pi}{\lambda} \left\{ \left(a_p{}^2 + z^2 \right)^{1/2} - z \right\}, \tag{3.1}$$

for wavelength, λ, and piston radius, a_p (Wells 1977).

Figure 3.1 shows the on-axis field pattern, from equation (3.1), of a piston transducer of 2.5 cm diameter at $z = 0$, emitting a continuous wave at 1 MHz. The field contains a series of maxima and minima, whose separation increases with distance from the transmitter. The position of the last maximum is taken as the transition between the so-called near and far fields, often termed the Fresnel and Fraunhofer diffraction regions, respectively. For figure (3.1), the last maximum occurs at $z = 0.105$ m. Whilst the near field ($z < 0.105$ m) is highly complex, plane wave propagation may be assumed to occur in the far field ($z > 0.105$ m).

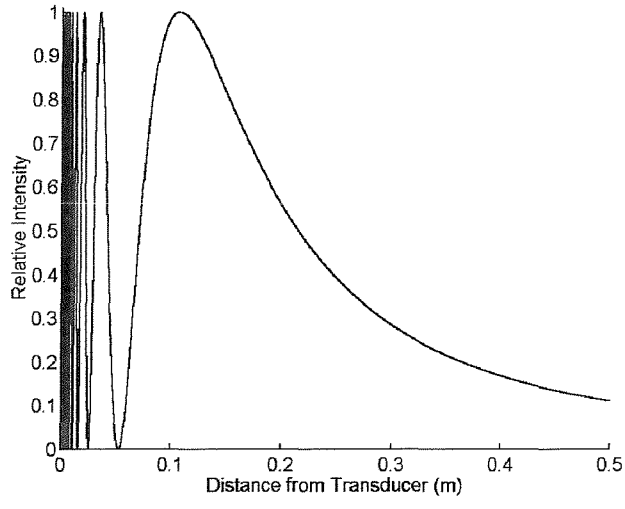

Figure 3.1 - On-axis beam pattern for a radiating piston of 25 mm-diameter at 1MHz.

Transient pulses do not produce the same interference pattern as continuous waves, and temporal information is required to predict a transient field (Beaver 1974). However, it may be assumed that transient excitation affects the amplitude variation in the near field more significantly than the far field (Kinsler *et al.* 1982). The on-axis position of the transition between near and far fields for a transient response may be approximated as that location predicted in the continuous case, by equation (3.1). Section 3.3.2 will consider a case where it is beneficial to probe a test object with the far field in practical measurement.

3.2.3 Ultrasonic Detection

The voltage output of a piezoelectric receiver is proportional to the average pressure over its sensing surface. Transducers of finite size may spatially average the pressure of an incident signal. For example, if a receiver is used to measure the maximum pressure at a focus smaller in area than the sensing surface, it will sense the peak, plus surrounding regions of lower pressure (figure 3.2). This variation will be averaged over the sensing area, producing a signal output lower than the actual peak pressure present (Leighton 1994). The transducer may only measure the true peak if that pressure is sustained over the whole sensing surface. The averaging of signal properties is considered later in section 3.3.2.

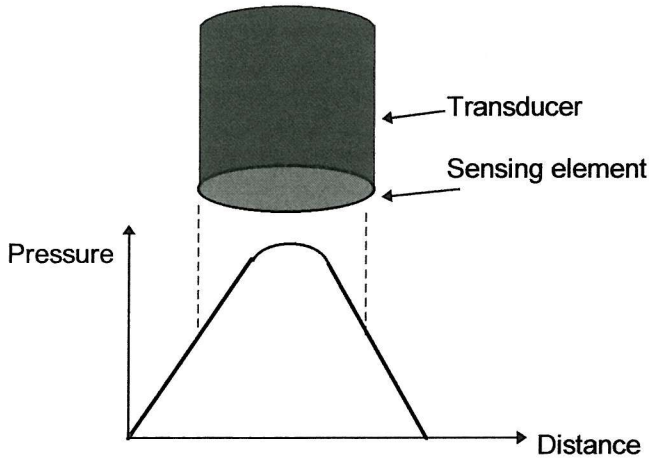

Figure 3.2 - Source of spatial averaging during measurement (Leighton 1994).

3.2.4 Non-linear Propagation

Linear wave propagation assumes fluctuations in particle velocity are much smaller than the speed of sound, and fluctuations in density are negligible compared to equilibrium density (Kinsler *et al.* 1982). However, particle displacements cause local fluctuations in density in sound fields of sufficient amplitude (often termed *finite amplitude*), such that density and pressure variations do not satisfy the linear wave equation. There are two possible sources of non-ideal behaviour: convection and material non-linearities (Leighton 1994).

Convection non-linearities occur if the particle velocity, v, is a significant proportion of the wave speed, c. For high peak pressures, parts of the wave will propagate with the combined speed, $(v + c)$. This causes the peaks to travel faster than other parts of the wave, whilst the troughs lag (Leighton 1994), in the manner shown in figure (3.3) for a sinusoid. *Material* non-linearities occur when a medium is compressed, causing its bulk modulus to increase locally. This leads to an increase in the local speed of sound, which enhances the peak-trough shift.

Both forms of non-linearity cause the waveform to distort, in the manner shown in figure 3.3. As a sinusoidal wave propagates through the medium, local effects cause parts of the wave to travel faster than others, skewing the sinusoid. The waveform becomes sawtooth at a distance from the source known as the *discontinuity length*. The shock which occurs causes increased absorption by redirecting energy from the fundamental frequency to harmonics, which are attenuated more strongly. After the discontinuity length, the amplitude of the shock decreases. Further absorption occurs after this (*old age*), and the waveform becomes a small amplitude sinusoid.

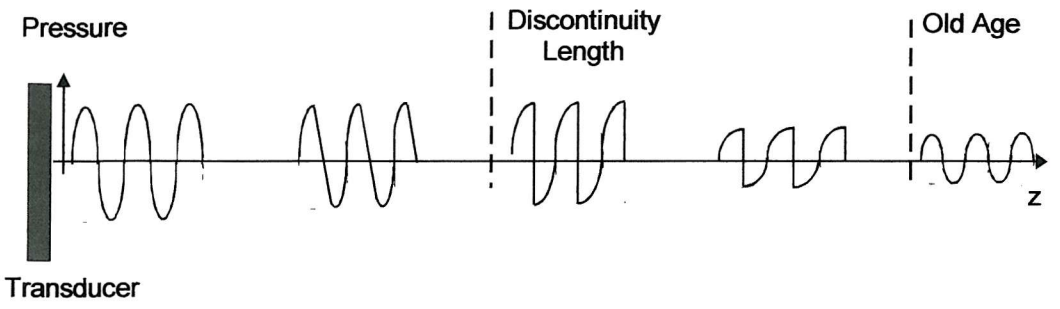

Figure 3.3 - Distortion of a sinusoidal wave due to non-linear propagation (after Leighton 1994).

The presence of non-linear propagation gives rise to various consequences for the practical experiment. Non-linear waveform distortion may interact with diffraction effects, causing a sinusoidal pulse to become non-symmetrical about the zero axis: generally, the peak pressure is increased, whilst the trough becomes rounded (Leighton 1994). In practice, analysis of the maximum and minimum peak pressures may reveal the presence of non-linear propagation. Amplitude scaling tests may also be performed. Both are used in these studies, as described in sections 3.5.2 and 4.2.2. Linearity may be approximated for small wave amplitudes in practice.

If comparisons are made between a theoretical model based on linear propagation, and the results from a practical non-linear case, discrepancies are likely to occur. For example, section 3.3.1 will later describe the evaluation of attenuation based on a linear propagation model, is evaluated as the ratio of amplitude spectra of reference and test trace, found using Fourier Transforms. Although Fourier analysis may be applied to any signal, it is not strictly valid to evaluate their spectral ratio if propagation is non-linear (Stremler 1990). Furthermore, non-linear waveform distortion and the absorption of higher harmonics may occur to different degrees in test and reference media. This will lead to differing waveforms in the respective media and may bias attenuation measures.

3.2.5 Configuration for Measurement of Bone

Pulse-echo measurements are commonly used in ultrasonic applications such as imaging and Doppler. A single transducer performs both the transmission and reception of signals. In this monostatic arrangement, the test pulse traverses a site twice, after the direct signal is reflected back at some rear interface. Bone is highly absorbent in comparison with soft tissue (Bamber 1997), and thus signals may be strongly attenuated over two traverses of a test site. Hence, measurements of bone are better suited to transmission techniques, where the test object is placed between a transmitting transducer and a receiving transducer.

Transmission tests may use a contact or a fixed-path arrangement, both of which have been applied to QUS bone assessment (for example, in the Lunar® Achilles and the Metra QUS-2™, respectively). In the contact method, probes are placed against the site surfaces, hence only generating waves normal to the surface. In contrast, the fixed-path are often performed under water, which provides acoustic coupling. The following sections discuss the evaluation of attenuation and phase velocity using transmission systems.

3.3 The Measurement of Attenuation

3.3.1 Definition and Evaluation

Attenuation is the reduction in acoustic intensity of a sound field. Intensity is defined as the rate of flow of energy through a unit area normal to the direction of propagation. The instantaneous intensity, $I(t)$, at time t, is given by,

$$I(t) = p(t).\, v(t)\,, \tag{3.2}$$

for pressure, $p(t)$, and particle velocity, $v(t)$. For a plane harmonic wave, pressure and particle velocity are related by $p = \rho_o c v$, for ambient density, ρ_o, and speed of sound, c. So, the intensity at time, t, is,

$$I(t) = \frac{p^2}{\rho_o c}. \tag{3.3}$$

However, intensity is often averaged[1] over time, by the integral over period, T,

$$I = \frac{1}{T}\int_t^{t+T} pv.dt\,. \tag{3.4}$$

Taking $p(x,\ t) = P_o.exp(-\alpha_a x).exp(j\omega t - qx)$ in this integral, for a harmonic plane wave, the time-averaged intensity is (Kinsler *et al.* 1982)[2],

$$I = \frac{(P_o e^{-\alpha_a x})^2}{2\rho_o c} = I(0)e^{-2\alpha_a x}\,, \tag{3.5}$$

where $I(0)$ is the intensity at time $t = 0$. The pressure amplitude will decay as $P_o exp(-\alpha_a x)$, whilst the intensity decays with $exp(-2\alpha_a x)$. The attenuation coefficient, α_a, is expressed in Nepers per metre, but may also be quantified in

[1] Output of ultrasonic equipment is often stated as a time-average at the spatial peak of intensity.
[2] Also, rms. pressure and particle velocity may be used for harmonic waves, to give $I = P_{rms}^2/\rho_o c$.

decibels per metre. Since acoustic intensity is commonly expressed in decibels, with respect to some reference, $IL = 10\log(I / I_{ref})$, attenuation may be evaluated as the decrease in measured intensity, with respect to some reference, as,

$$IL_1 - IL_2 = 10\log\left(\frac{I_1}{I_2}\right). \tag{3.6}$$

In practice, intensity is not generally measured, and the evaluation of attenuation relies on measurements of pressure. As mentioned in section 3.2.3, the output voltage from a piezoelectric transducer is proportional to the pressure over its surface. From equation (3.3), intensity is proportional to the square of pressure, and therefore also related to the square of voltage. Therefore, the reduction in intensity of equation (3.6), that is, the attenuation, may be calculated as a function of frequency, as the reduction in squared output voltage between two conditions,

$$atten(f) = -10\log\left[\frac{H_2(f)^2}{H_1(f)^2}\right], \tag{3.7}$$

where $H_1(f)$ and $H_2(f)$ are the amplitude spectra of two distinct signals. Ideally, the values of $H_1(f)$ and $H_2(f)$, should correspond to the outputs of the same signal being measured internally in a test medium at two different locations. This will be discussed further in the following section. However, in the insertion measurements, used in clinical QUS and in this research, the values of $H_1(f)$ and $H_2(f)$, correspond to the cases with and without the bone present, respectively.

Figure 3.4 (a:i - iii) is a flow diagram of the steps involved in evaluation of attenuation from two voltage signals (figure 3.4 (a:i)), and is used in the experiments of Chapter 4. First, the Fourier spectrum of each signal is evaluated by Fast Fourier Transforming (figure 3.4 (a:ii). The attenuation is then found from the ratio of the two spectra, and may be normalised for sample width. Figure 3.4 also shows the steps involved in the evaluation of phase velocity, which will be discussed later in section 3.4.

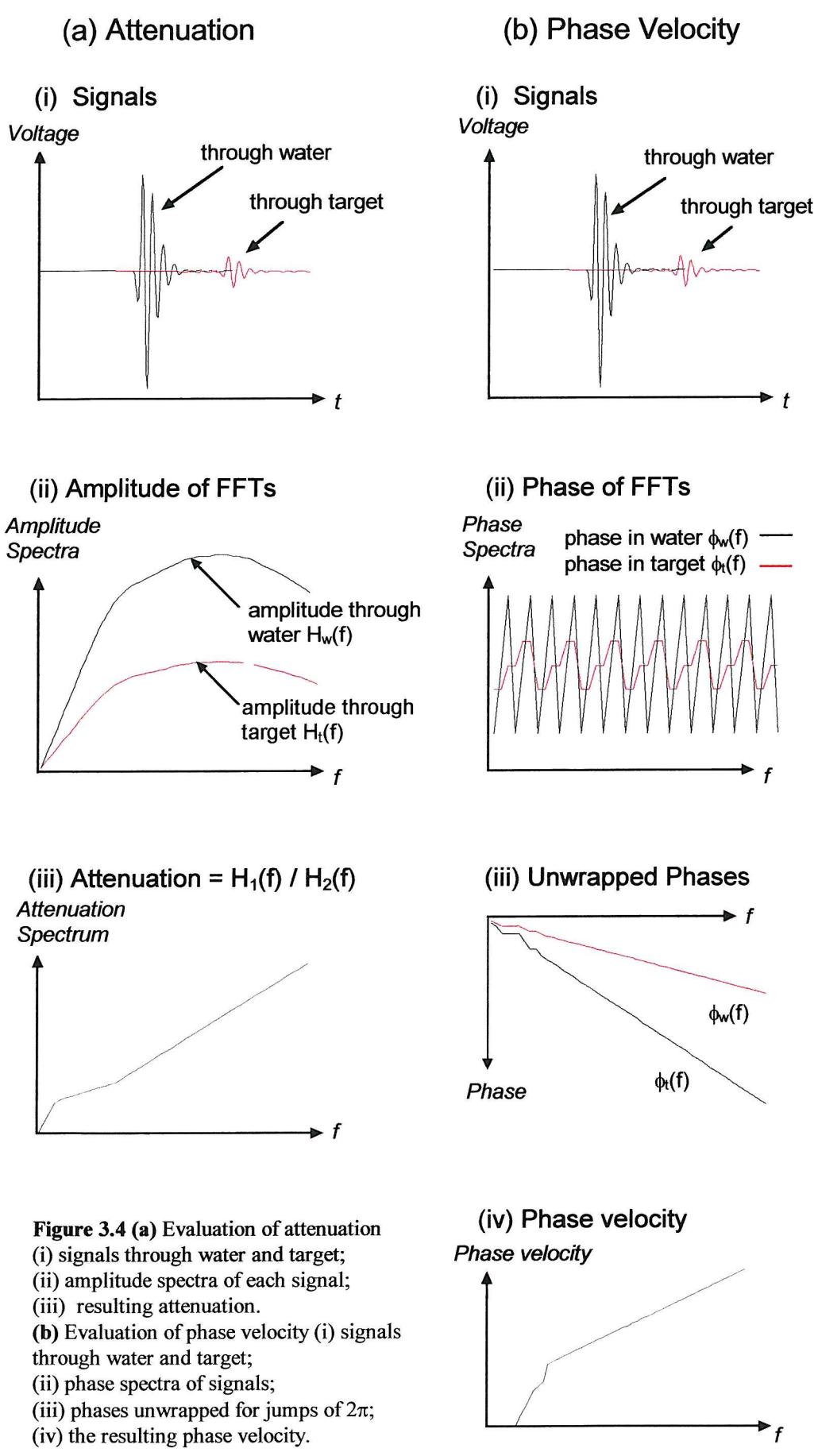

Figure 3.4 (a) Evaluation of attenuation
(i) signals through water and target;
(ii) amplitude spectra of each signal;
(iii) resulting attenuation.
(b) Evaluation of phase velocity (i) signals through water and target;
(ii) phase spectra of signals;
(iii) phases unwrapped for jumps of 2π;
(iv) the resulting phase velocity.

3.3.2 Factors Affecting the Measurement of Attenuation

The accurate evaluation of the attenuation through equation (3.7), depends on the ability of the method to quantify intensity. For a piezoelectric sensor, this refers to those factors affecting the determination of pressure. The energy incident on a receiver's surface may be reduced by factors other than the bulk absorption of the test specimen. Several measurement artefacts may be duplicated in both reference and test signals (such as quantisation and electronic noise), and eliminated by division in equation (3.7). However, the presence of the test medium itself will produce increased scattering and reflection losses, and may enhance the attenuating function of diffraction, phase averaging, and non-linear propagation. These subsidiary factors, and their influence on bone insertion measurements, are discussed in the following sections. Of particular importance to the measurement of BUA, are those factors that contribute a frequency-dependent attenuation. An attenuating factor that increases with frequency will bias the attenuation gradient (that is, the BUA value). The BUA value may therefore be too high, thus conceivably leading to a poor bone status not being recognised.

(a) Diffraction of the Projected Field

Section 3.2.2 discussed how diffraction influences the spatial variation of an acoustic field. Consequently, such effects contribute a frequency-dependent factor to the measured signal loss (Seki 1956). Methods of correcting for diffraction, pioneered by Papadakis (1966), may be applied to any parameter of the acoustic field, to yield a plane wave solution. Whilst several methods exist for correcting pulse-echo measurements, few exist for insertion measurements. Corrections can often be neglected where the velocities of the reference and test media are approximately equal, such as for soft tissue, but, if they are significantly different, diffraction loss may considerably add to attenuation, as found for immersion measurements on perspex (Xu and Kaufman 1993). However, diffraction corrections can make gross assumptions, and their usefulness is yet to be proved.

Owing to diffraction and interference, in parts of the field, wavefronts will not be planar. The assumption that intensity is related to pressure squared is only applicable to plane waves, and hence, the validity with which equation (3.7) can be applied may be called into question if diffraction is present. In practice, planar propagation within a specimen may be approximated by placing it in the far field, thus equation (3.7) may be used.

The influence of the presence of diffraction on measurements of attenuation and BUA in cancellous bone has been studied by previous authors. Diffraction loss is frequency-dependent, which may bias BUA gradients. or a model of the heel bone, diffraction loss has been estimated as 1.66 - 1.91 dB/MHz for insertion techniques, although it was found to be critically dependent on whether a contact or immersion technique is used (Strelitzki and Evans 1998). Discrepancies may result from contact and immersion measurements using regions of a field, such as that in figure 3.1, with differing spatial variations. Contact measurements are generally performed on sites of a few centimetres in thickness, and are likely to probe with the near field (that is, $z < 10.5$ cm in figure 3.1). By contrast, immersion techniques may operate in, or nearer to[3], the far field ($z > 10.5$ cm). Measurements will be subject to different diffraction effects and may therefore be expected to give significantly differing results. Furthermore, contact measurements in the near field will be more sensitive to variations from repositioning and site thickness variation than the fixed-path method, where the beam profile will be virtually consistent between measurements.

(b) Phase Cancellation

If the medium through which a wave propagates has locally varying acoustic properties, parts of the wave will travel at different speeds. Spatial fluctuations may occur along the wavefront as a result of variations in travel times, leading to the distortion of an originally planar wavefront (Marcus and Cartsensen 1975). If fluctuations are smaller than the receiver size, the different phases arrive at the sensor simultaneously and will be spatially averaged across its surface: an effect known as phase cancellation. Since the output of a piezoelectric receiver is

[3] Lunar Achilles has a fixed separation of 9.5 cm, operating at 0.2 to 1.0 MHz.

proportional to the average pressure over its surface, it is therefore sensitive to phase. Additionally, the phenomenon is proportion to frequency.

Phase cancellation will only occur during the measurement of propagation through an inhomogeneous medium. Therefore, when this is compared with that through an isotropic reference medium, it may bias estimations of the true attenuation. Since cancellous bone is extremely inhomogeneous, phase cancellation is a concern in the measurement of attenuation and BUA, which have tended to use isotropic reference media. In particular, since phase cancellation increases with frequency, measurements made with large receivers may overestimate the BUA value, conceivably resulting in a misdiagnosis.

Investigations into the effect of phase cancellation, have been carried out by contrasting phase sensitive and insensitive measurements made using transducer arrays (Petley 1994, Strelitzki *et al.* 1999). Phase sensitive measurements, such as those made using piezoelectric receivers, may be emulated by first combining signals from each transducer element in the time domain. The Fourier transform is then performed on the averaged signal. In contrast, performing the FFT on the time data first, and then averaging their spectra, is equivalent to a phase insensitive measurement. Thus, the two methods can be compared for the same data set. For measurements of attenuation and BUA in cancellous bone, Petley (1994) demonstrated a significant difference between phase sensitive and insensitive measurements when focused on a Region of Interest. However, in a similar study, Strelitzki *et al.* (1999) reported no significant difference between the two cases.

An additional factor influencing the extent of phase cancellation is the size of the receiver. For a given frequency and field with spatially fluctuating wavefronts, a receiver of certain surface area will produce an output subject to greater phase cancellation than that from one of smaller area. The consequences of receiver size have been studied for measurements of attenuation in bone (Petley 1994, Edwards 1998). Phase differences of up to 150° have been measured through os calces over a width of 37 mm at 400 kHz (Petley 1994). Such a variation is likely to contribute to phase cancellation, influencing estimates of attenuation. Indeed, attenuation made at 1MHz, measured for receivers of 0.5 mm- and 25 mm-diameter, were seen to differ by 9 ± 3 dB (Edwards 1998). This

gave reasonable agreement with predictions of 12 dB from a simple model developed by that author.

Finally, since the phase difference between components with different travel times is proportional to frequency, phase cancellation increases with frequency (Petley 1994). Hence, its occurrence may affect the attenuation gradient, and, as with diffraction effects, bias the BUA value.

(c) Reflection Losses

Losses resulting from the reflection of waves impinging on interfaces will also contribute to measured signal loss. Large impedance mismatches between reference and test media result in large reflection coefficients. For normal incidence, the pressure reflection coefficient, **R**, may be found using the formula,

$$\mathbf{R} = \frac{\rho_2 c_2 - \rho_1 c_1}{\rho_2 c_2 + \rho_1 c_1}, \tag{3.8}$$

for density, ρ_i and sound speed, c_i (Kinsler *et al.* 1982), where i is medium 1 or 2. Since the intensity of a harmonic plane wave is related to the square of pressure (equation (3.3)), the intensity reflection coefficient is $|\mathbf{R}|^2$ (Kinsler *et al.* 1982).

Equation (3.8) is valid for reflection from the surfaces of isotropic media, but the situation is somewhat more complicated for that from the surfaces of inhomogeneous media. When a sound wave impinges at normal incidence on a porous surface, part of the wave is reflected back into the reference medium, whilst part is transmitted into the medium as a fast wave, and part as a slow wave. The acoustic properties of a porous boundary are highly sensitive to the state of the surface (Johnson *et al.* 1994).

Some authors have employed a substitution method, where specimens of different widths are used to calculate bulk attenuation (Johnson *et al.* 1994, Hosokawa and Otani 1997). It is assumed that the reflection losses from the surfaces of both samples are identical and may be eliminated in dividing their spectra. However, for this to be achieved, all surfaces must display identical acoustic properties, which is often impractical for biological specimens.

For a water-cortical bone interface, the pressure reflection coefficient is 0.6 (for speeds in bone and water of 3000 m/s and 1500 m/s, respectively, and densities of 2000 kg/m^3 and 1000 kg/m^3, respectively). That is, the pressure amplitude of the reflected wave will be greater than that of the wave transmitted into cortical bone. The proportion of the energy that is reflected is approximately 36 %. Strelitzki and Evans (1998) incorporated dispersion into a prediction of the interface losses through a model of the heel bone. Their results suggest that frequency dependent losses of this kind could be up to 0.24 dB/MHz.

Reflection, discussed in the following section, is a form of scattering where the structures are much larger than the wavelength.

(d) Scattering

Scattering is defined as a change in amplitude, phase, frequency or direction of a wave as a result of spatial or temporal irregularities in a medium. The effect may be classified as *coherent* or *incoherent* (Chivers 1991). Coherent scattering is that which simply adds in amplitude to a plane wave such as general bulk, or volume. Incoherent attenuation implies that which adds a fluctuating intensity, such as specula scattering from distributed irregularities (Hill *et al.* 1978). Acoustic propagation in biological tissue is subject to both coherent and incoherent scattering (Bamber 1997). The contribution of each depends on how randomly multiple scatterers are distributed, and on the ratio of the wavelength to the size of the scatterers. If sound is scattered incoherently from randomly distributed sources, the scattering pattern contains fluctuations, which may be periodic if the tissue has a regular structure on some organisational level (Bamber 1997).

Waves propagating in a porous medium may suffer incoherent specula scattering from the randomly distributed material discontinuities. The scatterers may be taken as the fluid-filled pores, or the solid grains or struts, depending on the proportion of each constituent. As described in section 2.2, the slow wave may be considered as propagating mainly in the fluid of a porous medium. If a large impedance mismatch exists between the solid and fluid components, the fluid-

borne slow wave is likely to be subject to scattering losses from interactions with solid scatterers.

The slow wave will be subject to scattering when $1/|q_{slow}|$ (= V_{slow}/ω for slow wave velocity, V_{slow}) becomes small compared with the diameter of the discontinuity, a; that is, where the product, $q_{slow}.a$, is equal to or greater than unity[4]. Hence, with knowledge of the scatterer size, a, and wave speed, V_{slow} the frequency where this scattering sets in may be estimated and is termed the *scattering frequency*, $\omega_{scat} = (V_{slow}/a)$.

Scattering has been examined for cancellous bone (McKelvie and Palmer 1987; Tavakoli and Evans 1992). Propagation through cancellous bone exhibits negative dispersion (Nicholson *et al.* 1996), which is an observation that is in qualitative agreement with predictions from multiple scattering models (Schwartz and Plona 1984). Recent work by Kitamura *et al.* (1996) considered forward scattering from cancellous bone by modelling the structure as a diffraction grating. This will be discussed further in the Future Work of Chapter 7. Although these studies suggest scattering is present for waves in cancellous bone, its contribution to attenuation measurements has not been quantified.

(e) Attenuation of the Slow Wave in Porous Media

As discussed in section 2.2, the slow wave is highly absorbed owing to relative motion between fluid and solid. It may be further attenuated by scattering from interactions with solid discontinuities, to the extent that it may not be detectable in practice. Johnson and Plona (1982) proposed a *frequency window*, established from practical experience, within which the slow wave may be easily observed. This is defined as the bandwidth composed of frequencies greater than the viscous frequency, $\omega_{viscous}$ (from equation (2.23)), but less than the scattering frequency, $\omega_{scat} = (V_{slow}/a)$,

$$\omega_{viscous} < \omega < V_{slow} / a \,. \qquad (3.9)$$

[4] Using the wavenumber, q, shows that the scattering depends, not only on the ratio of the wavelength to the scatterer size, but also on the speed.

This is illustrated schematically in figure 3.5 (a). The slow wave will be highly attenuated by viscous or scattering losses at all frequencies outside this window, rendering it difficult to detect in practice.

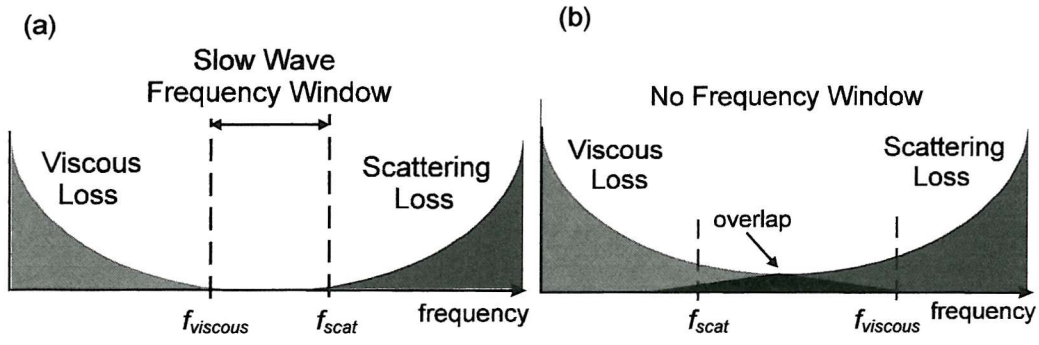

Figure 3.5 - (a) The slow wave frequency window; (b) the overlap of viscous and scattering frequencies. The rates of loss are arbitrary.

Since the product ($q_{slow}.a$) should be greater than unity to avoid significant scattering, for a given frequency, ω, the slow wave velocity, V_{slow} should be large to avoid large scattering losses. Johnson and Plona (1982) demonstrated that the slow wave velocity is proportional[5] to the combination of the frame bulk modulus, K_b, and the shear modulus, N_b, as ($K_b + {}^4/_3 N_b$). If the bulk moduli of the fluid and of the frame are of the same order, or the medium has a high porosity (see equations (2.25 - 2.28)), the factor ($K_b + {}^4/_3 N_b$), and hence the slow wave velocity, will be small. In such cases, the frequency to avoid scattering, must also be low, and, crucially, may even be lower that the viscous frequency, $\omega_{viscous}$. Since this is contrary to equation (3.9), the slow wave will be subject to viscous and scattering losses at all frequencies in media with moduli of the same order. This is illustrated schematically in figure 3.5 (b), where the rates of change of loss with frequency are arbitrary[6].

[5] in the form of a bulk wave, for speed, $c = (K_b + {}^4/_3 N_b)/\rho$.
[6] This analysis does not consider a threshold above which the slow wave may be observable.

The slow wave frequency window was investigated for cancellous bone saturated with various fluids. Previous work by the current author (Hubbuck *et al.* 1998) had shown that the bulk modulus of the cancellous frame (3.2 ± 0.6 GPa), is of the same order as that of the marrow (1.2 ± 0.5 GPa). This suggested that cancellous bone has a relatively weak frame, and may result in no frequency window being present for slow wave propagation.

First, the viscous frequency in Hertz, $f_{viscous}$, was calculated from equation (2.23), using the pore radii and trabecular widths for normal and osteoporotic human cancellous bone, estimated from Mellish *et al.* (1989). The fluid density was varied between 992 - 1047 kg/m^3, and the marrow viscosity was taken at two temperatures: 0.05 Pa.s at 37°C and 0.15 Pa.s of 20°C from Bryant *et al.* (1989).

Next, making the assumption that the fluid-borne slow wave may be scattered by interactions with the calcified trabeculae, the scattering frequency, f_{scat}, was evaluated from $f_{scat} = (V_{slow} / 2\pi d_{trab})$. Trabecular thickness, d_{trab}, was taken as 160 ± 40 μm for normal bone and 120 ± 25 μm for osteoporotic bone (after Mellish *et al.* 1989). Slow wave velocities were calculated as in section 2.3, using parameters given in Tables 2.1 for normal and osteoporotic human bone, taking the mean value at 1 MHz. The resulting slow wave frequency windows are summarised in Table 3.1.

Table 3.1 Slow wave frequency limits for marrow-saturated human bone

	Normal Bone (mean ± error)	**Osteoporotic Bone** (mean ± error)
Marrow at 20°C		
Viscous Frequency	6.3 ± 2.3 MHz	2.6 ± 1.6 MHz
Scattering Frequency	1.4 ± 0.4 MHz	1.7 ± 0.4 MHz
Marrow at 37°C		
Viscous Frequency	2.1 ± 0.7 MHz	0.9 ± 0.5 MHz
Scattering Frequency	1.4 ± 0.4 MHz	1.7 ± 0.4 MHz
Water at 20°C		
Viscous Frequency	425 ± 155 kHz	195 ± 108 kHz
Scattering Frequency	1.2 ± 0.3 MHz	1.6 ± 0.3 MHz

For marrow-saturated normal bone at 20°C (the *in vitro* condition), Table 3.1 shows that the mean scattering frequency is lower than the mean viscous frequency. That is, the limits of the slow wave frequency window overlap, and therefore the wave will be subject to viscous and/or scattering losses at all frequencies, as in figure 3.5 (b). Similarly, for such fluid conditions in osteoporotic bone, there is also no window. This suggests that the observation of the slow wave may be problematic in cancellous bone *in vitro*.

The viscous frequency decreases with increasing temperature in marrow, whilst the scattering frequency remains the same (to this accuracy). Consequently, whilst no window exists for normal bone at 37°C, a narrow bandwidth of frequencies may exist for the osteoporotic case (namely, 0.9 ± 0.5 to 1.7 ± 0.4 MHz), in keeping with figure 3.5 (a). This suggests that it may be easier to observe the Biot slow wave in osteoporotic bone *in vivo* than in healthy bone.

Finally, for a pore fluid of water, a window may exist for both bone conditions. The influence, or otherwise, of these losses on the slow wave in cancellous bone in practice is discussed in section 4.2.5.

3.3.3 The Measurement of Attenuation in a Porous Medium

The energy of an ultrasonic wave travelling through a porous medium will be partitioned between fast, slow and shear waves. The extent of such division will be related to the transmission coefficients of the three waves for a porous surface, defined with respect to Biot's theory (Johnson *et al.* 1994).

Attenuation, as defined in equation (3.7), is stated relative to a reference signal. Ideally, the attenuation of a single mode (whether fast, slow or shear) is measured by placing two probes inside the specimen at a certain separation, enabling the mode to be measured after it has travelled a known distance through the medium. The reference signal in this case is the wave recorded at the first probe. However, the technique faces practical obstacles, including the fact that the presence of the probe itself may alter the properties of the medium. Therefore, historic measurements of bone have generally used the substitution method where the reference signal is a single pulse recorded without a specimen present (called

the *no-specimen reference* here). However, if this no-specimen reference signal is used in the calculation of attenuation of either of the two compressional waves, the energy in the incident pulse will be counted twice: once for fast wave attenuation and once for slow wave attenuation.

The studies of Chapter 4 will compare measured wave properties with those predicted by Biot's theory. In doing so, it is essential that the same wave characteristics are contrasted. In accounting for energy partition, plus the additional factors affecting the accurate determination of pressure, the definitions of *absorption*, *attenuation* and *signal loss* should be carefully considered.

The true attenuation of a mode in a porous medium (*mode X*, where *X* denotes fast, slow or shear), measured with respect to a single pulse using substitution, may be expressed as,

$$\begin{bmatrix} \textit{empirical signal} \\ \textit{loss of mode X,} \\ \textit{from no-specimen} \\ \textit{reference} \end{bmatrix} \text{ subject to } \begin{bmatrix} \textit{energy} \\ \textit{partition} \\ \textit{of mode X} \end{bmatrix} = \begin{bmatrix} \textit{predicted} \\ \textit{absorption} \\ \textit{of mode X} \end{bmatrix} + \begin{bmatrix} \textit{additional} \\ \textit{losses affecting} \\ \textit{mode X} \end{bmatrix} \tag{3.10}$$

On the right hand side of equation (3.10), *predicted absorption* refers to the internal viscous loss of the wave (whether fast, slow and shear wave) from Biot's theory. The preceding sections discussed those *additional losses* (diffraction, scattering and phase cancellation), which are likely to modify the properties of all waves. It is worth remarking that these elements may affect each mode to a different extent. Indeed, section 3.3.2 already discussed how the slow wave may be subject to greater scattering owing to interactions with solid discontinuities and its relatively long wavelength at a given frequency. Strictly, the right hand side is equivalent to the "attenuation" found by measuring the *empirical signal loss* with respect to a no-specimen reference pulse, to which an *energy partition* weighting has been applied for that specific wave, determined from transmission coefficients.

It has been common practice in previous applications of Biot's theory to cancellous bone (Williams *et al.* 1996, Hosokawa and Otani 1997) to compare

predicted absorption with attenuation, calculated using a single reference pulse without allowing for energy partition. Hence, it is not surprising that these authors did not find correlation with Biot's predictions. Partition and the additional empirical losses must be known for the comparison between theoretical absorption and signal loss, measured by substitution with respect to reference in an isotropic medium, to be meaningful. Furthermore, it is unlikely, therefore, that measured empirical signal loss will provide information about bone properties directly, nor give direct agreement with Biot's predictions. Therefore, in seeking agreement between theory and observation, the phase velocity is used, the evaluation of which is described in the following section.

3.4 The Measurement of Phase Velocity

Previous workers have compared measured time-of-flight velocity (that is, group velocity) in cancellous bone with predictions of phase velocity from Biot's theory (Williams 1992, Lauriks *et al.* 1994, Williams *et al.* 1996). This comparison is only valid if propagation is non-dispersive. However, as previously discussed, waves in cancellous bone are dispersive, and therefore theory should be compared with experimentally determined phase velocity. The most commonly used algorithm for evaluating phase velocity in insertion experiments is known as the Phase Spectrum Method.

The Phase Spectrum Method (PSM) was developed by Sachse and Pao (1978) to measure the phase velocity in dispersive solids by a transmission technique. It was later modified by Lee *et al.* (1990) for the purposes of immersion measurements, and was applied by Alvarez-Arenas *et al.* (1994) in identifying Biot slow waves in porous fabric. The algorithm is only applicable for propagation at normal incidence, where no internal refraction occurs[7].

The output signal, after passing through a test specimen, may contain more than one waveform, arising from multiple echoes, scattering, or mode conversion (discussed further in section 3.6.2). Where a time trace contains more than one mode, they may be separated by temporal windowing, where the time axis is sectioned into intervals, each containing a single mode. Spectral analysis may then be performed on the mode contained in the chosen time interval. When a time series is truncated abruptly, errors may be introduced into the calculations because only part of the data stream is used. Fourier spectral analysis is based on the concept that a signal is the sum of contributions of all frequencies that extend in time to infinity (Oppenheim and Schafer 1975). Truncation results in bias errors and spectral smearing, reducing the low frequency content of the signal and the resolution of the Fourier Transform. To lessen these processing effects, shaped temporal windows are used, such as Hanning or Gaussian windows (Oppenheim and Schafer 1975).

[7] Section 5.5.2 considers an alternative method of evaluating phase velocity at non-normal angles.

The amplitude and phase of a mode may be computed using a Fast Fourier Transform (FFT) algorithm. The phase spectrum of the mode is,

$$\phi(\omega) = \tan^{-1}\left(Im(\omega) / Re(\omega)\right), \tag{3.11}$$

where $Re(\omega)$ and $Im(\omega)$ are the real and the imaginary parts of the FFT, respectively. The phase velocity, V_p of the mode is then

$$V_p(\omega) = \frac{d.\omega}{(-\phi_{ref}(\omega)) - \phi_{target}(\omega) + \frac{\omega}{V_w}(d + V_w t_c)}. \tag{3.12}$$

The terms ϕ_{ref} and ϕ_{target} are the phase spectra of the signal with and without the test specimen present, respectively. The term, V_w is the speed of sound in the reference medium (usually water), and d is the target thickness. The term, t_c, compensates for the path length through water displaced by the insertion of the specimen, which is included in the reference phase, ϕ_{ref}, and not present in the specimen phase, ϕ_{target}.

Prior to performing the FFT, the peak value of the waveform should be aligned with the centre of the window, otherwise the resulting phase will change rapidly, providing erroneous results[8]. The peak of waveform is aligned by adding (or subtracting) zeros from the start of the processing window. This is equivalent to moving the pulse by a delay equal to the ratio of the number of additional zeros to the sampling frequency. This delay is equivalent to t_c, in equation (3.12).

Figure 3.4 (b:i - iii) is a flow diagram of the steps involved in evaluation of phase velocity from two voltage signals (figure 3.4 (b:i)), and is used in the experiments of Chapter 4. First, the Fourier spectrum of each signal is evaluated by Fast Fourier Transforming (figure 3.4 (b:ii)). To ensure a smooth spectrum, the phase was unwrapped for jumps of 2π. The phase velocity is then found by using the phase spectra in the formula of equation (3.12).

[8] This achieves *zero phase* (at zero frequency), providing a reference for the subtraction of phases in eqn (3.2). Theoretically, zero phase occurs when a signal is symmetric around the time origin (Oppenheim 1975), approximated here by aligning the peak at the centre of the temporal window.

3.5 Experimental System

3.5.1 Apparatus and Arrangement

The two compressional waves of Biot's theory may be generated and observed in porous media using an impulse method. Plona and Johnson (1980) first reported the observation of fast and slow waves in a porous medium of fused glass spheres, using short pulses of ultrasound, which enabled distinct modes of differing frequency to be separated in time and observed on an oscilloscope trace. The technique was subsequently used by other authors to observe fast and slow waves in a variety of porous media (Lakes *et al.* 1983; Alvarez-Arenas *et al.* 1994; Hosokawa and Otani 1997). Therefore, a fixed-path transmission impulse technique was used in this study to generate Biot fast and slow bulk modes in marrow-saturated cancellous bone through mode conversion at the water-specimen interface. Water was used as the coupling medium, since its acoustic properties are well established, and its attenuating properties may be assumed to be negligible compared to bone (Bamber 1997).

The experimental configuration is shown in figure 3.6 and photographs of the apparatus are shown in figure 3.7. Two Panametrics 1 MHz-resonant 25 mm-diameter piezoelectric transducers were suspended and coaxially aligned in a tank filled with degassed water. The water temperature was recorded at the start and finish of each test. A single sinusoid, with a centre frequency 1 MHz and a pulse repetition frequency of 100 Hz, was produced by a Thurbly Thandar TG1304 programmable signal generator. This was fed to a ENI RF power amplifier (Model 240L), which amplified the signal by 50 dB. The amplified signal was fed to the transmitting transducer.

The test specimen was placed in a reflective polystyrene mount, coaxially aligned with the transducers, to prevent ultrasonic signal leakage around the side of the specimen. The signal passed through the specimen and was acquired by the receiver. The received waveform was recorded by a Lecroy 9314L Digital Storage Scope, sampling at 10 MHz, above the Nyquist frequency to avoid aliasing (Oppenheim and Schafer 1975). The output was averaged over 500 acquisitions to lessen the effects of electronic noise and stored on floppy disc. The signals were

analysed off-line on a Hi-Grade 486 PC, by first converting data from binary to ASCII format using the software package FGM, and then the MatLab Version 4.0 data processing package. A Hanning window and 2048 FFT points were used.

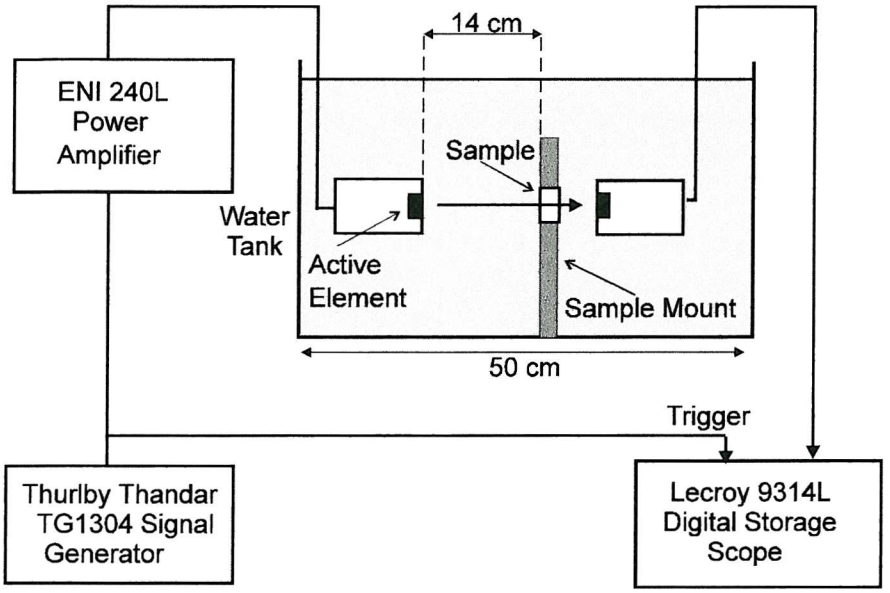

Figure 3.6 - Schematic diagram of experimental system

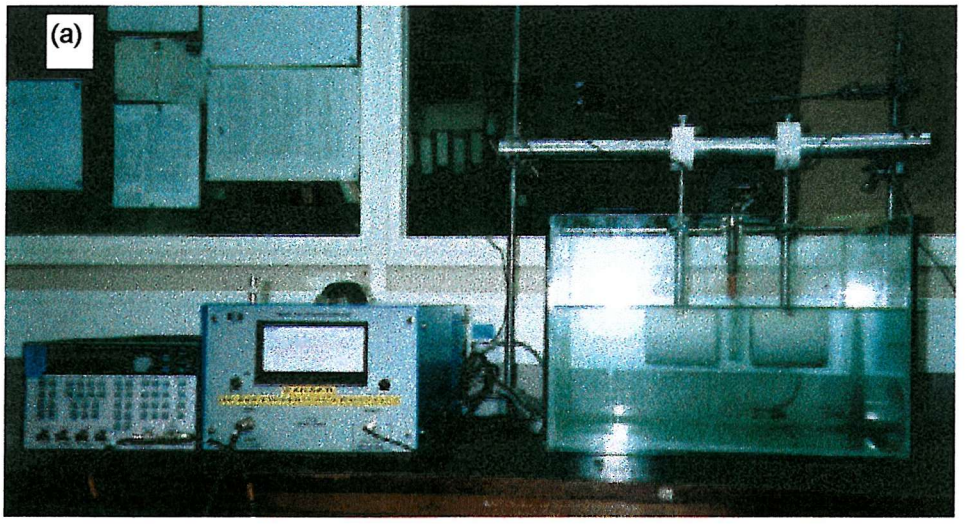

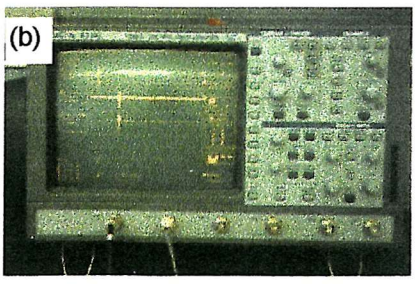

Figure 3.7 - Photographs of experimental equipment.
(a) l-to-r: signal generator, power amplifier, water bath;
(b) Lecroy oscilloscope;
(c) coaxially aligned transducers, showing active element.

3.5.2 Acoustic Field Characteristics

A transducer is generally most efficient when used at its resonant frequency. The resonance frequency of the 25 mm-diameter transducers was 1 MHz, and, from the discussion of section 2.4.2, this frequency was considered to be in that range where two Biot waves may be observed.

The acoustic field produced by the 25 mm-diameter transmitter was investigated for a single sinusoidal input pulse of centre-frequency 1 MHz. Figure 3.8 (a) shows the voltage output received by the second 2.5 cm transducer through water at an on-axis distance of 14 cm. The origin of the time axis is at the trigger, taken on the rising edge of the input pulse from the signal generator. The waveform is seen to have a prolonged decay, likely to result from both transducers being poorly damped at resonance. Such a response was seen to occur to some extent for excitations of both impulses and sinusoidal pulses, as expected for resonance. The duration of the pulse is around 4.5 μs. Waveforms of the type in figure 3.8 (a) were used as the reference signal for the calculations of phase velocity and attenuation throughout the experimental work of this thesis.

Figure 3.8 (b) is the power spectral density of the pulse in figure 3.8(a), showing a maximum value around 920 kHz. The -3 dB bandwidth, within which the signal-to-noise ratio may be assumed to be good, is roughly 0.85 - 1.02 MHz. It should be noted that the spectrum may also reflect the frequency response of the other elements of the system, such as the power amplifier.

The field transmitted by the transducers was characterised using the NPL Beam Calibration Unit. The system evaluates key parameters, such as maximum and minimum pressures, p^+ and p^- respectively; beam width, temporally averaged intensity, I_{spta} and total power output. Transducers were calibrated with a pulse input to the power amplifier of centre frequency 1 MHz, 800 mV peak-to-peak input, amplified by 50 dB, used throughout the experiments of Chapter 4 and 5. Details of the calibration procedure are summarised in Appendix A.I.

The maximum and minimum peak pressures of the field were found to be 48.4 kPa and -32.0 kPa, and the -6 dB beam width was 1.2 cm. This indicated that the pulse was not significantly distorted by the interference of non-linear and

diffraction interference. Further linearity tests, reported in section 4.2.2, were performed on samples of cancellous bone.

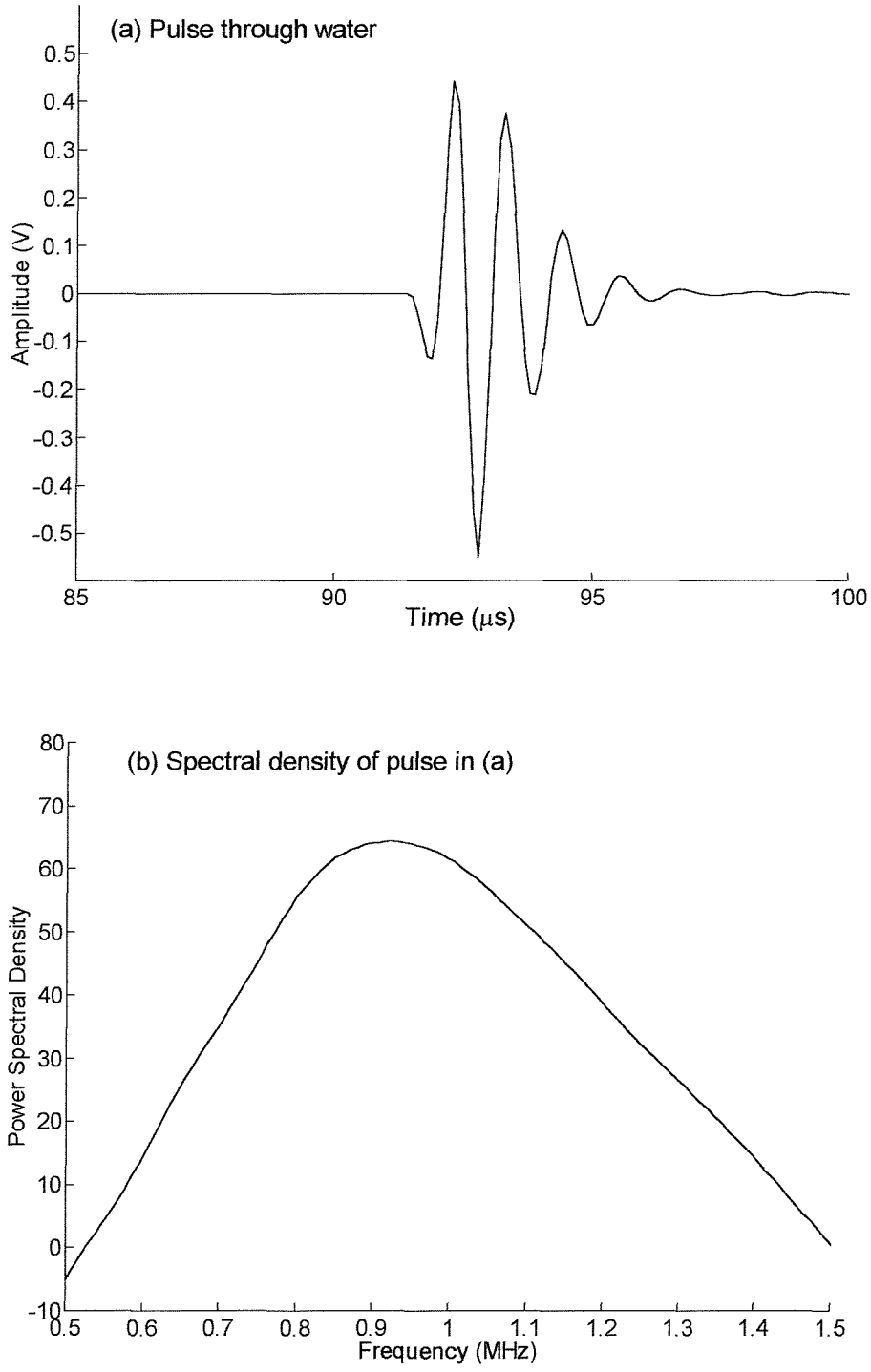

Figure 3.8 - (a) Waveform through water; (b) its spectral density (in dB/Hz).

The test specimen was placed in a reflective polystyrene mount, coaxially aligned with the transducers, to prevent ultrasonic signal leakage around the side of the specimen. To approximate plane wave propagation, the sample was placed in the far field. For a 25 mm transducer, operating at 1 MHz in water, the near-far field transition was found in section 3.2.2 to start at 10.5 cm from the transducer face. However, the signal had an operational bandwidth of 0.85 - 1.02 MHz, which may cause the transition to occur at 8.9 - 10.7 cm from the transmitter. Therefore, to ensure the sample was in the far field, it was placed at approximately 14 cm from the transmitter face, where plane wave propagation could be assumed.

3.6 Validating the Experimental Method

3.6.1 Introduction

At the beginning of an experimental study, the method should be validated for the results to be meaningful. The previous section already discussed the characterisation of the acoustic field and some tests of the presence of non-linear propagation. In addition, the function of the algorithms used to evaluate wave properties should be established, using various test objects.

3.6.2 Mode Separation and Reverberation

An acoustic wave in a finite-sized specimen may internally reverberate, as reflections arise from waves impinges on interfaces with the external reference medium. If reflections of the reverberated wave overlap with the direct wave, the output signal may be corrupted.

Figure 3.9 shows the problem for an isotropic medium. A direct signal propagates through the medium, and is partly reflected and partly transmitted at the rear interface. Some interference may occur between direct and reflected signals near this edge of the test object if the pulse duration is long, regardless of sample thickness. The first echo inside the sample is reflected a second time at the

front boundary, is finally transmitted into the reference medium. Thus the first reverberation travels an additional distance of $2d$.

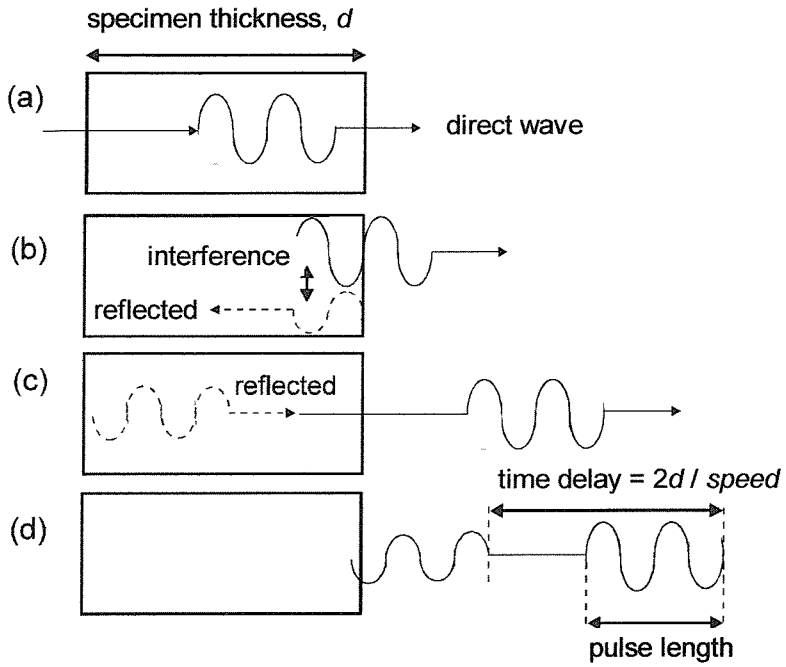

Figure 3.9 - Reverberation inside a specimen and the emerging signal.

To achieve clear temporal distinction between direct modes and echoes, the pulse duration should be less than the time delay between arrivals. From figure 3.9 (d), this delay is twice the thickness divided by the mode speed. Since the mode speed is determined by the medium, and the pulse duration is fixed by the measurement system, presence of this effect in practice is established by the sample thickness, d.

The velocity of a direct signal through cancellous bone has been measured as approximately 2600 m/s at 1MHz (Truscott *et al.* 1996)[9]. Since the duration of the pulse in figure 3.8 (a) is 4.5 μs, reflected and direct signals may overlap in the time trace if the sample has a thickness less than 0.585 cm (= (4.5 μs × 2600) /2). Therefore, to observe reverberant echoes distinct from the direct arrivals in the time domain, it is necessary that samples are thicker than 0.6 cm.

The scenario is further complicated for a porous medium, owing to the presence of more than one propagation mode. The emergent time history will

[9] Although not associated with a Biot wave, it is prudent to take the fastest speed available.

consist of a fast wave, followed by a slow wave and a sequence of reverberant echoes, separated by predictable time delays. The temporal separation between arriving modes depends on the thickness of the specimen.

It is possible to examine whether a signal contains echoes from reverberation using spectral analysis. Signal processing methods (known as *cepstral* analysis, or homomorphic filtering (Oppenheim and Schafer 1975)) exist for detecting and removing echoes from time series, commonly used in speech processing, sonar and seismic studies. If the echo, amplitude a_o, of a fundamental signal, $s(t)$, occurs at time t_o, the resulting signal is,

$$x(t) = s(t) + a_o s(t - t_o). \tag{3.13}$$

The Fourier transform of this signal gives the spectrum $X(f)$, as

$$X(f) = S(f)\left[1 + a_o e^{-j2\pi f t_o}\right]., \tag{3.14}$$

where $S(f)$ is the Fourier Transform of $s(t)$, and $e^{-j2\pi ft}$ is the Fourier Transform of a pure delay at t_o. Using the identity $e^{j\theta} = cos\theta + j.sin\theta$, the power spectral density may be written as,

$$|X(f)|^2 = |S(f)|^2 \{1 + a_o + 2a_o \cos(2\pi f t_o)\}. \tag{3.15}$$

The term in parenthesis {...} on the right hand side of equation (3.15) adds a sinusoidal ripple to the spectrum at a "frequency" of t_o (see figure 3.10). Therefore, the presence of reverberation in a signal through a test medium may be established by examining the power spectral density of the signal.

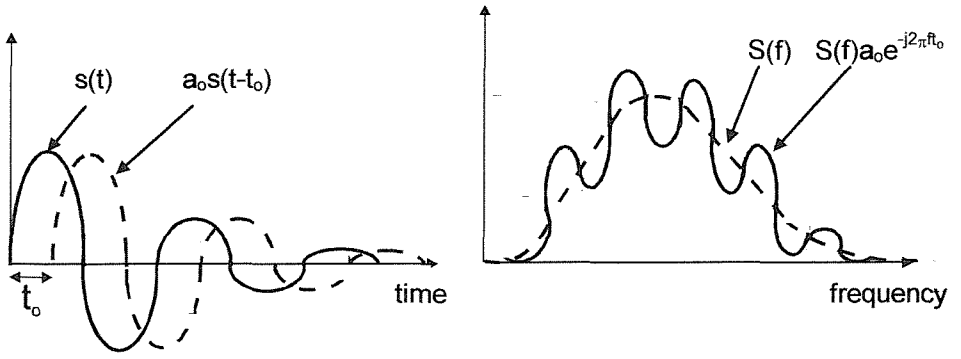

Figure 3.10 - (a) Signal composed of direct wave and echo; (b) schematic of its spectral density (Hammond and Peardon 1994).

3.6.3 Testing the Processing Algorithms

The Phase Spectrum Method for the evaluation of phase velocity, introduced in section 3.5, was programmed in MatLab and validated with real ultrasonic data. First, the speed of sound in water was evaluated and verified against its well-established value. With the transducer separation at 14 cm, a 1 MHz pulse was transmitted through water and recorded. In this test, the reference and test signal are the same (of the type in figure 3.8 (a)). As a result there should be no resulting phase change between the signals. It can be seen from equation (3.11), that the resulting phase velocity should therefore be equal to the speed of sound in the reference medium, V_w.

Figure 3.12 shows the computed phase velocity for a pulse in water, compared with its established value of 1480 m/s at 20°C. The speed of sound in an acrylic test object of thickness 0.6 cm, was also evaluated, and compared with an established value of 2650 m/s (Kinsler *et al.* 1982). Figure 3.11 shows the waveform received with the test object present, whilst figure 3.12 shows its phase velocity. At 1 MHz, the measured velocity gave agreement to the established values to within 0.5 % in water, and 5 % in acrylic. However, the presence of dispersion clearly affects performance at other frequencies. Nevertheless, the algorithm can be assumed to be operating correctly at the frequency of interest.

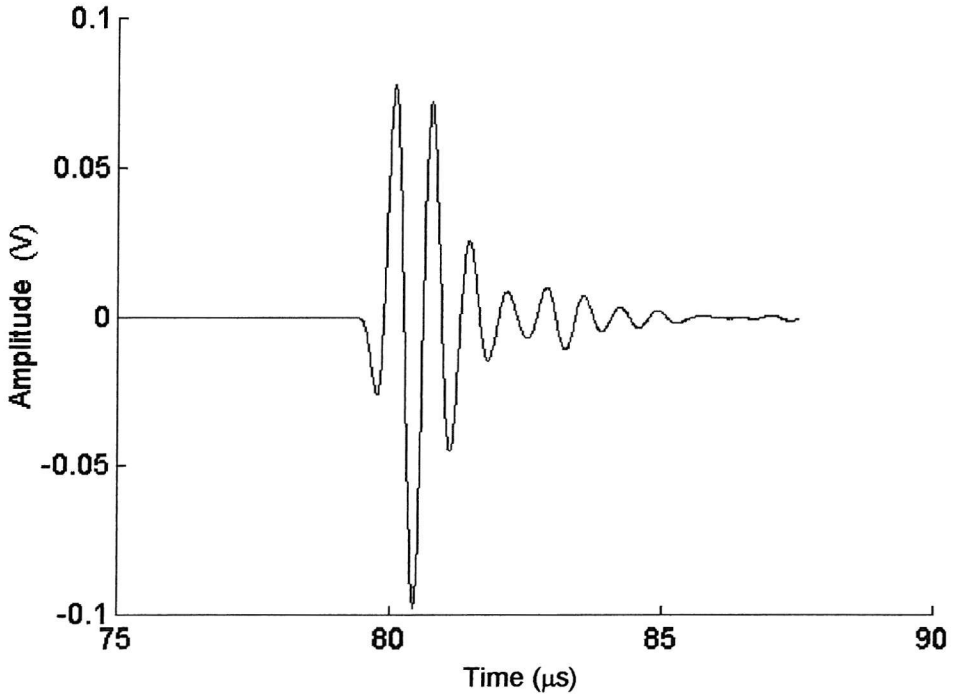

Figure 3.11 - Waveform through acrylic test object

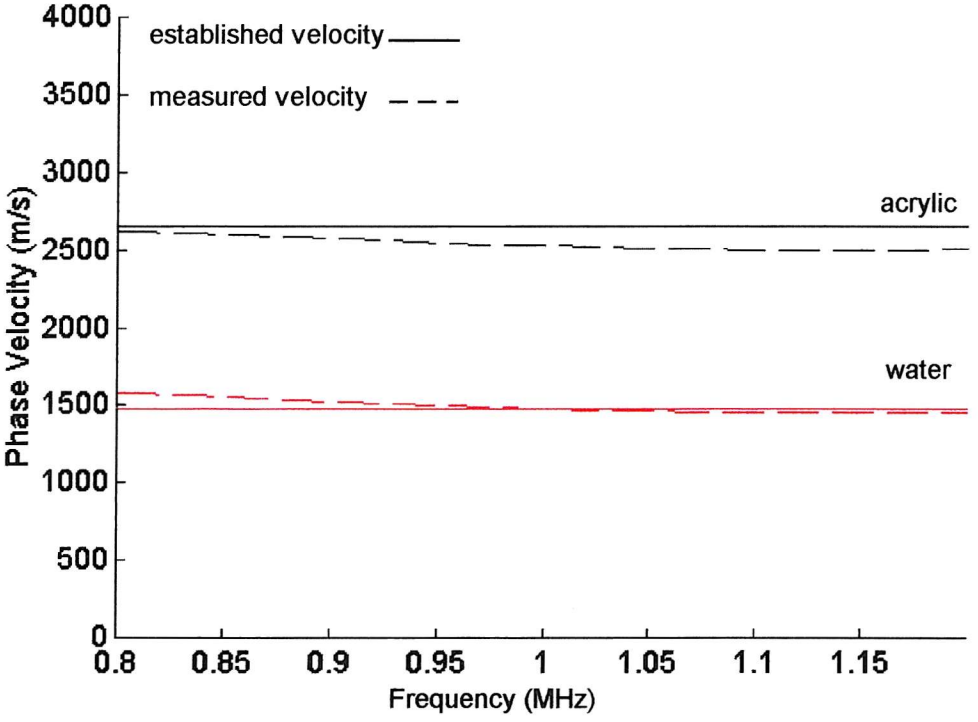

Figure 3.12- Established and measured phase velocities of pulses through water (fig 3.8 (a)) and acrylic (fig 3.11).

3.7 Cancellous Bone Specimens

3.7.1 Sample Preparation

Tests were performed on samples of bovine cancellous bone, which is generally acknowledged as having similar properties to human bone (Gibson and Ashby 1988). Bovine tibia and femora were obtained fresh from a local butcher. The proximal and distal epiphyses were known to contain regions of cancellous bone with a well-oriented trabecular structure.

The bone was first cleaned of cartilage with boiling water and the cortical shell was removed. Samples, of square cross-section 3.0 cm × 3.0 cm, were cut under running water, with thickness varying from 0.6 cm to 1.5 cm (± 0.05 cm). A specimen of cortical bone was also cut from the shaft of the tibia. Samples were stored in the preservative formalin, and were kept moist at all times.

Specimens were classified by the orientation of the internal trabecular structure. Those samples with trabeculae running parallel to the thickness will be referred to as *Parallel samples*, whilst those with structure normal to this will be distinguished as *Perpendicular samples*. Specimens were also prepared with internal structure at 30° and 45° to the cross-section, referred to as *Oblique samples*. Typical samples are shown in the photographs of figure 3.14, and figure 3.13 summarises the naming convention.

Chemical fixation affects ultrasonic propagation in tissue, since it causes linkages between adjacent molecules, producing higher absorption effects (Bamber 1997). Tissue stored in formalin may exhibit an increase in attenuation, particularly at high frequencies (10 % at 1 MHz, 50 % at 7 MHz), and the directional dependence of attenuation in tissue such as muscle, may be affected (Bamber 1997).

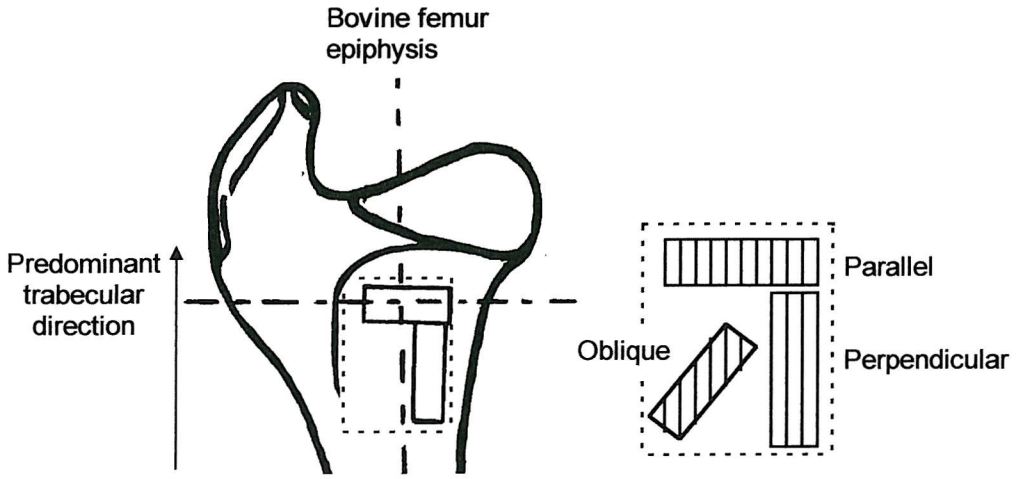

Figure 3.13 - Location and nomenclature of cancellous bone in the bovine femur.

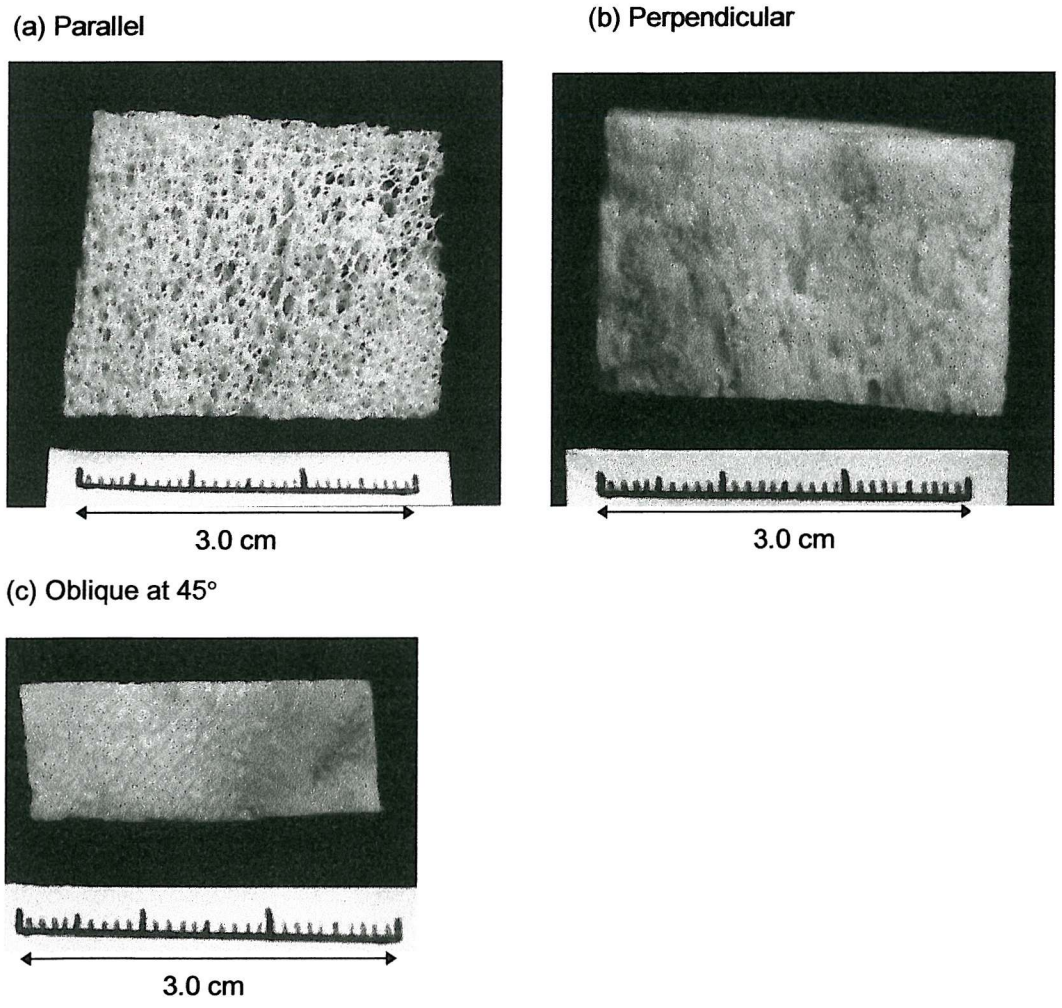

Figure 3.14 - Photographs of cancellous samples. (a) Parallel; (b) Perpendicular and (c) Oblique at 45°.

After ultrasonic testing, the marrow was extracted from the pores by immersing samples in trichloroethylene for a number of hours. Samples were cleaned and flushed through with water using a small submersed conduit, then re-saturated with water using the pipe. When this occurs tiny bubbles may become trapped within the pores, which may significantly affect ultrasonic propagation through the medium. Therefore, the water-filled samples were left for an hour before testing to ensure the surface bubbles were dissolved. However, some may have persisted internally, the potential effect of which is considered below.

The presence of air bubbles in a liquid will modify its bulk modulus, its sound speed and its attenuating characteristics (Leighton 1994). Such effects depend on the size and population of the bubbles, as well as the driving frequency. First, the bulk modulus is defined as the ratio of the change in pressure to the relative change in volume. Therefore, for a given change in pressure, the change in volume is greater when a bubble is present, than in the bubble-free liquid. It is possible to calculate the new bulk modulus (Leighton 1994), with knowledge of the bubble size and population, and use the modified value in propagation models such as Biot's theory (Alvarez-Arenas *et al.* 1994).

In general, a bubble resonates at a natural frequency inversely proportional to its radius (Leighton 1994). The ratio of resonant to the incident frequency determines whether the presence of a population of bubbles affects the sound speed. If their resonant frequency is above the incident frequency, the sound speed is reduced. However, large bubbles, with natural frequencies less than the driving frequency, tend to have little effect on sound speed (Leighton 1994). In both cases, they increase attenuation, with the major effect being scattering, owing to a high acoustic impedance mismatch of air-filled cavities with the surrounding water.

For a typical sample of bovine cancellous bone, it is reasonable to suppose that bubbles of radius less than 1 μm will be flushed from the pores or will dissolve rapidly. Hence, only those bubbles similar in size to the pore may remain in the sample. Whilst such bubbles could have a significant effect on attenuation, these relatively large ones are likely to have the least effect on bulk modulus and sound speed.

3.7.2 Validation of Intersample Comparison

To compare the acoustic results from different cancellous samples, it is necessary to define non-acoustic criteria for stating which samples classify as being the same. One factor, which is easy to establish and is required for modelling propagation, is the porosity.

The porosity of cancellous samples was found using Archimedes' technique. The volume of a cylinder of water is measured with and without a porous sample submersed (υ_{sample} and υ_{water}, respectively). The difference in volume in each case is equivalent to the volume of the solid phase, υ_{solid} in the sample. From a knowledge of the total volume of sample, υ_{cuboid}, if the sample is a cuboid, the porosity, β, may be found as,

$$\beta = 1 - \frac{\upsilon_{solid}}{\upsilon_{cuboid}} = 1 - \frac{\upsilon_{sample} - \upsilon_{water}}{\upsilon_{cuboid}}, \qquad (3.16)$$

where $\upsilon_{cuboid} = length \times breadth \times height$ of specimen (m^3). The method measures interconnected porosity, rather than due to isolated pores. It is, however, the former that is required by Biot's theory. Indeed, isolated pores will not occur in any biological tissue, owing to metabolic requirements.

Equation (3.16) was used to evaluate the porosity of samples of cancellous bone in order to classify samples as the same. First, it is necessary to establish how great a difference can be distinguished by a non-acoustic measurement of porosity. The measurement of porosity using equation (3.16) will have associated systematic and random errors. Taking the largest of these (systematic error bar or two standard deviations), two samples may be said to have the same porosity if their mean or average values are not separated by the error. Their subsequent acoustic measurement can be compared.

The systematic error represents the resolution (or systematic precision) to which the evaluation of equation (3.16) can be carried out, given uncertainties in input parameters. The sample dimensions were measured with a micrometer to $\pm$ 0.5×10^{-3} m (a fractional error in the order of $\pm$ 0.1 %), and the water volume can

be measured to a systematic precision of ± 5 ml (fractional error of ± 1 %). Fractional analysis[10] was carried out on equation (3.16) to find the uncertainty in the porosity as a result of these errors in the input variables.

The measurement of porosity may be biased by the presence of bubbles, which contribute to the perceived solid volume fraction (1 - β). Although this is likely to contribute to the error, it is difficult to quantify without knowing the bubble size of their population. The total systematic error in the evaluation of porosity from equation (3.16) was found to be no more than ± 1.3 %. The total random error in ten measurements was ± 3.6 %, which, being the greater of the two, was taken as the measurement error.

Figure 3.15 gives a summary of seven Parallel samples (*1* to *7*), three Perpendicular samples (*8* to *10*) and two Oblique samples (*11* and *12*) and their porosities, showing the maximum uncertainty in their values[11]. To determine whether two samples are the same, it is necessary to consider whether their mean values are separated by more than the measurement error.

Groups of samples may be assembled from this data. The porosities of Parallel samples *1* to *4* do not differ by more than the error (that is, 3.6 %), as with samples *5* to *7*. Therefore, samples 1 to 4 may be grouped as having a mean porosity of β = 74.5 %, with a standard deviation of 2.3 %, whilst Samples 5 to 7 can also be grouped, with mean porosity β = 80.5 %, standard deviation 2.8 %. Perpendicular samples *8 to 10* meet the criterion, such that they may all be considered as having the same porosity (mean 81.4 %, standard deviation 2.1 %). Oblique samples *11* and *12* give a mean porosity of 80.1 %, standard deviation 0.9 %. Therefore, the porosities of Parallel samples *4* to *7*, Perpendicular and Oblique samples, are equivalent to within the measurement error, enabling measurements from these samples to be compared.

[10] The random error in *F(x,y,z.)* resulting from errors in *x,y,z.* is given by (Trim 1983),

$$\pm\delta F = \pm\sqrt{\left(\frac{\partial F}{\partial x}\right)^2(\delta x)^2 + \left(\frac{\partial F}{\partial y}\right)^2(\delta y)^2 + \left(\frac{\partial F}{\partial z}\right)^2(\delta z)^2 \ldots .}$$

[11] Additional samples were tested, but their porosities were not recorded.

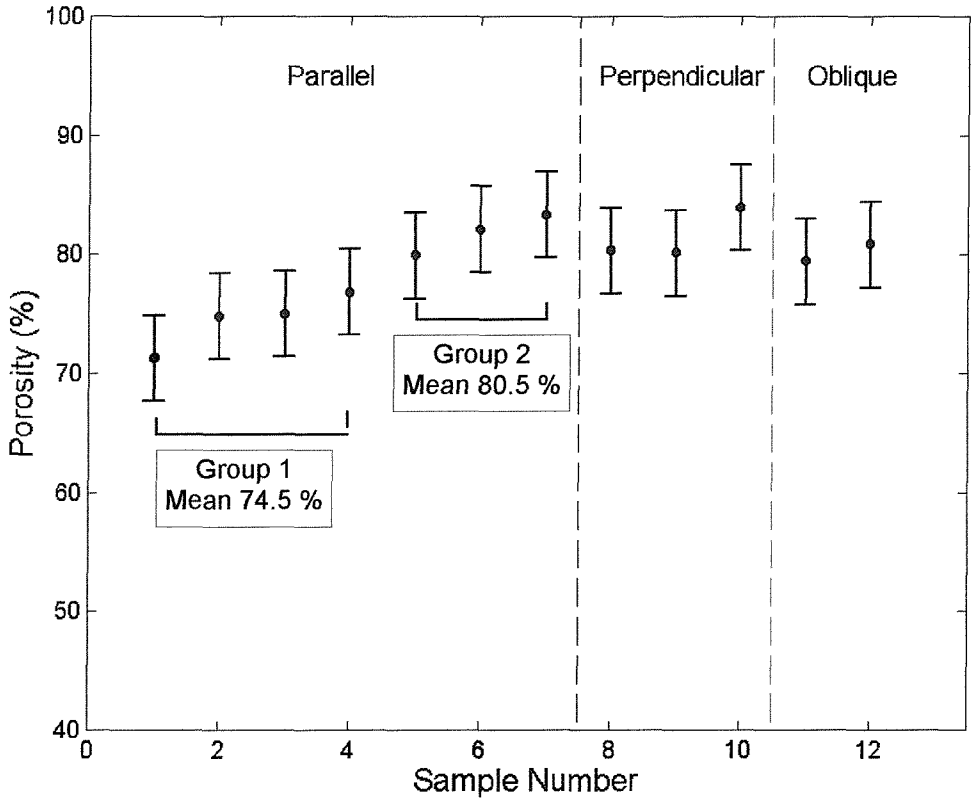

Figure 3.15 - Summary of porosities of cancellous samples used in experiments.

3.8 Summary

This chapter has outlined the principles of ultrasonic measurement and the measurement of ultrasonic wave properties. Deviation from ideal acoustic behaviour, caused by non-linear propagation, diffraction and additional empirical factors, have been discussed in some detail.

The following chapter outlines *in vitro* studies carried out to study the propagation of the two compressional waves predicted by Biot's theory in cancellous bone, using the techniques and specimens described here. Owing to problems in the precise evaluation and interpretation of measured attenuation, agreement with theory is found by comparing phase velocities.

Chapter Four

In Vitro Studies of Biot Waves in Cancellous Bone

4.1 Introduction

This chapter describes *in vitro* experimental studies compressional wave propagation in cancellous bone. The objectives were as follows:

- *To observe Fast and Slow compressional waves in cancellous bone.*

  The open and permeable structure of cancellous bone is favourable for the propagation of the slow wave in the High frequency region. At the outset of this work, the observation of two waves in cancellous bone had not been reported. Observation of these modes would give weight to models, such as Biot's theory, which predict two waves.
- *To study the effect of the interstitial fluid.*

  The viscosity of the interstitial fluid determines the frequency above which the slow wave will propagate in a porous medium. Therefore, it is predicted that varying the fluid will affect the wave properties of Biot waves.
- *To study the effect of the cancellous structure.*

  Applying Biot's theory requires the assumption that cancellous bone is mechanically and structurally isotropic. Real bone is highly anisotropic however, so the Biot assumption is not strictly valid. Propagation of fast and slow waves in anisotropic cancellous bone is likely to be dependent on direction.

4.2 Validation of Biot's Theory

4.2.1 The Observation of Fast and Slow Waves

The first study aimed to examine the existence of fast and slow waves in bovine cancellous bone *in vitro*. The apparatus and methods described in Chapter 3 were used to test Parallel samples, of mean porosity 74.5 %, and thickness varying from 0.6 to 1.5 cm, with the marrow intact.

Figures 4.1 (a - d:ii) show those waveforms received through samples tested at normal incidence. (Figure 4.1 (d:ii) shows the waveform of (d:i) on an expanded scale.) The origin of the time axis is at the trigger, taken on the rising edge of the input to the amplifier. Compared to the water-only waveform of figure 3.7 (a), those shown in figures 4.1 (a - d) exhibit a considerable amplitude modulation that suggests the presence two distinct wavepackets. Taking the arrival time as the first deviation from zero (or, if not clear, the rising edge), the separation of the arrival of these wavepackets is seen to vary from roughly 2.5 μs, for a sample 0.6 cm thick (figure 4.1 (a)), to 6.0 μs, for a sample 1.5 cm thick (figure 4.1 (d:i - ii)). Therefore, the delay between wavepackets is dependent on sample thickness. Such behaviour may arise for waves propagating through the specimen.

It was believed that the first wavepacket corresponded to the fast wave and the second to the slow wave. This assumption will be validated in the following sections. Strictly, the waves received are compressional waves in water, resulting from the mode conversion of the Biot wave at the rear face of the specimen.

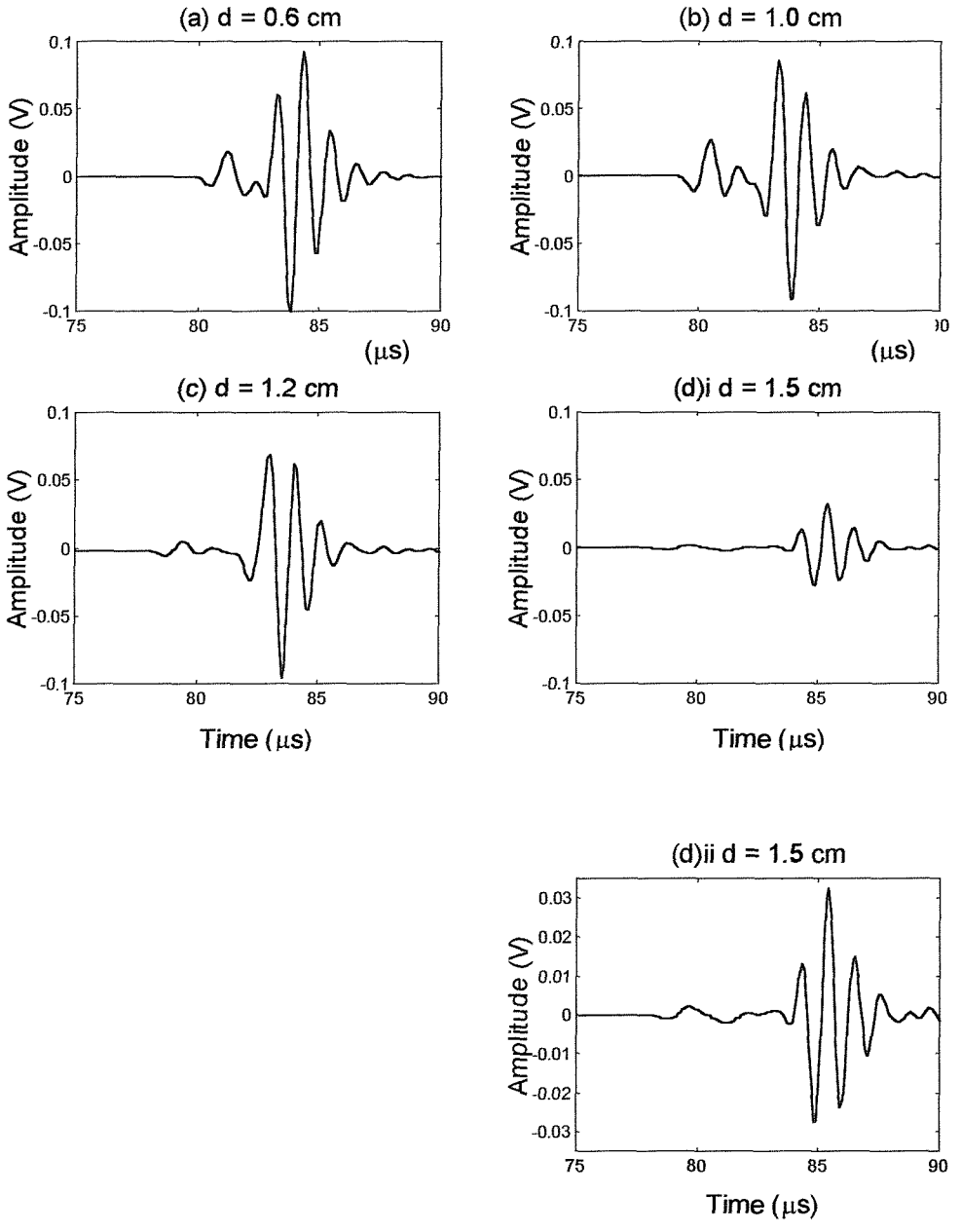

Figure 4.1 - Waveforms through Parallel samples of thickness (a) 0.6 cm; (b) 1.0 cm; (c) 1.2 cm; and (d): (i) 1.5 cm; (ii) on an expanded scale.

4.2.2 Linearity Tests

A scaling method was used to establish whether propagation, and the measurement system, were sufficiently linear. As discussed in section 3.2.4, this is investigated to determine the validity with which results may be compared with, and analysed by, those of linear propagation models. The presence of non-linear propagation may also bias estimates of empirical attenuation. Tests were performed using Parallel samples, with the marrow intact.

Figure 4.2 (a - c) shows the output waveforms from a sample 0.6 cm thick, for a sinusoidal pulse of 1 MHz. The input voltage to the power amplifier was first set at 1 V, and the positive peak amplitudes of fast and slow waves were noted from figure 4.2 (a), as 18 mV for the fast wave and 92 mV for the slow wave. Next, the input voltage was reduced to 900 mV, and the output amplitudes were noted from figure 4.2 (b), as 17 mV and 87 mV for fast and slow waves, respectively. Therefore, between the two cases, the input was scaled by a factor of 0.9, and the output amplitudes were seen to scale by a factor of 0.95 for both waves, that is, a linear change to 5 %. Next, the input was reduced to 500 mV, and fast and slow wave amplitudes were noted, from figure 4.2 (c), as 8 mV and 4 mV, respectively. In this case, the input was scaled by 0.5, and outputs by 0.44 for each wave: linear to 6 %.

The presence of discrepancies between controlled and measured scaling factors does not constitute a convincing argument for linear propagation. However, an additional test may be performed. Section 3.2.4 mentioned that a waveform will appear non-symmetrical if the effects of diffraction and non-linear propagation interact. Since it may be confidently assumed that diffraction is present, non-symmetrical fast and slow waveforms may therefore indicate non-linear propagation, or, at least, to its influence in these tests. Study of the magnitudes of positive and negative peaks of waves in figure 4.2 (a - c) shows the waveforms are relatively symmetrical. Therefore, it may be assumed that propagation and measurement system are sufficiently linear for an amplifier input of 1 MHz, 800 mV and amplified 50 dB, used throughout these studies. Consequently, this enables the application of methods of sections 3.3 and 3.4 for the calculation of phase velocity and attenuation.

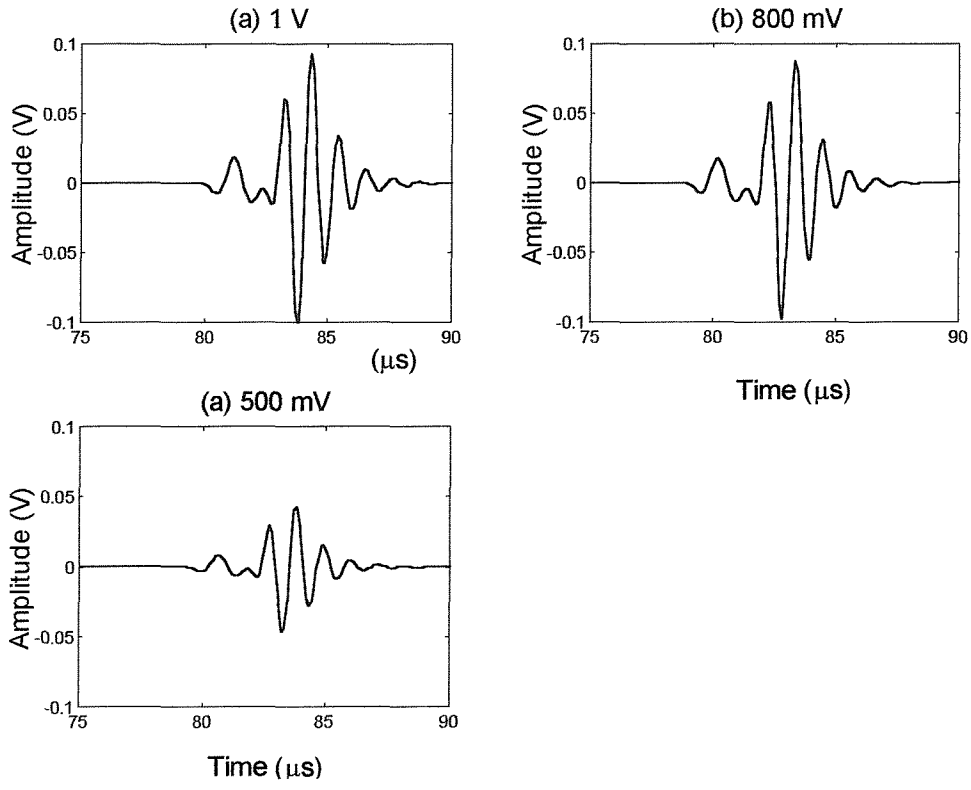

Figure 4.2 - Waveforms through Parallel sample, 0.6 cm thick, for power amplifier input amplitudes of (a) 1V; (b) 900 mV; (c) 500 mV.

4.2.3 Propagation Mode Identification

The first arrival observed in the recorded time histories was assumed to have travelled the shortest path to the receiver, that is directly through the specimen. To determine the origin of the second arrival, attention was turned to the influence of reflections from external and internal surfaces.

The shortest reverberant path to the receiver, from which a second arrival may arise, is that of a direct signal reflected from the receiver casing, to the rear face of the sample, and returning to the receiver sensing surface. Such a route covers a path length equal to twice the sample-receiver separation. In these studies, the sample and receiver were separated by a distance of 2.0 ± 0.05 cm, hence, a reverberant wave in water between the two surfaces would arrive 27 ± 3 μs after the direct arrival. Such a delay is clearly longer than that between first and second arrivals in figure 4.1 (a - d), previously noted as between 2.5 - 6.0 μs. Therefore, the second arrival could not originate as echo from an external surface.

Attention was turned to internal reverberation as a source of this wave. As section 3.6.4 described, the first reflection of reverberation within the sample may overlap with the direct wave in samples of certain thickness. In section 4.2.4 it will be shown that the speed of the first arrival at 1 MHz is approximately 3000 m/s (for porosity 74.5 %). For a reference pulse duration of 4.5 μs (figure 3.7 (a)), an overlap may occur for samples thinner than 0.68 cm (from (4.5 μs × 3000 m/s) / 2). Therefore, it would be expected that the waveform in figure 4.1 (a), from a sample of thickness 0.6 cm, would contain overlapping reverberant waves. However, whilst two distinct waveforms remain visible in this case, overlap is unlikely to occur in the waveforms of thicker samples of figure 4.1 (a - d).

In samples of thickness 1.0, 1.2 and 1.5 cm, the first reflection of the reverberation of a direct mode of 3000 m/s, would be expected to arrive at 6.6 μs, 8.0 μs, and 10.0 μs, respectively, from the rising edge of the first arrival. However, these predicted delays do not agree sufficiently with measured delays through samples of such thickness as 3.5 μs, 4.0 μs, and 6.0 μs, respectively. Therefore, there is not sufficient evidence to assuming that the second arrival is a reverberant wave using arrival times. Indeed, given that cancellous bone is a

dispersive medium, it is unlikely that this issue can be resolved with the use of times of flight[1]. The origin of the second arrival was investigated further.

As outlined in section 3.6.2, analysis of the spectrum of the waveform may be used to establish whether echoes of the direct signal were present in the time series of figure 4.1 (a - d). The power spectral density of the whole signal figure 4.1 (a), shown in figure 4.3, was found using a Fast Fourier Transform.

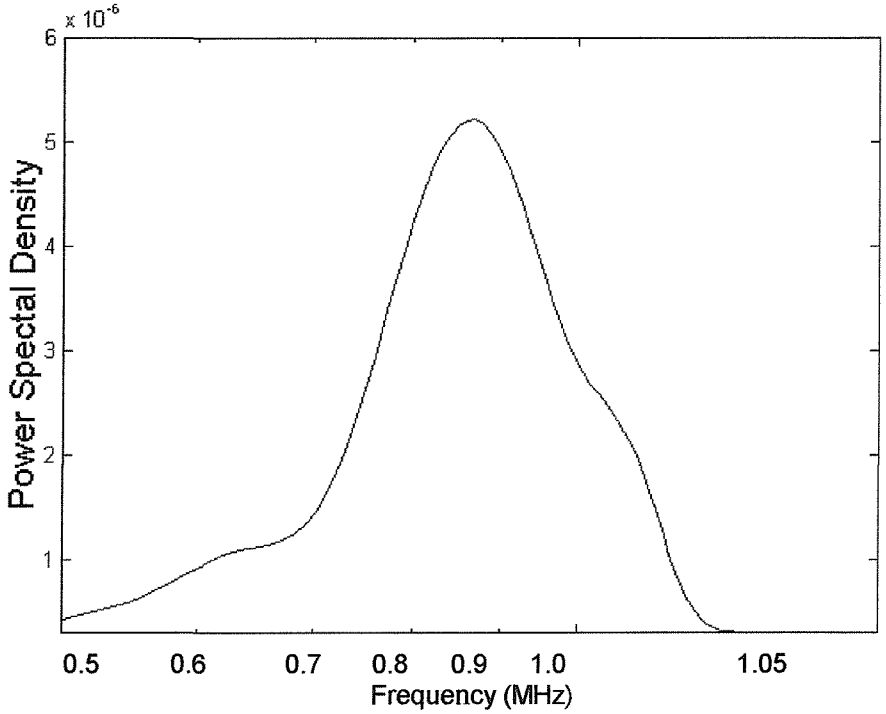

Figure 4.3 - Power Spectral density of a typical time series from a Parallel sample.

The spectrum of figure 4.3 does not clearly demonstrate the ripple effect associated with that of a reverberant signal. When processed this way, all the signals in figure 4.1 (b - d) exhibited similar spectra. Therefore, it could be concluded with reasonable certainty, that the second arrival was not an echo from reverberation of the direct signal within the sample. Since no shear wave would be generated at normal incidence, the arrivals were assumed to be bulk compressional modes.

[1] It is questionable whether a direct signal of relatively low amplitude would give rise to an echo of higher amplitude, after attenuation of the initial wave over subsequent traverses of the sample.

In porous media acoustics, the first arrival is generally associated with the fast wave and the second with the slow wave of Biot's theory. However, this should not be automatically assumed. Biot's theory predicts phase velocity (the speed of the wavefronts), whilst arrival time is determined by group velocity (the speed of energy propagation). In a dispersive medium, phase and group velocity are generally not equal. Thus, strictly, speeds derived from arrival times cannot reliably be used in identify Biot waves. Under specific conditions in a porous medium, the velocity of the slow wave may theoretically be faster than that of the fast wave (Lawrence and Don 1996). To classify the modes with respect to fast and slow waves of Biot's theory, experimental phase velocities were compared with theory. This is described in the following section.

4.2.4 Phase Velocity and Measured Signal Loss

Signal loss and phase velocity were evaluated using the methods described in sections 3.3 and 3.4. A waveform of the type in figure 3.8 (a) was used as the reference signal for the calculations throughout.

Systematic errors in the measured phase velocity and signal loss arise from the measurement of sample thickness (± 0.05 cm), water temperature (± 0.05°C) and the effect of temporal windowing. These produce a total systematic error, through the equations of the PSM of section 3.4, of no greater than 2 % for velocity. It was necessary to establish that the data was representative of the general response of Biot waves in cancellous bone. This was established by investigating its spread and precision. Reproducibility was examined in a number of ways, being evaluated as a coefficient of variance (%CV = {std / mean} × 100). Table 4.1 summarises the coefficients of variance for apparatus, positioning and intersample precision.

Table 4.1 - Reproducibility coefficients of variance for measurement system.

Parameter (at 1MHz)	Apparatus Reproducibility (%CV)	Positioning Reproducibility (%CV)	Intersample Reproducibility (%CV)
Phase Velocity	1.7 %	3.4 %	(β = 74.5) 6.0 % (β = 80.5) 4.5 %
Signal Loss	2.6 %	4.5 %	(β = 74.5) 8.4 % (β = 80.5) 9.7 %

First, the *apparatus precision* was established, that is, the reproducibility in the measurement of one sample a number of times without repositioning. This term reflects the uncertainty in measurements owing to variations in factors such as electronic and quantisation noise, and water temperature. It was found by testing the same sample ten times without repositioning, and finding the spread in the values of phase velocity and signal loss at the centre frequency of 1 MHz.

Next, the reproducibility in a number of measurements of one sample with repositioning was assessed, that is, *positioning precision.* This coefficient of variance will naturally include the above *apparatus* errors, plus additional uncertainties from removing and replacing a sample in position to test. It may be expected to be larger than the apparatus coefficient of variance. The same sample was tested ten times, being removed from the sample holder and repositioned each time. The coefficient of variance was found for velocities and signal loss.

Finally, the *intersample precision* was determined; that is, the reproducibility between measurement of a number of samples. This uncertainty will include both apparatus and positioning errors, but will include an addition from variations between samples, and may therefore be larger than the previous two coefficients. Samples within the same porosity groups were tested once each, and the coefficient of variance found for the data, for each porosity.

The values in Table 4.1 are consistent with those quoted for commercial QUS systems, which range from 1.34 % to 9.44 % (Greenspan *et al.* 1997). It can be seen in Table 4.1 that the measurement of velocity has a higher reproducibility than that of signal loss, a trend compatible for BUA and SOS from commercial

systems (Greenspan *et al.* 1997). This is not surprising in the cases of positioning and intersample precision, given that the empirical factors that contribute to signal loss may vary between cases.

Figure 4.4 shows the phase velocities of fast and slow waves as functions of frequency for the two porosity groups ((a) 74.5 ± 2.3 % and (b) 80.5 ± 2.8 %). The solid curves shown are the mean values of all the data in those groups (that is, with and without repositioning, for all samples), with error bars in solid lines, associated with the largest uncertainty. This convention is used throughout this thesis for plotting data. This corresponds to the intersample error of 6.0% for the curves of figure 4.4 (a), and 4.5 % for (b).

Experimental wave properties were compared with predictions by Biot's theory. The dashed lines in figure 4.4 show the maximum and minimum predictions of phase velocity from Biot's theory, found by the method of section 2.4. The parameters used for a model of marrow-saturated bovine bone for a measured water temperature of 20.0 ± 0.5°C are shown in Table 4.1. Pore size was estimated using a scanning microscope to be 815 ± 32 μm, the range arising from experimental uncertainties. The value of the Young's modulus of the solid is taken in the propagation direction in order that isotropy may be approximated. The values in Table 4.1 were used to predict phase velocity and absorption, for each porosity group studied.

Figures 4.5 (a) and (b) give signal loss in dB/m for the two porosity groups. The solid lines correspond to the experimentally derived signal loss, normalised for sample thickness, for the mean values of all the data in those groups (that is, with and without repositioning, for all samples). Solid error bars are associated with the largest uncertainty on the data, being the intersample uncertainty at 8.4 % for porosity, β = 74.5 %, and 9.7 % for β = 80.5 %. Dashed lines in figure 4.4 show the maximum and minimum predictions of absorption from Biot's theory, found by the method of section 2.3.3. The parameters used for a model of marrow-saturated bovine are shown in Table 4.2.

Table 4.2 - Input parameters to the Biot model for marrow-saturated bovine cancellous bone at 20°C.

Parameter	Value
Variable	
Density of cortical bone, ρ_s	1800 - 2000 kg/m^3
Density of marrow, ρ_f	992 - 1047 kg/m^3
Young's modulus of cortical bone, E_s	18.1 - 22.6 GPa
Porosity, β	(a) 0.745 ± 0.023 (b) 0.805 ± 0.028
Pore radius, r	815 ± 32 μm
Constants	
Bulk modulus of marrow, K_f	2.2 GPa
Viscosity of marrow at 20°C, η	0.15 Pa.s
Index of power law, n	1.23
Poisson's ratio of cortical bone, ν_s	0.32

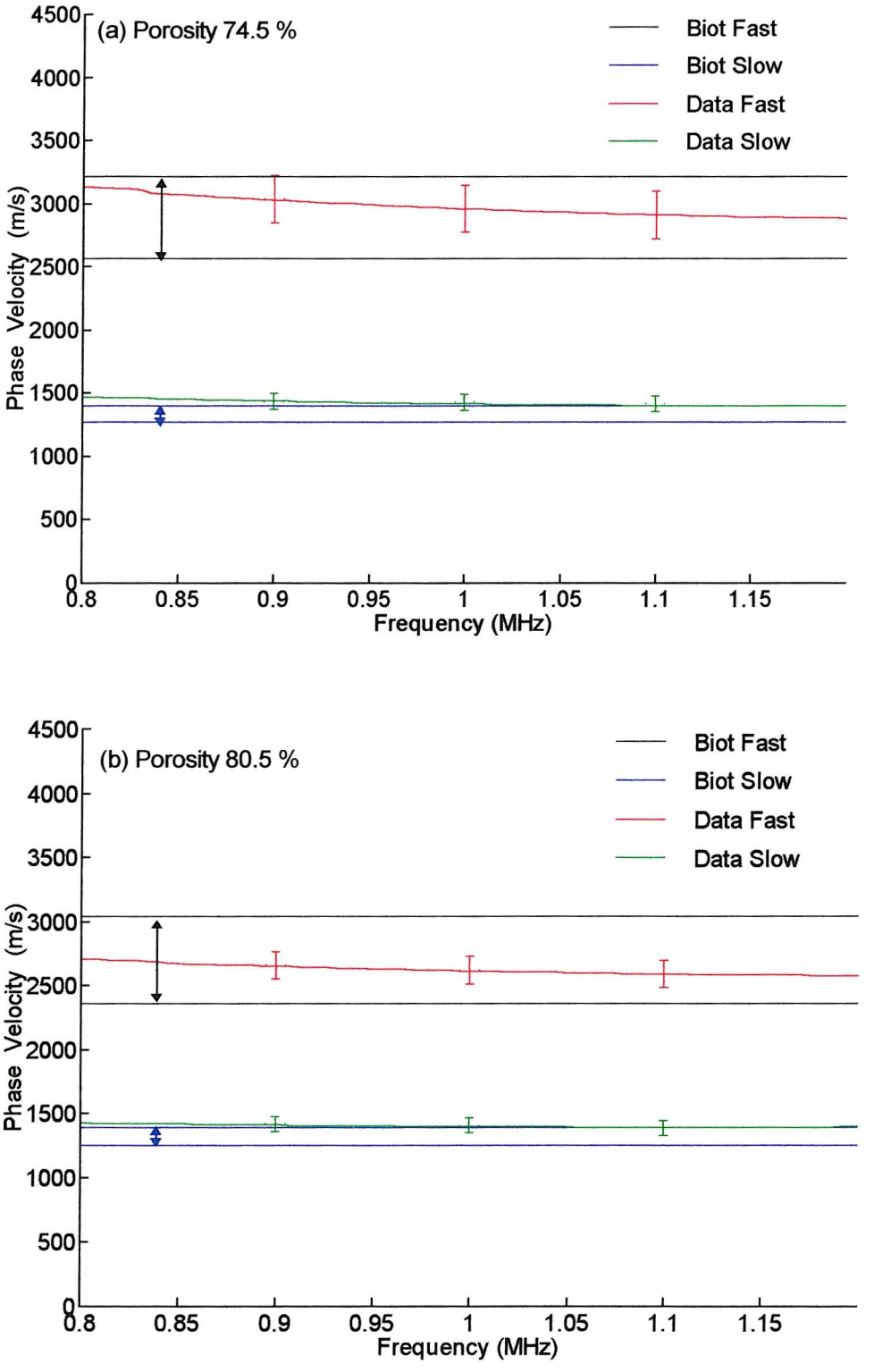

Figure 4.4 - Measured and predicted phase velocities of fast and slow waves for mean porosity: (a) 74.5 % and (b) 80.5 %. Error bars on data show intersample precision.

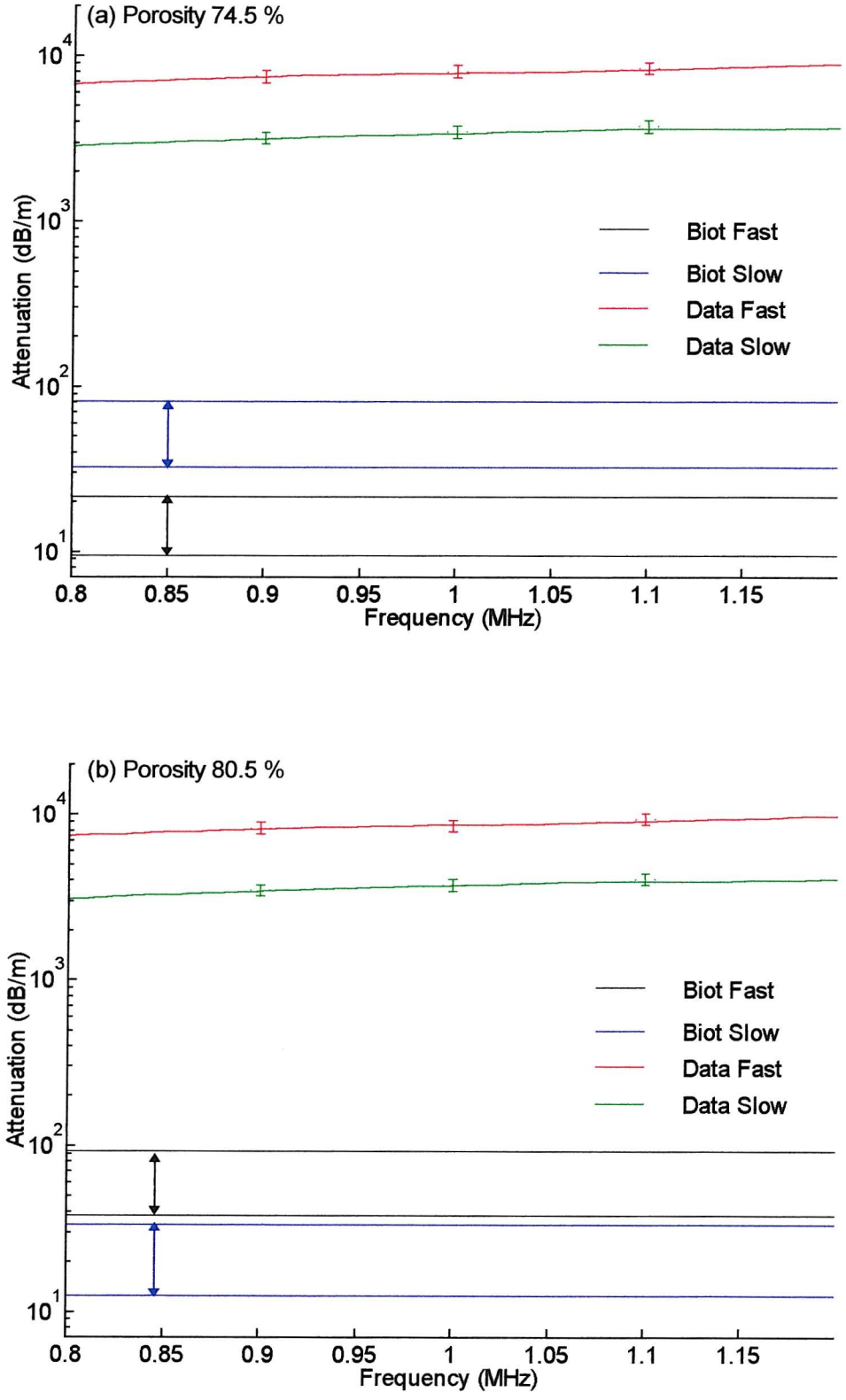

Figure 4.5 - Measured signal loss and predicted absorption of fast and slow waves for mean porosity: (a) 74.5 % and (b) 80.5 %. Error bars on data show intersample precision.

4.2.5 Discussion of Experimental Results

(a) Identification of Fast and Slow Waves

To identify the origin of the two modes in figures 4.1 and 4.2, experimentally determined wave properties were compared with those predicted by Biot's theory for a model of cancellous bone. As has been stated already, since it is problematic to compare empirical attenuation with predicted absorption, waves were classified through the analysis of phase velocities.

Figures 4.4 (a) and (b) clearly show that the phase velocity of the first arrival is consistent with that predicted for the fast wave. Similarly, the phase velocity of the second arrival is consistent with that predicted for the slow wave. For both porosity groups, experimentally determined fast wave velocities and its uncertainty, lie within the limits predicted by theory, although its frequency-dependence is not predicted. Experimental slow wave velocities lie at the upper limits of the predictions. It could therefore be concluded that the fast and slow waves of Biot's theory had been observed. The first arrival will be referred to as the *fast wave*; and the second as the *slow wave* for the remainder of this work. Finally, these findings contradict the hypothesis in section 3.3.7 that the slow wave may be attenuated to the extent that it could not be observed.

(b) The Effect of Porosity

Comparison of figures 4.4 (a) and (b) shows that the porosity affects the values of both measured and predicted phase velocities. The measured fast wave velocity at 1 MHz decreases from 3080 m/s in figure 4.4 (a) to 2640 m/s in (b), a reduction of 14 %, subject to the stated error. Such trends are in keeping with porosity-dependent decreases in velocity in bone measured by previous authors (Tavakoli and Evans 1992, Hosokawa and Otani 1997).

Two points are made here regarding these results, but not pursued further. First, Biot's theory predicts shifts in the extreme bounds of the theory with

porosity. A porosity, $\beta = 80.5$ % renders bounds which are 5 - 8 % less than $\beta = 74.5$ %. The analysis of whether this is a statistically significant decrease would require careful study, outside the scope of this work. Second, it was observed that there was a relatively large change in measured velocity with porosity. This may imply that the acoustic method is more sensitive than the Archimedes' technique (of section 3.7.2) for determining changes in porosity.

(c) Wave Amplitudes

The wave amplitudes in cancellous bone display an unexpected behaviour compared with the general response of porous media in this frequency range. Ordinarily, in cases where Biot fast and slow waves have been observed in synthetic and natural porous media, the slow wave amplitude has been much lower than that of the fast wave (Plona and Johnson 1980). Indeed, Biot's theory predicts that the slow wave will be subject to greater absorption than the fast wave. However, in this study, it appears that the reverse is true, since the slow wave is the dominant arrival. In samples thicker than, say, 2 cm, the fast wave may be attenuated to the extent that it may be undetectable by the system's dynamic range. This is the most probable reason for the lack of observation of two waves in previous studies of cancellous bone.

Plona and Johnson (1980) showed that the slow wave will have a relative amplitude larger than the fast wave for a specific case. This occurs when the frequency is close to where scattering sets in, as defined in section 3.3.6. At this frequency both viscous and scattering losses are minimal (the former is negligible in the High frequency region; and the latter is relatively small owing to $q_{slow}a$ being close to unity) and so do not significantly attenuate the slow wave. Section 3.3.7 gave the scattering frequency for marrow saturated cancellous bone at 20°C as around 0.7 MHz. This is sufficiently close to the incident frequency of 1 MHz to render a large amplitude slow wave here.

The anomalous trend in the relative wave amplitudes possibly arises from the boundary conditions, which may assist the setting up of a high amplitude slow wave. In Parallel sample, the pores are open to the reference medium (water).

There is a good impedance match between water and marrow, since they have similar densities (1000 and 970 kg/m^3, respectively) and sound speeds (both near 1500 m/s). Wave motion in the water will effectively couple into the marrow at the specimen interface, and hence the slow wave, which may be thought of as propagating in the pore fluid.

(d) Absorption and Measured Signal Loss

There is a clear quantitative disagreement in measured signal loss and predicted absorption in figures 4.5 (a) and (b). This is as anticipated from the discussions in section 3.3.3, where it was remarked that the measured signal loss of a single mode could be confidently compared with theoretical predictions only if energy is partitioned between the modes is included. Such division is not incorporated here, and these results are consistent with the findings of previous workers who neglected partition (Williams *et al.* 1996, Hosokawa & Otani 1997).

The measured signal loss of the slow wave is less than that of the fast wave, and such a discrepancy from the predicted trend is significant. It is most likely that this inconsistency arises from the neglect of partition and the losses of empirical factors. As the above discussion on wave amplitudes has shown, the conditions of the porous boundary are crucial to the transmission of waves into the medium. Complex models for the transmission coefficients of porous surfaces, based on Biot's theory, do exist (Johnson *et al.* 1994), but their application is outside the scope of this study.

Some practical factors of empirical signal loss, such as diffraction, phase cancellation and bulk scattering, may only contribute to a quantitative constant or frequency-dependent signal loss of both fast and slow waves. Such factors will not contribute to the error in trend. However, factors that affect the properties of each wave to a unique degree, such as specular scattering of the slow wave in section 3.3.2, may reduce the difference, or reverse the trend in signal loss. Again, whilst establishing these contributions may be essential to appreciating the cause of the trend, their evaluation is beyond the scope of this work. Owing to these confounding problems, which could not be easily rectified without further work, subsequent studies focus on measurement of velocity.

4.2.6 Bone-Mimicking Materials

Owing to the poor performance of commercial ultrasonic bone assessment systems, bone-mimicking materials have been developed for monitoring performance (Clarke *et al.* 1994, Hodgskinson *et al.* 1996, Asaba *et al.* 1999). Clarke *et al.* (1994) constructed a phantom from epoxy resin, to mimic calcified tissue, and a gelatine/water mixture, to mimic marrow. These materials were chosen to have acoustic properties similar to those of the components of real bone. The gelatine formed pore-shaped granules, with the porosity controlled by the proportion of each component. Other phantoms have been constructed from perspex (Hodgskinson *et al.* 1996) and plaster (Ashaba *et al.* 1999).

Velocities and attenuation[2] of ultrasonic waves in Clarke's phantom varied with porosity. Phase velocities at frequencies around 500 kHz were found to cover a higher range than those measured in real bone (1844 to 3118 m/s compared with 1465 to 2084 m/s for real bone). Attenuation and BUA of the phantom agreed reasonably well with those of real bone. Of particular interest, is that attenuation and BUA in both media display a parabolic relationship with porosity. A peak was observed around 50 % porosity for the Clarke phantom, and at 65 - 75 % for real bone (Hodgskinson *et al.* 1996). It was proposed that this response is caused by scattering from the isolated inclusions (fluid filled pores) at low porosities and from the continuous phase (solid matrix) at high porosities.

Whilst propagation in bone phantoms raises interesting questions, the fundamental propagation mechanisms involved are not compatible with those in real cancellous bone. The propagation of fast and slow waves relies on the assumption that the fluid and solid are interconnecting, which does occur in real bone. In a homogeneous medium containing isolated particles, such as Clarke's phantom, only one direct compressional wave will propagate and Biot's theory cannot be applied. This disparity makes it unfeasible to directly compare the results of this study with those for a phantom where only one wave is present.

In conclusion, bone phantoms display macroscopic properties, such as scattering, which mimic real bone, and are therefore useful in monitoring the performance of systems measuring attenuation. However, since propagation

[2] with respect to a single reference pulse

mechanisms differ in the two media, comparisons of the measurement of phase velocity should be carefully considered.

4.2.7 Frequency and Implications for Historical *In Vitro* Studies

Section 1.5.2 mentioned the bar equation has been used to approximate propagation in cancellous bone within various frequency bands (Strelitzki *et al.* 1997, Rho 1998). Ashman *et al.* (1984) hypothesised that bar propagation may transform into bulk propagation as the frequency increases, but this mechanism has not been thoroughly investigated. The effect may be equivalent to *geometric dispersion* for homogeneous media. This occurs where the propagation is dependent on the product of the specimen length and the wavenumber (Thurston 1978, Ashman *et al.* 1984). However, in porous media, there may be another cause for the change in propagation mechanisms with frequency, namely, that approaching the viscous frequency, $\omega_{viscous}$, of equation (2.23), above which fast and slow waves will propagate.

Strelitzki *et al.* (1997) investigated propagation in os calces at 37 kHz, where the continuum assumptions of the bar equation are valid. Measured velocities were lower than those at frequencies in the BUA range. For a pore radius in human bone of 250 ± 50 μm (Mellish *et al.* 1989), and a viscosity in water of 0.001 Pa.s at 20°C (Kinsler *et al.* 1982), the viscous frequency, $\omega_{viscous}$, of equation (2.23), is 50 ± 14 kHz. The frequency is close to the 37 kHz used in bar propagation investigations by Strelitzki *et al.* (1997).

Therefore, rather than being a geometrical dispersion effect, it may be postulated that limit of the viscous frequency, $\omega_{viscous}$, is the point of a suggested transition from apparent bar propagation at low ultrasonic frequencies to that bulk propagation observed at frequencies near 1 MHz.

4.3 Study into the Effect of Pore Fluid

4.3.1 Introduction and Objectives

Alves *et al.* (1996) showed that, at frequencies from 0.5 - 1 MHz, velocity in bovine cancellous bone increased by 2 % and attenuation (with respect to an isotropic medium) decreased by 6 % when marrow was replaced by water. This suggests that the role of the pore fluid is important at ultrasonic frequencies.

Most previous studies considering Biot's theory in cancellous bone have replaced marrow with water before testing (Hosokawa and Otani 1997, Williams 1992, Lauriks *et al.* 1994). This displacement will influence wave propagation, since the viscosity of water differs from that of marrow substantially (see section 2.3.2). This is also demonstrated for cancellous bone in the viscous skin depth graph of figure 2.4. A reduction in viscosity for the same frequency, will lessen viscous coupling, and enhance relative motion between fluid and solid. Therefore, propagation in samples saturated with marrow may be expected to differ from those with water.

4.3.2 Method

The effect of replacing marrow with water in the pores of cancellous samples was investigated. The same methods and experimental apparatus of the previous study were used. Parallel samples of both porosity groups with marrow intact were tested, and the data was processed to evaluate wave properties. The marrow was then removed as detailed in section 3.7.1. Samples were re-saturated with water, and left before testing to ensure the surface bubbles were dissolved. The wave properties of the water-saturated samples were then established.

4.3.3 Results and Discussion

Figure 4.6 (a - f) shows the waveforms through cancellous samples with marrow and with water in the pores. The results from three Parallel samples are shown (Samples 5 - 7 from figure 3.15 with porosity 80.5 ± 2.8 %).

The presence of different saturating fluids in the pores clearly has an effect on the propagation of Biot waves in cancellous bone. Fast and slow modes are recognised in figure 4.6 (a), (c) & (e) with marrow intact, as investigated in the previous study. The inclusion of water in the pores has the effect of altering the appearance of the emerging waveform, as can be seen by comparing figures 4.6 (b), (d) & (f) with (a), (c) & (e), respectively. Corresponding modes are reduced in amplitude, and the second arrival is delayed. Eliminating echoes and reverberation, as in section 4.2.3, the modes observed through the water-saturated samples were found to have propagated through the specimen as compressional waves.

The phase velocities and signal loss of the waveforms were evaluated for the two modes, shown in figures 4.7 (a - b) and figure 4.8 (a - b), respectively. It should be noted that the figures 4.7 (a) and 4.8 (a), velocity and signal loss for marrow-saturated samples of mean porosity 80.5 %, are the same as figures 4.4 (b) and 4.5 (b), respectively; reproduced to aid comparison. The intersample reproducibility coefficient of variance for the phase velocity of modes in the water-saturated case was 8.5 %, higher than the coefficients from the previous study in Table 4.2. Predictions from Biot's theory are also shown in figure 4.7, using the values in Table 4.1, evaluated for two values of viscosity at 20°C: 0.15 Pa.s for marrow, and 0.001 Pa.s for water, and a porosity of 80.5 ± 2.8 %

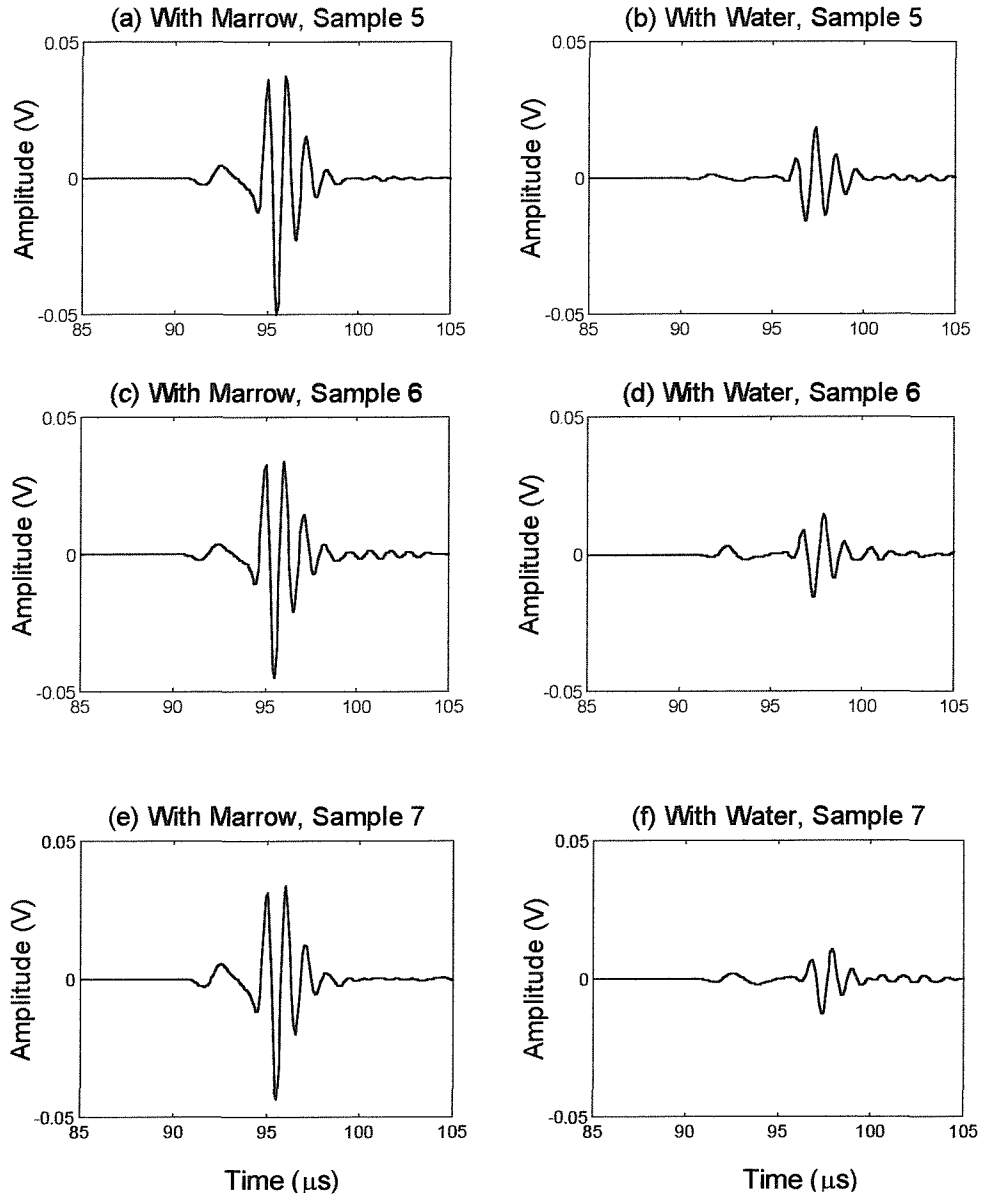

Figure 4.6 - Waveforms through Parallel Sample 5 with (a) marrow and (b) water in pores; Sample 6 with (c) marrow and (d) water in pores; and Sample 7 with (e) marrow and (f) water in pores.

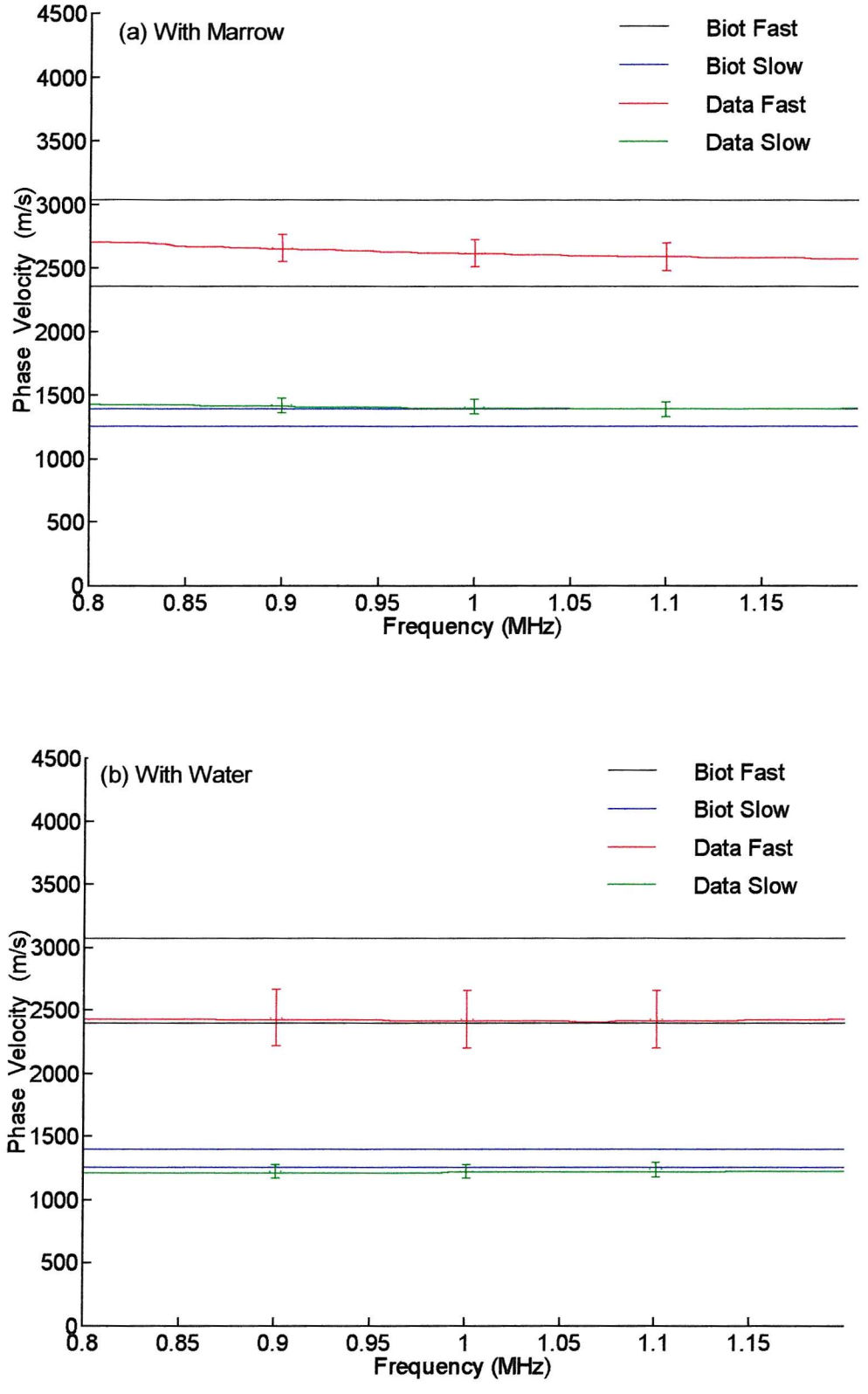

Figure 4.7 - Measured and predicted phase velocities of fast and slow waves with (a) marrow and (b) water in the pores.

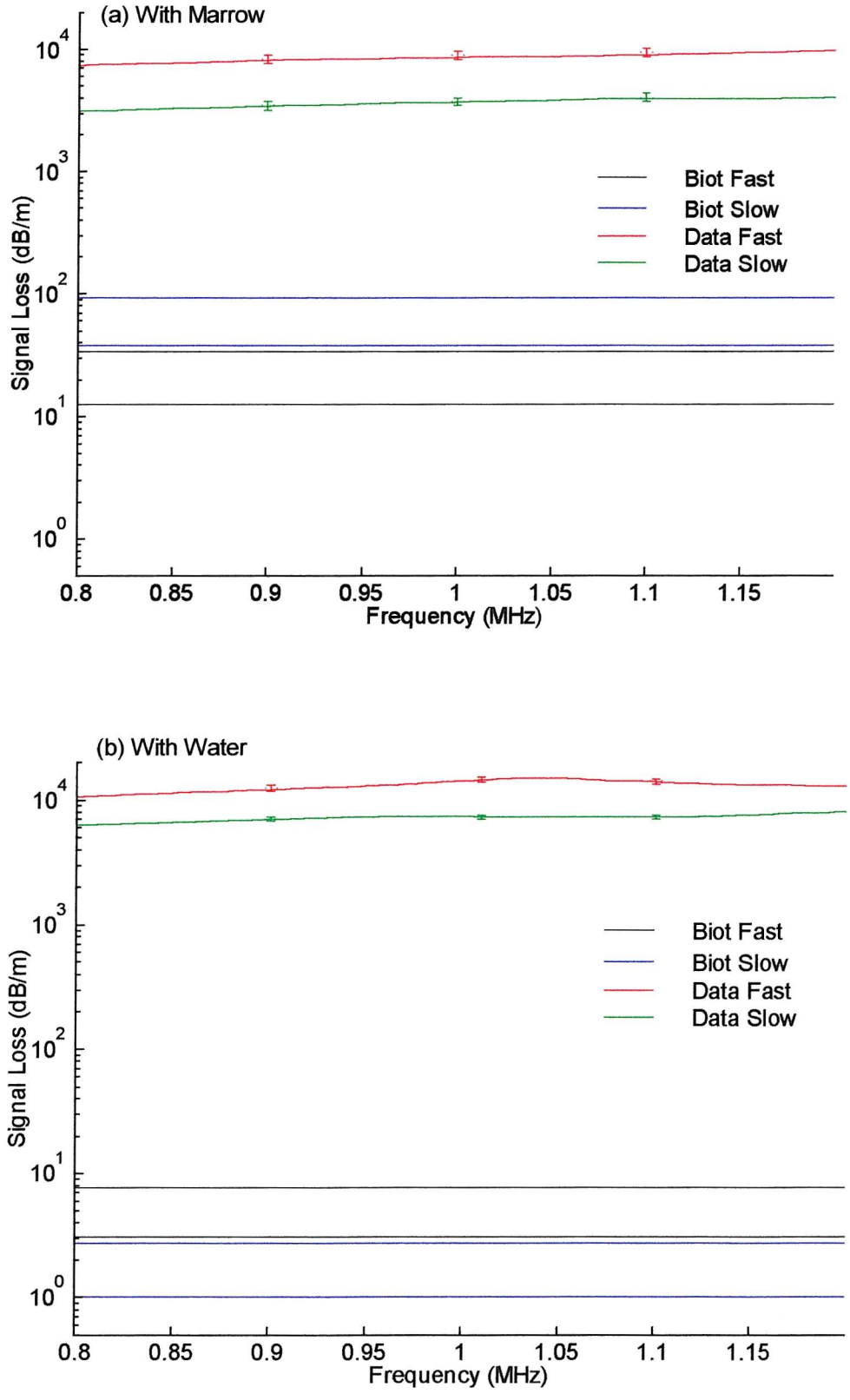

Figure 4.8 - Measured signal loss and predicted absorption of fast and slow waves with (a) marrow and (b) water in the pores.

Comparison of figures 4.7 (a) and (b) demonstrates that the phase velocities of fast and slow waves, in samples of the same porosity, are influenced by the interstitial fluid. The fast wave velocity increases with the substitution of marrow with water, by roughly 8 %, whilst the slow wave velocity decreases by roughly 13 %. In contrast, when the prediction is modified by replacing the viscosity value of marrow at 20°C with that for water at this temperature, the maximum and minimum velocity bounds do not appear to alter significantly. Whilst viscosity is a defining parameter regarding the extent of propagation regimes, such a variation in viscosity produces a difference in predicted phase velocity at frequencies near 1 MHz of less than 1 %.

Figures 4.8 (a) and (b) illustrate that the measured signal loss of both fast and slow modes is marginally higher for water-saturation than marrow-saturation. Unlike predicted velocity, predicted absorption at 1 MHz is seen to change by an order of magnitude between the two cases. The increase in signal loss of the fast wave, with the insertion of water, may arise from viscous coupling not being as effective with a fluid of lower viscosity. In addition, the lower viscosity encourages the relative motion associated with the slow wave, which causes greater frictional losses[3].

An alternative explanation for the increase in signal loss with the second pore fluid, is that the presence of unwanted bubbles within the sample may cause increased scattering losses. As discussed in section 3.7.1, air-filled cavities have a high acoustic impedance mismatch with the surrounding water and will scatter effectively. Such effects will be significant in the slow wave, which has a smaller wavelength. Random scattering from varying bubble distributions in each sample may account for the poor intersample reproducibility, compared with measurements in marrow-saturated bone, in Table 4.2. However, although the presence of bubbles may validate the modification of some of the input parameters to the Biot model (specifically the fluid bulk modulus), the bubbles likely to be contained in the trabecular matrix will be relatively large and therefore unlikely to alter its properties significantly.

[3] It is a paradox of Biot's theory that a fluid of lower viscosity, which should instinctively *reduce* viscous lagging losses, enables increased relative motion and actually *increases* viscous losses through such motion.

4.4 Study into the Effect of Trabecular Orientation

4.4.1 Objectives and Method

Previous applications of Biot's theory in cancellous bone investigated propagation in the trabecular direction only (Williams 1992; Hosokawa and Otani 1997). Isotropy was assumed for propagation in that direction for which the solid Young's modulus was defined. Other researchers investigated the effect of trabecular orientation on ultrasound. Many authors have reported significant differences in measured velocities for three orthogonal axes. Nicholson *et al.* (1994) noted such a result for vertebral bone, whilst Strelitzki *et al.* (1997) studied a similar effect for propagation at 37 kHz in os calces. Njeh *et al.* (1996) noted considerable variance with direction for relationships between velocity and Young's moduli. Variations in BUA with orientation have also been demonstrated (Hodgskinson *et al.* 1996).

The effect of trabecular structure on the propagation of fast and slow waves was studied here, using the method and apparatus described in section 3.5. Propagation through Parallel samples, of mean porosity 80.5 %, could be compared with that through Perpendicular samples, of mean porosity 81.4 %, since the difference between mean porosities was less than the error in their measurement (section 3.7.2). Samples were tested at normal incidence with marrow intact.

4.4.2 Results

Figure 4.9 (a) shows a pulse transmitted through a Parallel sample of thickness 1.2 cm, at normal incidence. This may be compared with figures 4.9 (b) and (c) through Perpendicular samples of varying thickness, and (d) for an Oblique sample, all having similar porosity. Trabecular orientation clearly influences the waveforms emerging from in cancellous bone. Only one pulse is seen in figure 4.9 (b - d), compared with two in (a). Eliminating reverberation, as in section 4.2.3, the mode observed through the Perpendicular samples was found to have propagated through the specimen as a compressional wave.

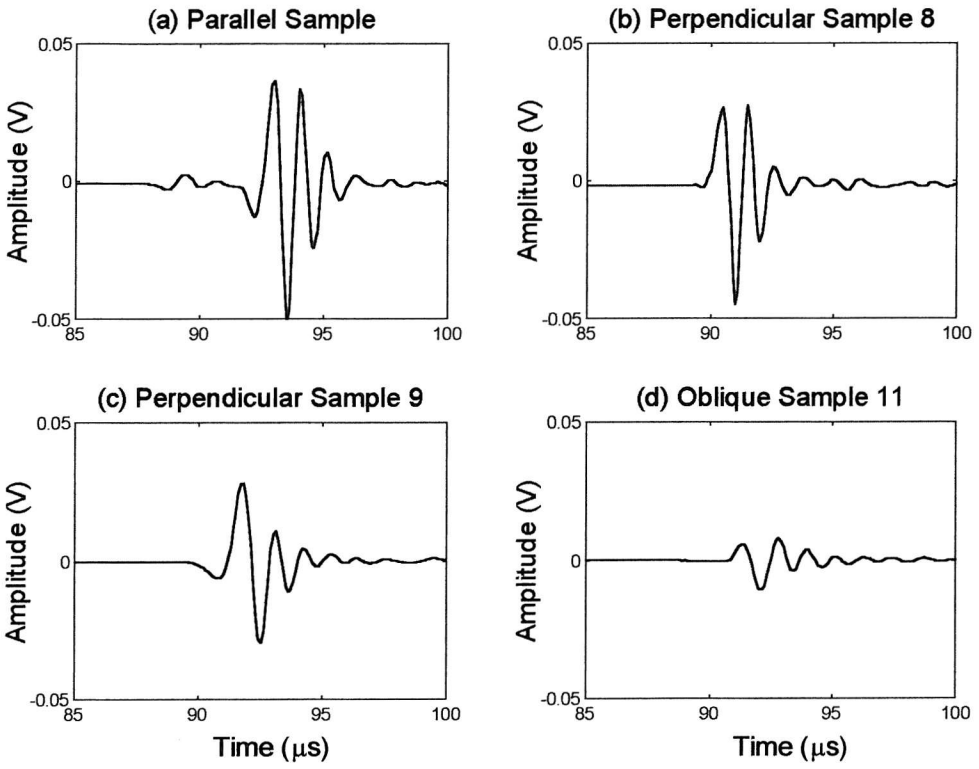

Figure 4.9 - Waveforms through (a) a Parallel sample; (b - c) Perpendicular samples and (d) an Oblique sample.

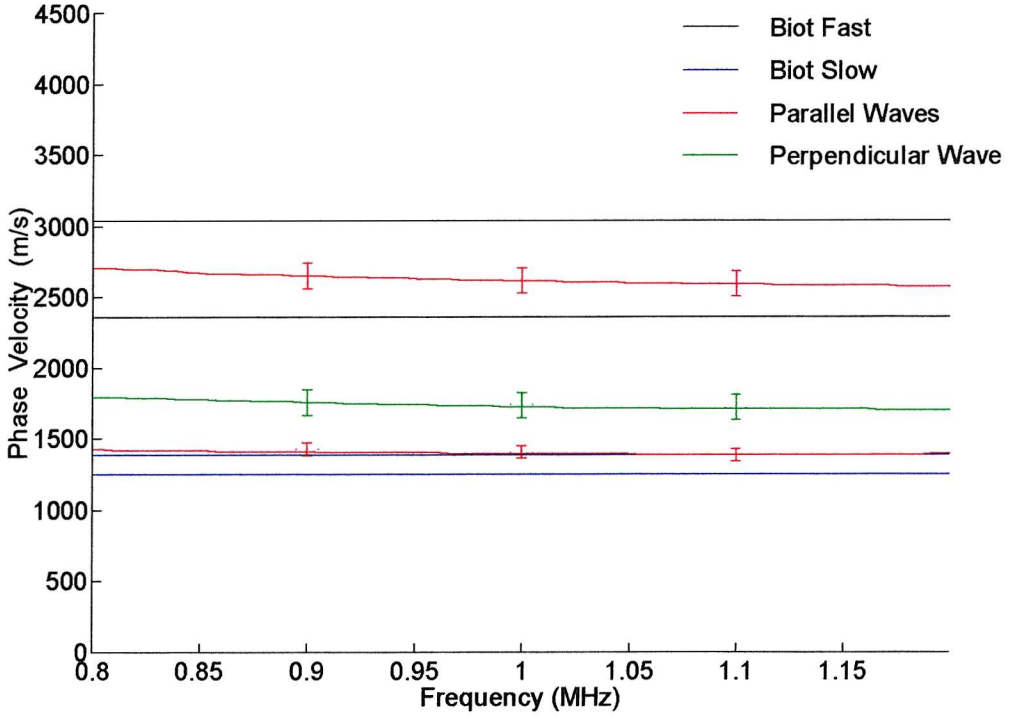

Figure 4.10 - Measured and predicted phase velocities of fast and slow waves from Parallel samples, and that of the mode from Perpendicular samples.

The lack of discrimination of two modes prevents the temporal windowing required to evaluate wave properties for separate fast and slow waves, if indeed both modes are present. Such deficiency may occur because the slow wave has been attenuated to such an extent that it cannot be distinguished by the dynamic range of the system. As a result, it was necessary to analyse the wave from Perpendicular samples as a single mode. The results from the Oblique samples are relevant to the later studies of Chapter 5 and not studied further here.

The experimental phase velocities were evaluated and compared with those derived from Biot's theory. Attenuation was not studied in this case. Figure 4.10 shows the phase velocities along with predictions for the wave received in the Parallel and Perpendicular samples. The intersample reproducibility in the measurement of phase velocity of the Perpendicular mode was found to be around 4 %, which compared well with measurements in Parallel samples in Table 4.2.

From figure 4.10, the phase velocity of the single mode does not agree with predictions of fast and slow wave velocity. Its value at 1 MHz is roughly 1700 m/s, and thus well outside the error bounds from data or theory for either fast or slow wave. Therefore, it was not certain whether the mode was a fast or slow wave. Further investigation was required to establish the origin of this wave, and some such studies are described in the following chapter.

4.5 Conclusions

This chapter has presented the results of an *in vitro* experimental study into some aspects of ultrasonic wave propagation in bovine cancellous bone. The aims of the study were to observe the Biot slow wave, and to examine correlation with Biot's theory. The influence of marrow and the orientation of the trabeculae were also investigated.

This study has shown that the slow wave does propagate in cancellous bone and maye be observed at ultrasonic frequencies. Furthermore, the medium appears to support slow waves very effectively under certain conditions. This is likely to be because the structure is highly permeable, and, at these frequencies, viscous coupling does not significantly impede fluid-solid relative motion.

As regards the modelling of wave properties, the phase velocities of fast and slow waves may be accurately predicted using a Biot model of propagation in cancellous bone for propagation in the trabecular direction. However, as expected, significant differences were apparent between measured signal loss and predicted absorption, highlighting the importance of other factors contributing to signal loss, such as energy partition. Therefore, only phase velocity was thought to be of practical use for comparison with theory. In addition, propagation at ultrasonic frequencies was predicted, and observed, to be dependent on the properties of the pore fluid, such as its viscosity and presence of bubbles.

Finally, the observation of fast and slow waves is dependent on the orientation of the trabecular structure. Both Biot modes are clearly observed in the trabecular direction, but are not apparent for propagation normal to this. To investigate the effect of trabecular orientation in more detail, further studies of the anisotropic response of bone were conducted. The following chapter outlines these studies, and introduces an alternative theory of propagation in cancellous bone.

Chapter Five

A Stratified Model for Ultrasound in Cancellous Bone

5.1 Introduction

The previous chapter showed that trabecular orientation influences the observation of two compressional modes in cancellous bone. Biot's theory, in the form discussed in Chapter 2, is unable to model this anisotropic behaviour. This chapter presents a new approach to considering cancellous bone, which is able to model the anisotropy. Predictions of waves properties in cancellous bone, with respect to angle of propagation are compared with data from an *in vitro* study.

5.2 Models of the Trabecular Structure

Cancellous bone consists of a permeable network of osseous strands or plates called trabeculae. Historically, devising a suitable simple geometrical or mathematical model to describe this complex architecture has been problematic, since many representations have been proposed, without consensus. Structural characterisation is not only required for propagation models, but also for analysing its mechanical behaviour, which, as mentioned in section 2.3.2, is desirable in the design of prosthetic bone. Some of the idealisations of the cancellous architecture are described below. It is assumed that, since the mechanical properties of cancellous bone can be analysed using these models, they may help ultrasonic examination.

Trabecular models may be categorised, first, as those having a permeable cellular matrix; and, second, those imagined to have developed as a pattern through mechanical loading. Of those models with a cellular structure, a common version is a network of cubes, each containing a spherical void (figure 5.1 (a)). The cubes may be staggered (Gibson and Ashby 1988), or vertically stacked, the latter having been used in finite element analysis of stress in cancellous bone (Beaupre and Hayes 1985). A variation is the *fabric ellipsoid*, found by constructing a characterising ellipsoid, whose principal axes as the average pore radii in three orthogonal axes, found from image processing (Turner and Cowin 1987). Bone texture has been analysed using fractals (Lesspessailles *et al.* 1996),

Gibson and Ashby (1988) presented models of trabecular architecture imagined to have developed from either uniaxial or biaxial loading. From loading in one direction, an array of prismatic tubes may develop, similar to a honeycomb structure (figure 5.1 (b)). From loading in two directions, an array of parallel plates separated by thin cross members, may develop (figure 5.1 (c)). These more regular geometric models are suitable for use in examining the influence of structure on ultrasonic propagation, since they may be most easily analysed mathematically. In particular, the layered structure of figure 5.1 (c) is attractive for further analysis because there exist well-established theories for acoustic propagation in layers. Once such theory, Schoenberg's approach, is investigated for ultrasonic propagation in bone in the following section.

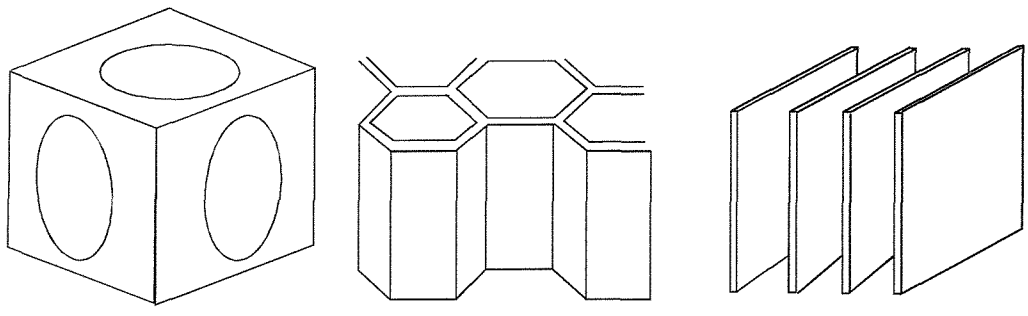

(a) (b) (c)

Figure 5.1 - Idealisations of cancellous bone: (a) a cell with a spherical void (Beaupre & Hayes 1985); (b) honeycomb tubes; (c) parallel plate structure (Gibson & Ashby 1988).

5.3 Schoenberg's Theory of Propagation in Stratified Media

5.3.1 Introduction

The analysis of wave propagation in periodically layered fluid-solid systems was first reported by Rytov (1956) and Brekhovskikh (1981), for propagation only in those directions parallel and perpendicular to stratification. Later, Schoenberg (1984) studied propagation in alternating fluid-solid layers in any direction, which was verified experimentally by Plona *et al.* (1987). Schoenberg's theory has since been used to describe propagation in various natural and man-made stratified media, such as geological structures and laminated composites.

5.3.2 Fundamental Equations

In 1984, Michael Schoenberg published his theoretical study into acoustic wave propagation in a medium composed of periodically alternating fluid-solid layers. The layering is parallel to the x_1 and x_2 directions, with spatial period H in the x_3 direction (figure 5.2), being infinitely extending in all directions (that is, there are no external interfaces). In one period of a medium with porosity β, the region of $0 < x_3 < (1 - \beta)H$ is occupied by an elastic solid (that is, it obeys Hooke's Law), with density ρ_s, compressional speed, V_s, and shear speed, V_{sh}. The region $(1-\beta)H < x_3 < H$ contains an ideal fluid, of density, ρ_f, and sound speed V_f.

Ideal fluid behaviour is a valid assumption for frequencies where the viscous skin depth, d_s, is much smaller than the fluid layer thickness. Schoenberg's model is therefore only applicable in the High frequency region of Biot's theory (section 2.4.2), where viscosity may be neglected. Furthermore, as with Biot's theory, the length scale of the discontinuities is also considered and Schoenberg's theory is only valid for the *long wavelength regime*; that is, the wavelength should be long compared to the period, H. This is shown schematically in figure 5.3.

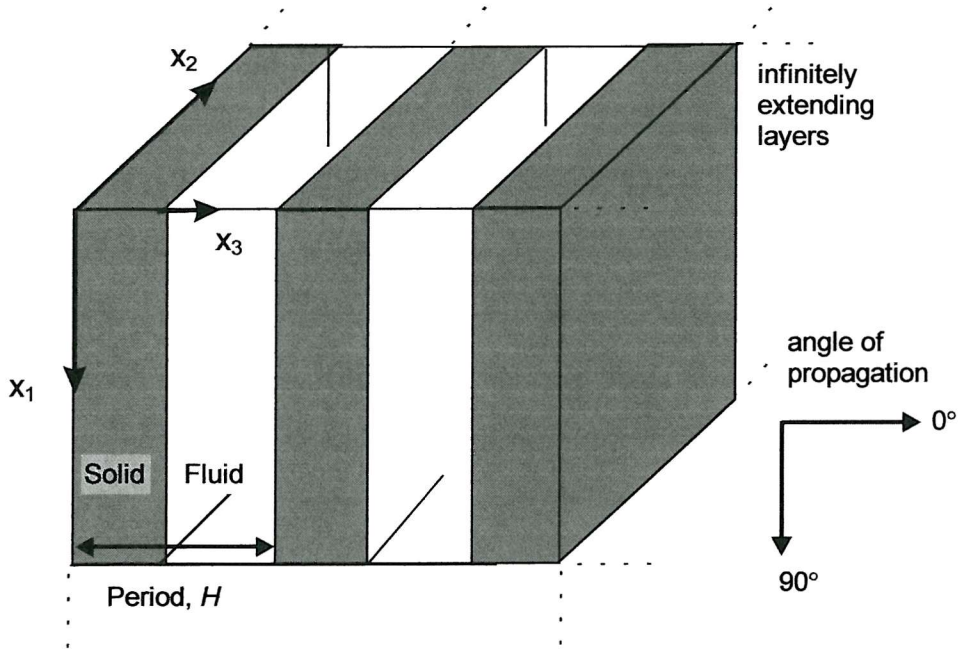

Figure 5.2 - Schematic diagram of a system of infinitely extending parallel fluid-solid layers, periodically alternating with period, H. The x_3-axis is 0° and the x_1-axis is 90° .

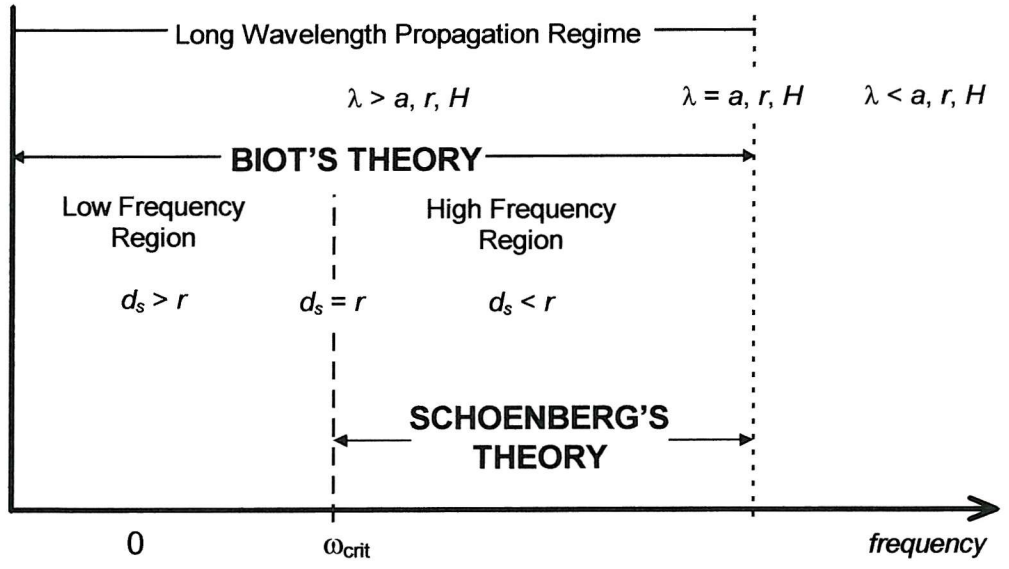

Figure 5.3 - The frequency regions within which Biot and Schoenberg theories are valid.

Schoenberg's derivation is briefly summarised here, but may be found in full in his 1984 paper. Schoenberg derived the dispersion relation for this medium by relating continuous acoustic field variables in one period to those in the next by propagator matrices. Acoustic wave propagation is expressed in terms of a slowness vector, $\boldsymbol{s} = (s_1, s_2, s_3)$. This vector has magnitude equal to the inverse of phase velocity, with phase angle equivalent to the angle of propagation through the layers relative to stratification[1].

For low-frequency harmonic waves, of $exp\ j(s_1x_1 - t)$, the dispersion relation becomes independent of frequency, ω. This leaves a relationship between the components of the slowness vector, $\underline{s}$, such that s_1, the parallel component, and s_3, the normal component, are found from the dispersion relation to be related as

$$(s_3^2 / \langle\rho\rangle) - \left\{ \frac{\beta(V_f^{-2} - s_1^2)}{\rho_f} + \frac{(1-\beta)(V_s^{-2} - s_1^2)}{\rho_s(1 - V_{pl}^2 s_1^2)} \right\} = 0 \qquad (5.1)$$

where $<\rho>$ is a thickness-weighted average density, equivalent to $\beta\rho_f + (1-\beta)\rho_s$, and V_{pl} represents the speed of extensional waves in an elastic plate,

$$V_{pl} = 2(1 - \frac{V_{sh}^2}{V_s^2})^{1/2} . V_{sh} \qquad (5.2)$$

as given by Plona *et al.* (1987). From equation (5.1), expressions for the magnitude and phase of the slowness vector, **s**, may be found as,

$$|\mathbf{s}| = \sqrt{[\ s_1^2 + s_3^2]}\ , \qquad (5.3)$$

$$\angle\mathbf{s} = \tan^{-1}(\ s_3 / s_1\ ). \qquad (5.4)$$

The magnitude of the phase velocity may then be found as a function of angle, $\angle\mathbf{s}$, in a stratified medium as the inverse of the magnitude of slowness, $1/|\mathbf{s}|$. The angle

[1] The slowness vector is an established convenient way of representing propagation in anisotropic media.

$\angle s$ corresponds to the angle of propagation through the layered structure, with reference to the direction of those layers.

Equations (5.1 - 5.4) predict two compressional waves that are equivalent to the waves of the first and second kind of Biot's theory. The waves have a direction dependence, with both waves propagating for all angles, except for propagation perpendicular to the plates, where there is only one mode.

Viscosity is omitted from the model. The phase velocity is purely real, and, since the absorption coefficient is usually found from the imaginary part of the complex phase velocity, Schoenberg does not therefore predict absorption. Furthermore, viscous coupling neglected in this model.

The direction dependence of the two propagation modes may be explained by considering inertial coupling in this system. For propagation perpendicular to the layers, inertial coupling is large and the motion of fluid and solid are fully locked together. Only the fast wave propagates, since relative motion associated with the slow wave is impeded. Inertial coupling decreases as the angle of propagation, with respect to x_3, increases, causing relative motion to occur, and allowing the slow wave to propagate. Parallel to the layers, the inertial coupling is zero. This means no coupling occurs between fluid and solid, and their respective motions are independent. Section 6.4.1 will later describe a tortuosity term (and hence inertial coupling), which may be found for a system of parallel plates that is a function of angle to the layering.

5.4 A Stratified Model for Cancellous Bone

Equations (5.1 - 4) were used to plot phase velocity against angle of refraction for a layered model of cancellous bone, using the values in the second column of Table 5.1. The resulting prediction is plotted in figure 5.4.

Figure 5.4 shows two distinct phase velocity contours (coloured lines) when plotted versus angle of propagation, with respect to x_3. These contours correspond to two compressional mode speeds, analogous to the Biot fast and slow compressional waves (Plona *et al.* 1987). The fast wave corresponds to the upper curve, and its velocity varies significantly with angle of propagation, being greatest parallel to the layering at 90°. In contrast, the slow wave phase velocity varies little with angle, such that it is approximately constant at angles close to the direction of layering.

The response is clearly symmetrical around 90°. This is owing to the theoretical layers being infinitely extending in two dimensions: there are no external boundaries to the medium. The response of the system may be thought of as arising from the coupling of an anisotropic fluid mode with an extensional plate mode (Plona *et al.* 1987). The velocity curves are bounded by two asymptotes, shown in figure 5.4, to which the curves display limiting behaviour. The first asymptote represents the solid plate mode of equation (5.2). The second limit corresponds to an anisotropic fluid mode, which may be found from the relation between components of the slowness vector, written in the form of an ellipse, as,

$$\frac{s_1^2}{V_s^{-2}} + \frac{s_3^2}{\left(\left[\frac{\langle\rho\rangle\beta}{\rho_f}\right]^{1/2} V_{pl}^{-1}\right)^2} = 1 \quad . \tag{5.5}$$

Plona *et al.* (1987) noted that the principle axes of this ellipse (and therefore the shape and value of the fluid asymptote) were govern by the ratio between porosity and density of the layers. Therefore, the asymptotes provide a physical explanation to the shape of the velocity curves predicted by Schoenberg.

Table 5.1 - Input parameters to a Schoenberg model of propagation in oriented cancellous bone for the figures 5.4 and 5.8.

Parameter	Value for Fig 5.4	Range for Fig 5.8
Density of solid bone, ρ_s	2000 kg/m^3	1800 - 2000 kg/m^3
Density of fluid, ρ_f	992 kg/m^3	992 - 1047 kg/m^2
Porosity, β	0.8	0.804 ± 0.028
Solid compressional speed, V_s	3150 m/s	3100 - 3200 m/s
Fluid compressional speed, V_f	1500 m/s	1500 m/s
Shear speed, V_{sh}	1650 m/s	1650 - 1800 m/s

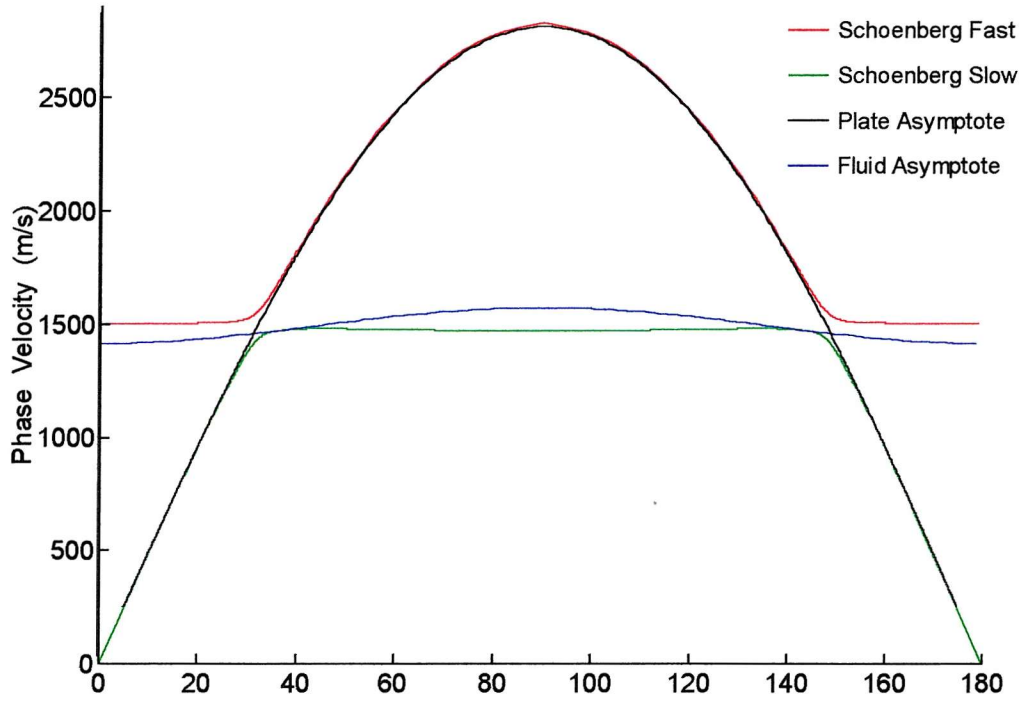

Figure 5.4 - Predicted phase velocities of fast and slow waves versus propagation angle for layered bone system, for 90° parallel to layers. Plate asymptote from eqn (5.2) and fluid asymptote from eqn (5.5) are shown.

5.5 *In Vitro* Study into the Effect of Trabecular Orientation

5.5.1 Objective and Method

Figure 5.1 (c) illustrated that the cancellous geometry may be considered as an array of bone-marrow layers. Therefore, Schoenberg's theory may be appropriate in understanding the anisotropic response of cancellous bone to ultrasound. Since Schoenberg's theory omits fluid viscosity, it may be applied to propagation at frequencies around 1 MHz, where viscous effects may be neglected.

Investigations were undertaken to establish whether Schoenberg's theory was compatible with measurements of direction dependent velocity, to a certain level of precision. The immersion and acquisition systems described in section 3.5 were used, with the addition of a revolving specimen holder. This mechanism allowed samples to be rotated manually about a pivot coaxially aligned with the fixed transducers. The angle of incidence was indicated on an angular scale, and the output was acquired after each 5° ± 0.5° increment in the sample position. Three Parallel, three Perpendicular and two Oblique samples were used, with marrow left intact.

When samples were rotated, care was taken to ensure that the beam width was covered, to avoid signal leakage around the sample. An erroneous output may arise if a direct wave is measured. Calibration tests, described in Appendix A.I, showed that the width of the beam was 1.2 cm at 1 MHz. From figure 5.5, a sample, of width 3 ± 0.05 cm, could be tested at angles of incidence from 0° - 60° before signal leakage occurred. Therefore, Parallel and Perpendicular samples of such width could be tested to cover the an angular range 0° - 90°.

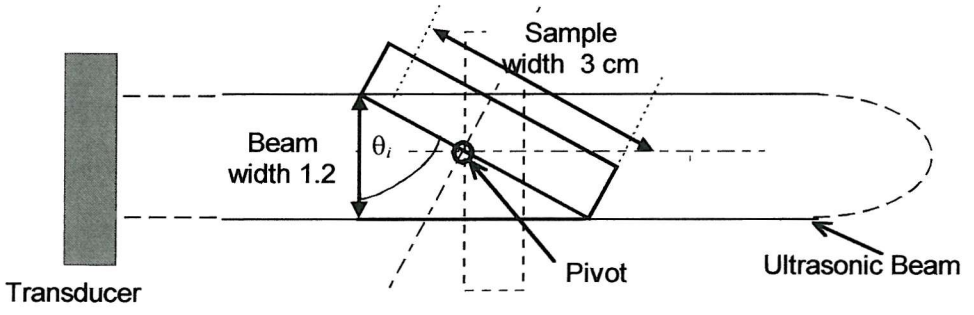

Figure 5.5 -Rotation of a sample in an ultrasonic beam.

5.5.2 Evaluating Phase Velocity for Refracted Waves

The Phase Spectrum Method, described in section 3.5.1 for evaluating phase velocity, is only applicable to propagation in samples tested at normal incidence. At non-normal angles of incidence, the difference in the velocities of test and reference media causes refraction to occur at a fluid-porous solid interface. For an isotropic sample, the path length of the wave will always be greater at non-normal angles of incidence than at normal angles. Rotating a sample from normal incidence, the wave is bent away from the normal in all cases, for any velocity in the sample. A longer path length will cause the pulse to arrive later, *appearing* as if its velocity has decreased with angle[2]. An alternative method for determining phase velocity overcomes this by accounting for refraction, and is outlined below.

The phase velocity of a refracted wave may be calculated using a technique developed by Smith (1972), and later modified by Plona *et al.* (1987) for ultrasonic immersion tests. This algorithm accounts for the fact that the path through the sample lengthens by an amount dependent of the angle of refraction.

The group velocity of a dispersive wave (introduced in section 1.5.2) is generally different from the phase velocity, hence the latter will be refracted at a different angle. Figure 5.6 shows an ultrasonic beam is incident at the target at an angle θ_i in the *yz*-plane. The phase velocity component makes an angle, θ_r with the normal to the sample face, whilst the group velocity makes an angle, θ_g. In a non-dispersive medium, the angles, θ_g and θ_r will be the equal.

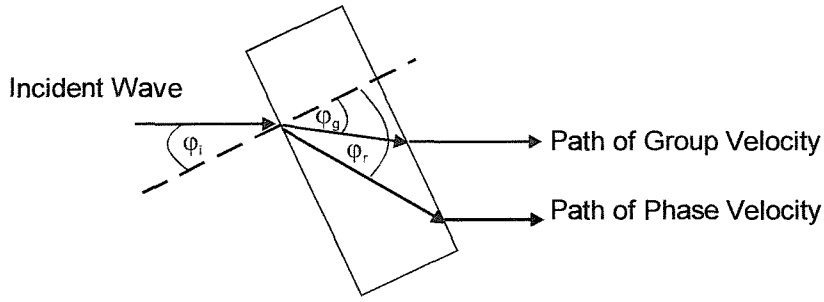

Figure 5.6 - Refraction through a finite-sized sample, for angle of incidence, θ_i; and the angles of refraction of group and phase velocities, θ_g and θ_r , respectively.

[2] An apparent increase in velocity, where the wave arrives earlier than at normal incidence, only occurs if the properties of the specimen are anisotropic. No increase is observed if the specimen's properties are the same as those of the reference medium.

Using trigonometry and Snell's law (Leighton 1994), the angle of refraction, θ_r may be found in terms of the known quantities: specifically, the angle of incidence, θ_i; the phase difference between a pulse with and without the specimen present (that is, the time difference between group velocities in each case); the speed of sound in the reference medium, V_w; and the sample thickness, d. For an angle of refraction, θ_r, where,

$$\tan\theta_r = \sin\theta_r(\cos\theta_i - g), \tag{5.6}$$

the phase velocity, $V_p(\omega)$, can be expressed as

$$V_p(\omega) = V_w / \left(1 + g^2 - 2g\cos\theta_i\right)^{1/2}. \tag{5.7}$$

where V_w is the velocity in water and,

$$g = \left(V_w \phi_b(\omega)\right) / \omega d, \tag{5.8}$$

where d is the thickness of the target. The term $\phi_b(\omega)$ is the phase difference between pulses with and without the target present. If $Re(\omega)$ and $Im(\omega)$ are the real and imaginary parts of the Fourier Transform of a signal, respectively, the phase may be evaluated as $\phi(\omega) = \tan^{-1}(Im(\omega) / Re(\omega))$. The phase difference can be expressed in degrees as

$$\phi_b(f) = \left(-\phi_{ref}\right) - \left(\phi_{target}\right) + 360 f L_c. \tag{5.9}$$

In equation (5.9), the frequency, f, is in Hertz. The phases, in degrees, of pulses received with and without the target present are ϕ_{target} and ϕ_{ref}, respectively. The term L_C is a time-compensating distance, which accounts for the phase change present in the reference signal as a result of a section of water displaced by the insertion of the target. At normal incidence, equation (5.7) reduces to,

$$V_p(\omega) = V_w / (1 - g). \tag{5.10}$$

In a dispersive system, the phase velocity will vary with frequency, and thus it may be expected that each frequency component will refract at a different angle. By substituting equation (5.8) into (5.6), that the angle of refraction, θ_r, is frequency dependent. Hence, the processing algorithm utilises the fact that different frequencies will refract at different angles, thus allowing for bandwidth.

The phase velocity at angle of incidence, θ_i was calculated using the equations (5.6 - 5.9). This algorithm was programmed in MatLab.

5.5.3 Data Representation and Errors

Establishing the compatibility of Schoenberg's theory with measurements of direction dependent velocity, to a certain precision, involved the evaluation of first, the experimental error, and, second, the uncertainty in the predictions. An acrylic test object was used to verify the processing method of section 5.5.2. The operation of the MatLab code used to evaluate the Schoenberg predictions was verified against data of Plona *et al.* (1987). Both these tests are outlined in Appendix A.II.

The reproducibility of the experimental results, for one sample, and for samples of the same porosity, were established. First, phase velocity and angle of refraction were found from the algorithm of section 5.5.2. However, these evaluated properties are not independent of one another, that is, for any velocity there is a unique angle of refraction (as Snell's Law would suggest). Therefore, it is not possible to find the distribution, and hence uncertainty, in velocity at one particular refraction angle using this method. Instead, precision must be evaluated for another parameter for which a spread in phase velocity may be defined. The simplest parameter for which this may be achieved is the angle of incidence.

Theory and experiment were to be compared against an apparent angle of incidence, defined below with respect to the trabecular plate direction, 0° being perpendicular to the plates. Care is taken here to detail the angular conventions used throughout this study, since confusion may arise between definitions of angles with respect to the external and internal structure of samples of differing trabecular configurations.

First, two configurations of sample (Parallel and Perpendicular) were tested to cover the entire range of the angle of refraction, from 0° to 90°. The significance of the following angles should be noted. First, the angle of incidence, θ_i, *with respect to the sample face*, was controlled in the experiments, and the angle of refraction, θ_r, with respect to the sample face, which was calculated from equation (5.6). However, the data was to be plotted against the angle of incidence *with respect to the internal trabecular structure.* Since Parallel and Perpendicular samples had differing internal structure, an expression for the experimental *apparent angle of incidence* was established for each sample. Specifically, for a Parallel sample, the apparent angle of incidence, θ_{ia}, equals (90° - θ_i), for angle θ_i with respect to the external face; whilst, for a Perpendicular sample, θ_{ia}, is simply equivalent to θ_i.

Second, Schoenberg's theory predicts the angle of propagation, $\angle\mathbf{s}$, with respect to the layers in an infinitely extending medium. The theory does not account for interaction at external boundaries with secondary media, thus no angle of incidence is specified. To compare experimental results with predictions, the latter must be plotted versus the angle of incidence (as opposed to the angle of propagation in figure 5.4). Consequently, the theoretical angle of propagation through the layers, $\angle\mathbf{s}$, from equation (5.4), must be re-expressed as an angle of incidence for an imaginary half-space, where water is the reference medium and 0° is the trabecular direction (figure 5.7). Using Snell's Law, a theoretical *apparent* angle of incidence, θ_{ia}, may be expressed as,

$$\sin\theta_{ia} = \frac{V_w}{|\mathbf{s}|^{-1}}.\sin\angle\mathbf{s}, \qquad (5.11)$$

where terms are defined in equations (5.6 - 5.9).

Finally, the angular convention for the Oblique samples should be noted. These samples were tested at normal incidence, such that the angle of refraction was equivalent to that of the internal trabecular structure (that is, no additional refraction occurred). To present the data in terms of the apparent angle of incidence, equation (5.11) was again used, where the terms $|\mathbf{s}|$ and $\angle\mathbf{s}$ were replaced by V_p and θ_r (which was 45° or 60°), respectively.

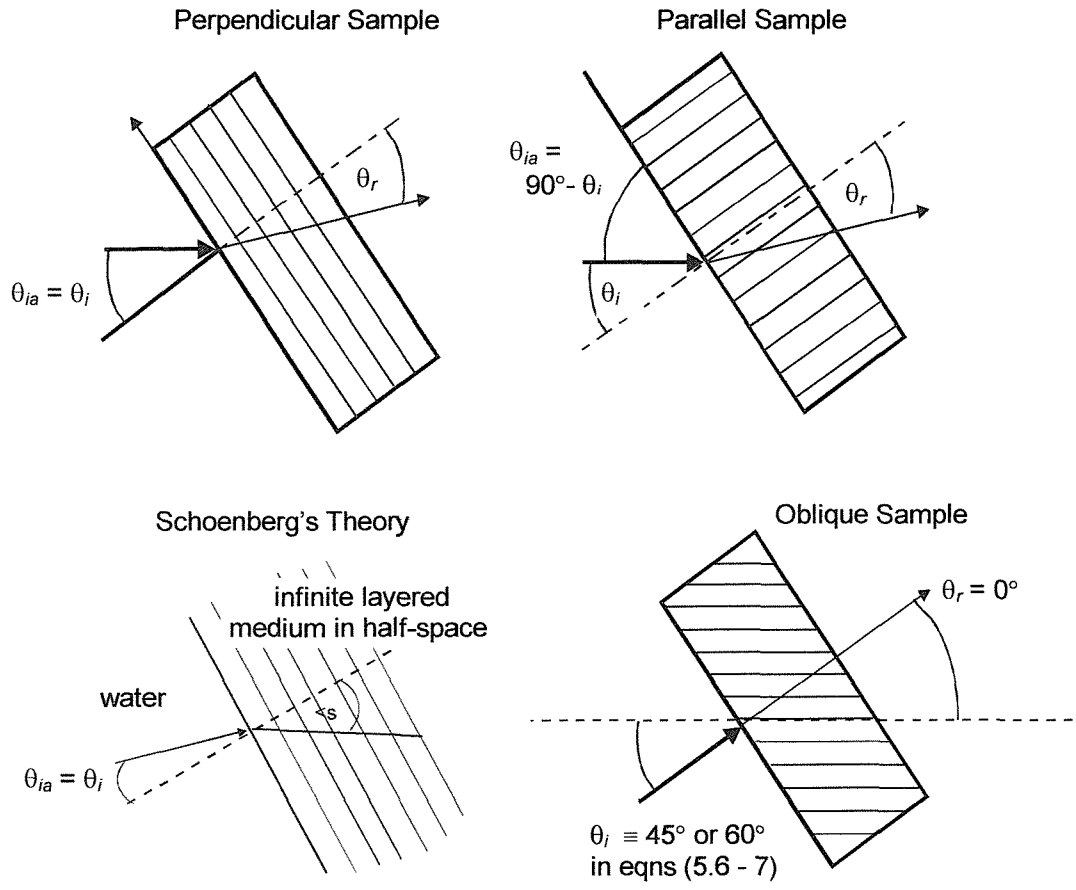

Figure 5.7 - The definition of the angles in representation of theory and data.

As with the studies on Biot's theory, the error in the predictions of Schoenberg's theory owing to uncertainties in the input parameters, may be represented by the maximum and minimum predicted bounds. Optimisation methods, introduced in section 2.3.3, may be used to find the extremes for Schoenberg. First, linearity in the equations for the given limits, was established (as presented in Appendix A.III), before proceeding with the optimisation.

Upper and lower bounds of the fast and slow wave velocities were evaluated using equations (5.1 - 5.4), using the values in column three of Table 5.1. The porosity of the cancellous samples was found in section 3.7.2 as 80.5 ± 2.8 %. The remaining parameter values were found from literature. If the experimental data, and its largest uncertainty, lie within the theoretical extremes of Schoenberg's theory, it may be said that no discrepancy has been observed at that precision, and that in this respect propagation in cancellous bone behaves as that in a system of parallel plates.

5.5.4 Results and Discussion

Figure 5.8 shows computed fast and slow wave phase velocities at 1 MHz from three Parallel (solid circles, from 30° to 90°) and three Perpendicular samples (empty circles, from 0° to 25°). Note, the results are plotted versus angle of refraction, θ_r, as found by equation (5.6), and the trabecular direction is at 90°. Figure 5.8 illustrates the spread in the data. The intersample precision at one angle had previously been calcuated for these specimens as 6.0 %. The data was re-expressed against the apparent angle of incidence, and its distribution was evaluated at each apparent angle of incidence. Figure 5.9 shows the phase velocities of fast and slow waves versus apparent angle of incidence, θ_{ia}, with the error bars as the intersample reproducibility.

For measurements taken at non-normal angles of incidence, it was necessary to ensure that shear waves were not recorded and corrupting the results. Oblique samples were tested at normal incidence, where shear propagation does not occur. Figure 4.9 (d) showed that only one mode was observed for these samples. The velocity of this mode was found to be 3210 m/s for the 30° specimen (θ_{ia} found as 76°), and 2805 m/s for the 45° specimen (θ_{ia} = 68°). When plotted on figure 5.9 these velocities give agreement within the bounds of surrounding data, which supports the assumption that the waves measured as non-normal angles in other samples were consistent with compressional propagation.

Figures 5.8 and 5.9 clearly demonstrate the reproducible result that fast and slow wave velocities in cancellous bone depend on direction. The fast wave velocity is seen to increase, although the slow wave, but for those angles where its velocity could be calculated, its value remains approximately constant. Figure 5.9 demonstrates that experimental fast and slow wave velocities are consistent with the predictions of Schoenberg's theory, to within the specified precision. Therefore, it may be concluded that ultrasonic propagation in cancellous bone is consistent with that in a layered system as modelled by Schoenberg's theory. The origin of the mode observed from Perpendicular samples the data between 0° and 25° was not apparent from initial analysis of the data. However, comparison with Schoenberg's predictions suggests that the mode observed is the fast wave at these angles.

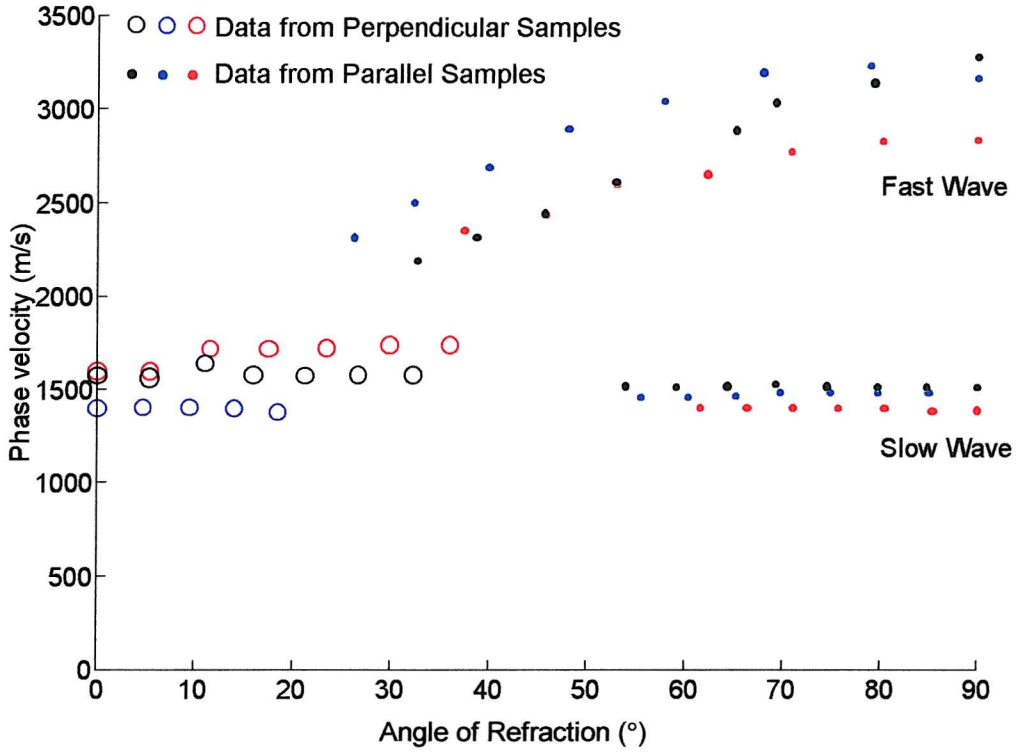

Figure 5.8 - Measured phase velocities versus angle of refraction from various samples.

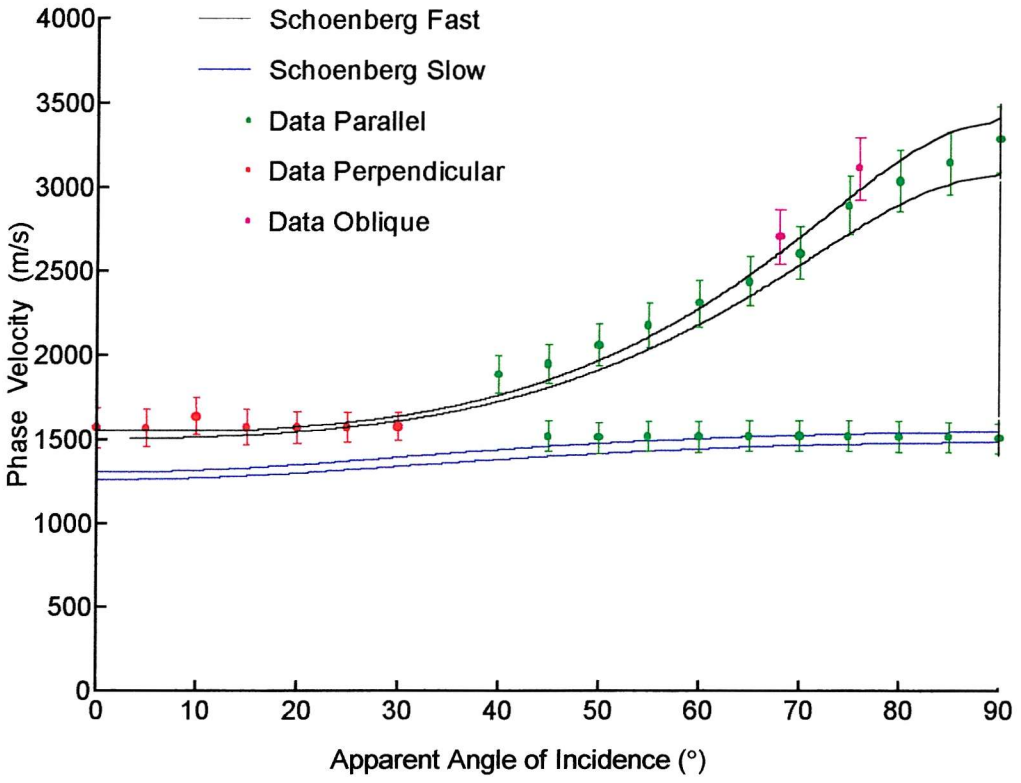

Figure 5.9 - Measured and predicted phase velocities of fast and slow waves versus apparent angle of incidence. Curves show bounds of Schoenberg theory; error bars show intersample precision on data points.

5.5.5 Lateral Shift

The presence of refraction results in a displacement in the measurement plane of the position of arriving peak pressure. Fast and slow waves, having different velocities, will refract by different amounts in the *y*-direction. At high refraction angles (and high velocities), the lateral shift may cause the peak pressure to fall outside the sensing surface of the receiver. Such a displacement would cause signal level to drop, leading to perceived high attenuation or the removal of a measurable wave. Checks were performed to establish whether signal leakage had occurred during these tests.

With reference to figure 5.10, the shift in the *y*-direction, may be quantified, using simple geometry and Snell's Law, with knowledge of the angles of refraction, θ_r, and incidence, θ_i. The shift, *Y*, may be expressed as,

$$Y = \frac{d}{\cos\theta_r}\sin(\theta_r - \theta_i), \qquad (5.12).$$

where *d* is the sample thickness, and θ_r and θ_i are angles of refraction and incidence, respectively, defined in figure 5.10.

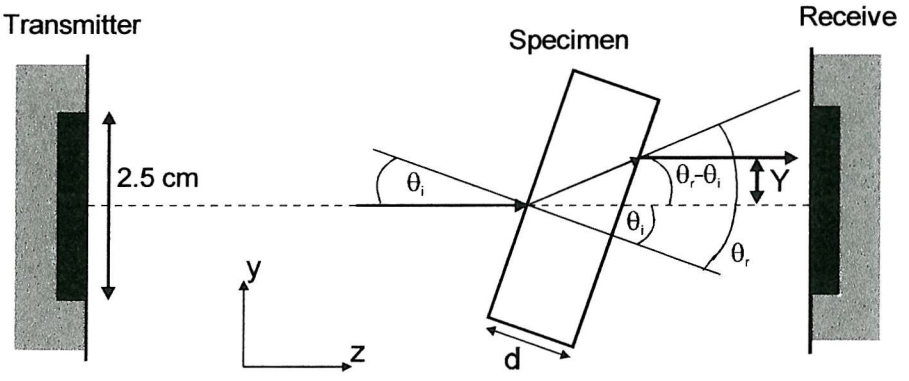

Figure 5.10 - The lateral shift in a wave through a sample tested an a non-normal angle of incidence.

Acoustic energy may not fall on the sensing surface if the distance Y is greater than the radius of the transducer. For these studies, the transducer radius was 1.25 cm. From equation (5.12), it may be seen that if the angle of refraction and incidence are approximately equal, or where the wave velocity is close to that in the reference medium, the shift will be negligible. The velocity of the slow wave is close to that in water, and the wave is unlikely to experience much lateral shift. Hence, it will be fully recovered by the sensor. For example, for a Parallel sample of thickness 1 cm, with an angle of incidence of 20°, corresponding angle of refraction[3] of 22°, the lateral shift, Y, in the slow wave, is less than 1 mm. In contrast, for an angle of incidence of 20°, and angle of refraction of 30° in the same sample, the fast wave shift Y is 2 mm. The maximum shift in the fast wave achievable using this set up, is around 2 cm, This occurs at angles of incidence and refraction of 55° and 79°, respectively.

The bandwidth of the signal may also affect the shift, since the phase velocity, and hence the angle of refraction, θ_r, are functions of frequency. Figure 4.4 (a - b) showed that the slow wave velocity is approximately constant in the bandwidth 0.8 - 1.2 MHz. Thus, the lateral shift is unlikely to alter over this range. The fast wave experiences negative dispersion, of around 0.1 % in its value within the given bandwidth. However, such a change in minor velocity would produce a negligible variation in shift over these frequencies.

In conclusion, refraction of the fast wave at angles of incidence above 50° (with respect to external sample dimensions) may result in shifts of the position of the peak response in the y-direction. In such tests, wave energy may be fall outside the sensing surface, thus altering measurements of wave properties. However, this is adequately tackled by the use of both Parallel and Perpendicular samples to each cover angles of incidence up to 45°, lessening the need for data at high incidence angles.

[3] The angles quoted here are given with respect to the external sample dimension, and not the trabecular direction, as plotted in figures 5.4, 5.8 and 5.9.

5.6 Summary

During this chapter, a new theoretical approach to modelling the propagation of ultrasonic waves in cancellous bone has been proposed. This model assumes that the trabecular structure is a periodic array of parallel fluid-solid layers, to which Schoenberg's theory is applied. *In vitro* investigations of direction dependent wave velocities in cancellous bone demonstrate two results. First, the anisotropic response of fast and slow compressional waves is reproducible. Second, evidence exists that ultrasound in cancellous bone containing a dominant trabecular structure behaves like that in a stratified array of bone-marrow layers. Qualitative agreement has been found between theory and experiment to within specified uncertainties.

The stratified model proposed here is clearly a simplification of the cancellous architecture. Although it is unable to model viscous effects, which may be important at ultrasonic frequencies, it uses fewer input parameters than the Biot model. Therefore, it has the potential to be usefully employed to investigate ultrasonic propagation in cancellous bone further. It is also able to provide descriptions of physical and dynamic forces which lead to an anisotropic response in bone. The following chapter presents a comparison between the Biot and Schoenberg theories.

Chapter Six
Comparison of Biot and Schoenberg Theories

6.1 Introduction to Theoretical Study

6.1.1 General Comments

Although both porous media theories of the previous chapters predict the existence of two compressional waves, they are derived from fundamentally differing perspectives. Biot considers the motion of fluid and solid separately, and then coupled. The porous geometry is described through four of the fourteen parameters. Schoenberg's use of matrices to relate acoustic field properties in consecutive periods inherently constructs a layered geometry. Such conceptual differences mean that Biot perceives cancellous bone as an isotropic matrix of fused calcified spheres saturated with viscous marrow, whilst Schoenberg sees calcified plates filled with an ideal fluid. Section 5.3.2 stated that the omission of pore fluid dynamics by Schoenberg, which are comprehensively incorporated by Biot, prevents the former from predicting viscous absorption, and restricts its application to the High frequency region.

The crucial distinction between representations is shown in figure 6.1. The figure compares the predictions with direction to trabecular alignment from Schoenberg and the isotropic Biot model, using the parameters in Table 6.1, some of which are common to both models.

Table 6.1 Input parameters to a Biot model of marrow-saturated bovine bone at 20°C, and a Schoenberg model, showing coincident terms.

Parameter in Schoenberg Model	Value	Parameter in Biot Model
Solid Compressional Speed, V_s	3150 m/s	
Solid Shear Speed, V_{sh}	1650 m/s	
Fluid Speed, V_f	1500 m/s	
Density of solid, ρ_s	2000 kg/m^3	Density of solid, ρ_s
Density of fluid, ρ_f	992 kg/m^3	Density of fluid, ρ_f
porosity, β	0.78	porosity, β
	0.266 mm	pore radius, r
	22.6 GPa	Youngs modulus of solid, E_s
	2.2 GPa	Bulk modulus of fluid, K_f
	0.32	Poisson's ratio of solid, ν_s
	1.23	Index of power law, n
	0.15 Pa.s	Viscosity of fluid, η

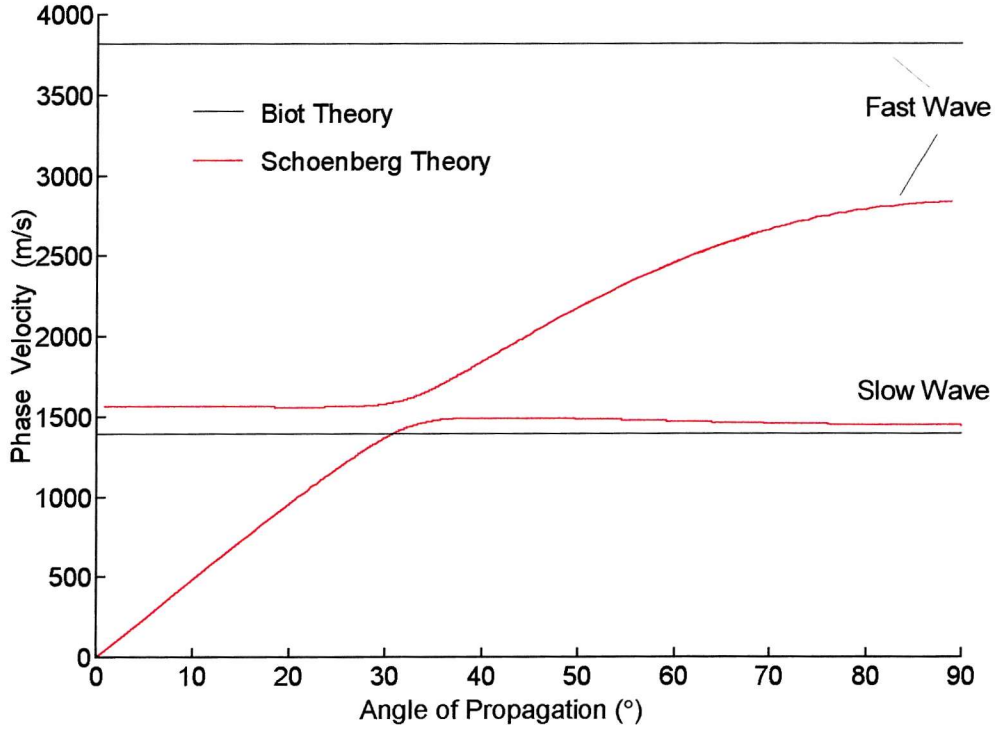

Figure 6.1 - Phase velocities of fast and slow waves versus angle of propagation predicted by the Biot and Schoenberg theories. 0° is perpendicular to the layers in Schoenberg; Biot is isotropic.

6.1.2 Aim of Theoretical Study

An investigation was undertaken to establish whether the predictions of phase velocities of Biot and Schoenberg may become equivalent with modifications. As shown in Chapter 5, the variation with direction of material properties of a porous medium influences wave propagation. Changes in wave properties with direction originate from two characteristics of a porous matrix. First, the compressibility of the frame will depend on direction, thus affecting propagation through it. Second, the pores may be elongated or skewed, such that the motion of the pore fluid is angle-dependent. Whilst both details depend on the porous geometry, they may be analysed separately. Since Biot's theory comprehensively includes frame and fluid effects, anisotropy has been introduced into Biot's theory on various occasions, not least, by Biot himself (Biot and Willis 1957). The following sections compare Biot's predictions, where anisotropy is introduced, to those of Schoenberg. The values in Table 6.1 were used, unless otherwise stated.

6.2 Introducing Transverse Isotropy into Biot's Theory

6.2.1 Transverse Isotropy in Bone

A medium is transversely isotropic if its material properties are consistent in all directions at right angles to a principle axis or azimuth (see figure 6.2 later). This condition occurs in many natural media, such as sedimentary rock and the ocean, which may be treated as a series of layers of varying density and ambient pressure.

Cortical bone displays a clear transversely isotropic behaviour (Duck 1990). Table 6.2 shows Young's moduli and Poisson's ratios for cortical bone. It is seen that, first, the parameters vary with direction, but also that, since the Young's moduli are approximately equal in directions x and y, the medium is transversely isotropic, where the azimuth as the long axis (shaft) of the bone.

Chapter 5 showed that cancellous bone could be modelled as a transversely isotropic array of parallel layers. Hence the introduction of transverse isotropy to the mechanical definitions of Biot's theory may enable it to approximate Schoenberg's stratified model. This is considered next.

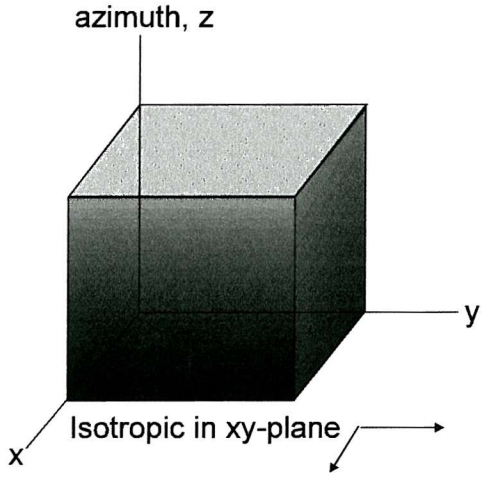

Figure 6.2 - Co-ordinate system for a transversely isotropic medium, with layers in the xy-plane having same properties.

Table 6.2 Anisotropic material parameters for bovine cortical bone* (Duck 1990)

Parameter	Value	Parameter	Value
Young's Modulus, E_x	10.2 - 13.3 GPa	Poisson's ratio, ν_{xy}	0.30 - 0.51
Young's Modulus, E_y	10.2 - 14.6 GPa	Poisson's ratio, ν_{xz}	0.11 - 0.24
Young's Modulus, E_z	18.1 - 22.6 GPa	Poisson's ratio, ν_{yz}	0.20 - 0.22
Shear Modulus, N_{xy}	3.4 - 5.3 GPa	Poisson's ratio, ν_{yx}	0.38 - 0.51
Shear Modulus, N_{xz}	3.6 - 6.3 GPa	Poisson's ratio, ν_{zx}	0.21 - 0.42
Shear Modulus, N_{yz}	3.6 - 7.0 GPa	Poisson's ratio, ν_{zy}	0.22 - 0.40

*Shear modulus, N_{ij}, is the ratio of the shear stress to shear strain for shear in the ij-plane. Poisson's ratio, ν_{ij}, is the ratio of contraction in the i-direction to expansion in the j-direction.

6.2.2 Theory

The influence of direction on the mechanical properties of a transversely isotropic porous medium may be considered in a straightforward way. Moduli and the Poisson's ratio are generally defined by considering the mechanical response in one axis, to a stimulus (whether extension or compression) in an orthogonal axis. For example, as section 2.3.2 stated, the Poisson's ratio is the quotient of lateral contraction to longitudinal extension under lateral stress. Thus, it may be expected that the values of such mechanical properties will vary with the frame of reference in a transversely isotropic medium.

The introduction of transverse isotropy to the mechanics of a fluid-saturated porous matrix may be achieved through fundamental relationships between stress and strain. As discussed in section 2.2.2, the derivation of Biot's theory begins by considering these relationships, given in equation (2.1) for an isotropic system.

For a transversely isotropic porous medium, the stresses in solid and fluid (σ_{ij} and σ, respectively) are related to the strains (e and ε, respectively),

$$\begin{aligned}
\sigma_{xx} &= 2Ne_{xx} + A(e_{xx} + e_{yy}) + Fe_{zz} + M\varepsilon, \\
\sigma_{yy} &= 2Ne_{yy} + A(e_{xx} + e_{yy}) + Fe_{zz} + M\varepsilon, \\
\sigma_{zz} &= Ce_{zz} + F(e_{xx} + e_{yy}) + Q\varepsilon, \\
\sigma_{yz} &= Le_{yz}, \quad \sigma_{zx} = Le_{zx}, \quad \sigma_{xy} = Ne_{xy}, \\
\sigma &= M(e_{xx} + e_{yy}) + Qe_{zz} + R\varepsilon. \qquad (6.1)
\end{aligned}$$

In the isotropic case of equation (2.1), four elastic coefficients, A, N, Q and R (and $P = A + 2N$), are required to describe the solid frame. However in the transversely isotropic case of equation (6.1), eight are required: A, N, F, M, C, Q, L and R (simply, four in the azimuth axis, and four orthogonal to this). The term N is the shear modulus and parameters A, Q, and R were previously given in equations (2.2 - 2.4).

As an aside, the coefficients of the anisotropic case are related by,

$$F = \mathbf{f}A, \qquad L = \mathbf{l}N, \qquad M = \mathbf{m}Q, \qquad C = F + 2L, \quad (6.2)$$

where the terms **f**, **m**, and **l** relate the elastic coefficients in orthogonal directions. Therefore, if the parameters A, N, Q and P were defined for the azimuth direction in figure 6.1, the terms F, L, M and C would be the equivalent properties, respectively, defined for the xy-plane. If **f** = **m** = **l** = 1, the material is isotropic, since the parameters reflect the degree of anisotropy. However, the terms **f**, **m** and **l** need not be known for the evaluation of the coefficients, which may be found instead from real data.

The elastic coefficients of a transversely isotropic porous medium may be found in a similar way to those in the isotropic case, using properties evaluated for the relevant axes. Specifically, equations (2.2 - 2.4), (2.26 - 2.28) are used to find parameters A, N, Q and P, using the Young's modulus and Poisson's ratio for the azimuth direction, whilst F, L, M and C may be found using those equations and input values defined for an orthogonal direction. For example, for transversely

isotropic cancellous bone, the term A, may be evaluated using the Young's modulus defined in the azimuth direction, E_z = 18.1 - 22.6 GPa. Consequently, F, orthogonally related to A through equation (6.2), will be evaluated with the Young's modulus perpendicular to this, $E_x \approx E_y$ = 10.2 - 14.6 GPa. The remaining elastic coefficients may be evaluated in a similar way.

Having treated the mechanical properties of a transversely isotropic porous medium in this way, expressions may be found for wave properties. This is briefly outlined in the following section.

6.2.3 Phase Velocities in a Transversely Isotropic Porous Medium

Sharma and Gogna (1991) derived equations for the phase velocities of fast, slow and shear waves, following the derivation of Biot's theory and using the stress-strain relations of equation (6.1).

As in the isotropic case, coupled linear equations of motion may be found for compressional and shear propagation. In the isotropic case there are two set of coupled equations, with equation (2.5) representing compressional propagation and equation (2.6) representing shear propagation. In the case of transverse isotropy, there are three sets of coupled equations, one of which is easily solved for shear waves. The coefficients of the remaining two sets for longitudinal propagation may be formed into a four-by-four matrix equation,

$$\begin{vmatrix} (A+2N)\frac{1}{c^2}+Lq^2-\rho_{11} & \frac{q}{c}(F+L) & \frac{M}{c^2}-\rho_{12} & \frac{q}{c}M \\ \frac{M}{c^2}-\rho_{12} & \frac{q}{c}Q & \frac{R}{c^2}-\rho_{12} & \frac{q}{c}R \\ \frac{q}{c}(F+L) & \frac{L}{c^2}+Cq^2-\rho_{11} & \frac{q}{c}Q & q^2Q-\rho_{12} \\ \frac{q}{c}M & q^2Q-\rho_{12} & \frac{q}{c}R & q^2R-\rho_{22} \end{vmatrix} = 0, \tag{6.3}$$

where $c = (V / \sin\theta)$ and $q = (\cos\theta / V)$, for a wave of velocity, V, propagating at an angle, θ, with the z-axis. The terms ρ_{11}, ρ_{22} and ρ_{12} were given in equations

(2.7) and (2.8). With some algebra and matrix transformation, equation (6.3) may be re-expressed as a cubic equation in terms of velocity, V^2, as,

$$T_{31}V^6 + \left(T_{32}\sin^2\theta + T_{21}\cos^2\theta\right).V^4 + \left(T_{33}\sin^4\theta + T_{22}\sin^2\theta\cos^2\theta + T_{11}\cos^4\theta\right).V^2 + T_{34}\sin^6\theta + T_{23}\sin^4\theta\cos^2\theta + T_{12}\sin^2\theta\cos^4\theta + T_0\cos^6\theta = 0 \quad , \qquad (6.4)$$

where the values of the coefficients T_{ij} are given in Table 6.3. Equation (6.4) may be solved by applying Cardano's method (Trim 1983), to find an expression for, the phase velocities of three modes, V_n (n = 1, 2 and 3 ≡ fast, slow and shear respectively), as

$$V_n = \sqrt{(\Lambda_n - A_1)/A_0}\,, \qquad (n = 1, 2, 3) \qquad (6.5)$$

$$\text{where} \quad \Lambda_n = 2\sqrt{-B}.\cos\left(\frac{\phi + 2\pi(n-1)}{3}\right) \quad \text{and} \quad \phi = \tan^{-1}\left(\sqrt{|\Delta|}/-G\right) \qquad (6.6)$$

The term, $\Delta = G^2 + 4B^3$, where,

$$G = D_0^2 D_3 - 3D_0 D_1 D_2 + 2D_1^2,$$
$$B = D_0 D_2 - D_1^2\,, \qquad (6.7)$$

where the terms D_n are functions of angle of propagation relative to the azimuth, θ, as shown in Table 6.3. The terms ρ_{11} and ρ_{22} are evaluated from equation (2.7), whilst ρ_{12} is found from equation (2.8), using the tortuosity, α, of equation (2.22).

Table 6.3 - Coefficients of eqn (6.4) for the Transversely Isotropic Biot model.

Term	Expression
T_{11}	$-(XZ + \rho_{22}LY)$
T_{12}	$\rho_{22}\{(2N+L)X + M[Q(F+2L)-CM] + Q(MF-AQ) + R[AC-F(F+2L)]$
T_{21}	$(Y + \rho_{22}L)Z$
T_{22}	$\rho_{11}\rho_{22}[Q^2+M^2-(C+A+2N)R] - \rho_{12}^2[2MQ-2(F+2L)R] - 2\rho_{22}LY + 2\rho_{22}^2(L-N)C + 2\rho_{12}\rho_{22}[(C+A+2N)M-2(F+2L)Q] + \rho_{22}^2[F(F+2L)-AC]$
T_{23}	$\rho_{22}\{3NX + [AC-(F+2L)F+L(A+2N)-CN]R + (FM-AC)Q + NQ^2 - LM^2 + (F+2L)MQ-CM^2\}$
T_{31}	$-Z^2$
T_{32}	$(Y' + \rho_{22}L)Z$
T_{33}	$-(X'Z + \rho_{22}LY')$
T_{34}	$\rho_{22}LX'$
X	$CR - Q^2$
X'	$(A + 2N)R - M^2$
Y	$\rho_{11}R + \rho_{22}C - 2\rho_{12}Q$
Y'	$\rho_{11}R + \rho_{22}(A + 2N) - 2\rho_{12}M$
Z	$\rho_{11}\rho_{22} - \rho_{12}^2$
D_0	T_{31}
D_1	$(T_{21}\cos^2\theta + T_{32}\sin^2\theta) / 3$
D_2	$(T_{11}\cos^4\theta + T_{22}\cos^2\theta \sin^2\theta + T_{33}\sin^4\theta) / 3$
D_3	$T_0\cos^6\theta + T_{12}\cos^4\theta \sin^2\theta + T_{23}\cos^2\theta \sin^4\theta + T_{34}\sin^4\theta$

Table 6.4 - Input parameters for the elastic coefficients for the TI Biot model.

Parameter	Value	Details
Azimuth Direction		Used to find K_{sz}, K_{bz} & N_{bz} from eqns (2.26 - 2.28), used in eqns (2.2 - 2.4) for A, Q & R. $P = A + 2N$, for $N = N_{bz}$.
Young's modulus in z-dir'n, E_z	18.0 GPa	
Poisson's ratio for z-y plane, ν_{zy}	0.3	
X-Y Plane		Used to find K_{sx}, K_{bx} and N_{bx} from eqn (2.26 - 2.28). Values of K_{sx}, K_{bx} and N_{bx} then used to find F from eqn (2.2) and M from eqn (2.3). $C = F + 2L$, for $L = N_{bx}$.
Young's modulus in x-dir'n, E_x	12.0 GPa	
Poisson's ratio for x-y plane, ν_{xy}	0.4	

6.2.3 Comparison of the Predictions of TI Biot model with Schoenberg

Phase velocities as functions of the angle of propagation were evaluated for the transversely isotropic Biot model (which will be called the TI Biot model for convenience), from equations (6.5 - 7), and the coefficients of Table 6.3, using the values in Table 6.1 and Table 6.4. Care was taken to evaluate the elastic coefficients, *A, N, F, M, C, Q, L* and *R*, using values of the Young's modulus and Poisson's ratios defined for the relevant direction. The use of their values is summarised in Table 6.4. Predictions from Schoenberg's model, were evaluated as in section 6.1. As an aside, in Schoenberg's stratified medium, the azimuth is taken *perpendicular* to the layers. In real bone, however, this axis is *parallel* to the layers, which reflects the fact that much real bone is composed of rods, not plates.

Figure 6.3 shows phase velocities versus angle of propagation as predicted by two models. The TI Biot model is seen to predict fast and slow wave speeds which vary with the angle of propagation. Thus, modification of basic equations of Biot's theory yields an anisotropic response. The fast wave velocity is seen to increase with angle, being around 3200 m/s at 0°, rising to 4000 m/s at 90°. However, although the contour of the TI Biot fast wave velocity resembles that of the Schoenberg fast wave, its magnitude is twice that of the Schoenberg wave at 0° and a third greater at 90°. Poor knowledge of the input parameters may have given rise to this discrepancy. The TI Biot model uses orthogonal Young's moduli and Poisson's ratio for cortical bone, and which therefore makes the assumption that the inherent anisotropy of cancellous bone arises solely from the change in properties of individual calicifed trabeculae with direction. It is conceivable that the transverse isotropy in cancellous bone is instead a result of the fabric of its structure. However, without accurate biomechanical models or data, this cannot be included into the TI Biot model.

The slow wave velocity predicted by TI Biot shows little correspondence to the curvature or magnitude of that from Schoenberg, being around 100 m/s at 0° and 650 m/s at 90°. Significantly, the TI Biot slow wave does not fall to 0 m/s at 0°, the azimuth direction. In the Schoenberg model, the slow wave velocity is 0 m/s perpendicular to the layers, owing to the absence of a path through the layers through which a fluid-borne wave may propagate. However, in the TI Biot model,

the structure is defined by the tortuosity for the case for a structure of fused spheres (from equation (2.2.2)). Therefore, conceptually, channels will exist through the porous matrix in the azimuth direction, through which a fluid-borne wave may propagate and hence, the slow wave velocity is not 0 m/s for the TI Biot model at this angle.

In conclusion, although the mechanical properties of the solid frame are accounted for in the TI Biot model, subtleties in fluid flow associated with the layered structure of Schoenberg's model are poorly represented by the case of fused spheres. The following investigation discusses a version of the tortuosity for a layered structure, which may more closely approximate those inertial effects in Schoenberg's theory.

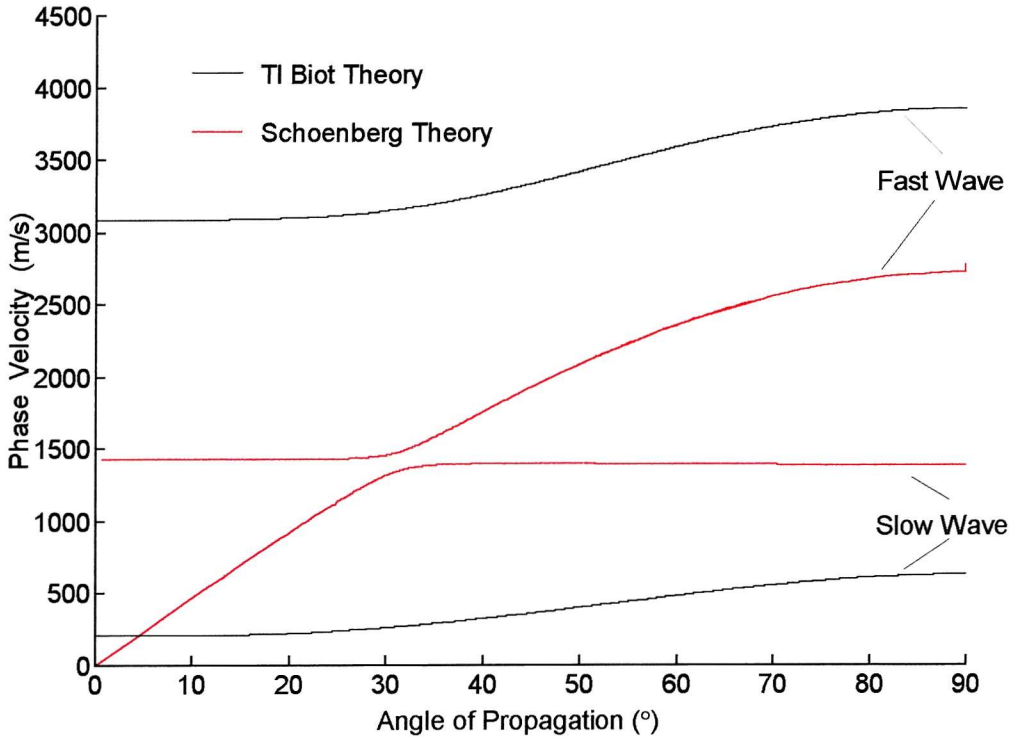

Figure 6.3 - Phase velocities of fast and slow waves versus angle of propagation predicted by the TI Biot and Schoenberg models. 0° is perpendicular to the layers (azimuth).

6.3 Introducing Anisotropic Fluid Effects in Biot's Theory

6.3.1 Theory

The macroscopic compressibility of the frame of a porous medium, considered in the previous section, may be related, in part, to the shape of the microscopic pores. Biot considered both the frame anisotropy (Biot and Willis 1957) and, later, that of the pore fluid motion, by introducing a visco-dynamic operator matrix, representing viscous and inertial coupling in three dimensions (Biot 1962). However, for the purposes of approximating a stratified structure, this operator is neglected here in favour of a simpler and novel approach, described below.

Section 2.2.4 discussed the representation of the dynamics of the interstitial fluid by the frequency-dependent tortuosity, $\alpha(\omega)$, of equation (2.21). At sufficiently high frequencies, the second term on the right hand side of this expression, which includes the viscosity, η, may be neglected, and the tortuosity may be approximated as the term, α_∞, being purely dependent on the porous geometry. Strictly, this accounts for the fact that, at high frequencies, viscous coupling is dominated by inertial coupling.

As mentioned in section 5.3.2, the dependence of velocity on the direction in a stratified medium reflects the variation in inertial coupling. If the Biot and Schoenberg models are to become equivalent, it may be assumed that the degree of inertial coupling at an intermediate propagation angle in Schoenberg's layered system is equivalent to that in a fluid with a tortuosity in a Biot model with anisotropic fluid motion. Therefore, introducing anisotropic fluid effects into Biot's theory requires finding an expression for the tortuosity, α, in a stratified structure as a function of the angle of propagation to the layers, θ.

Such an expression may be obtained by equating expressions for phase velocity from the two theories: from Biot's theory in terms of α, and from Schoenberg in terms of angle, θ. Equation (2.9) relates the phase velocities of Biot's theory to the tortuosity, α, through the definition of ρ_{12} from equation (2.8). This may be equated with the inverse of the magnitude of slowness, $|\mathbf{s}|^{-1}$, for

a wave in a stratified matrix as function of propagation angle, θ (Schoenberg and Sen 1983),

$$|\mathbf{s}| = \left(\frac{\langle 1/K\rangle / \langle 1/\rho\rangle}{\sin^2\theta + \cos^2\theta / \langle\rho\rangle\langle 1/\rho\rangle}\right)^{1/2}, \qquad (6.8)$$

where $<\rho> = \beta\rho_f + (1-\beta)\rho_s$, $<1/\rho> = \beta/\rho_f + (1-\beta)/\rho_s$ and $<1/K> = \beta/K_f + (1-\beta)/K_s$; and where $\theta = 0°$ for propagation perpendicular to the layers. The calculation may be substantially simplified if, rather than a fluid-solid system, the case of two fluids is considered. This allows for the values of the frame bulk modulus, K_b, and shear modulus of the solid, N, to be set to zero. The tortuosity as a function of angle, $\alpha(\theta)$, can then be found by equating equations (2.9) and (6.1), as,

$$\alpha(\theta) = 1 + ((1-\beta)\rho_s / \langle\rho\rangle)\cot^2\theta. \qquad (6.9)$$

Equation (6.9) gives the tortuosity parameter of Biot's theory as a function of the angle of propagation to the layering in a stratified structure.

6.3.2 Comparison of the Predictions of AF Biot model with Schoenberg

The angular tortuosity of equation (6.9) was incorporated into Biot's theory to model anisotropic fluid effects. (This model will be referred to as the AF Biot model, for an anisotropic fluid.) Phase velocities of fast and slow waves were predicted as a function of angle using the AF Biot model, and compared with those of Schoenberg, using parameters in Table 6.1.

Figure 6.4 shows the predictions of the two theories. The AF Biot model predicts fast and slow wave properties vary with the angle of propagation. Hence, as in the TI Biot model, modification of the basic equations of Biot's theory yields anisotropic wave properties. The fast wave velocity predicted by the AF Biot

model increases with angle and follows a similar curvature to that predicted by Schoenberg. However, it does not agree in magnitude with the Schoenberg fast wave, although the discrepancy is less than that of the TI Biot model in figure 6.3.

In contrast, the slow wave velocity predicted by AF Biot model shows considerable resemblance to the curvature and magnitude of that from Schoenberg. It is 0 m/s at 0°, increasing to a value of around 1450 m/s at 90°. Its value is to within 7 % of the Schoenberg slow wave curve at all angles. Such correspondence is likely to arise since the tortuosity relates to the motion of the fluid in the pores, through which the slow wave may be considered to propagate.

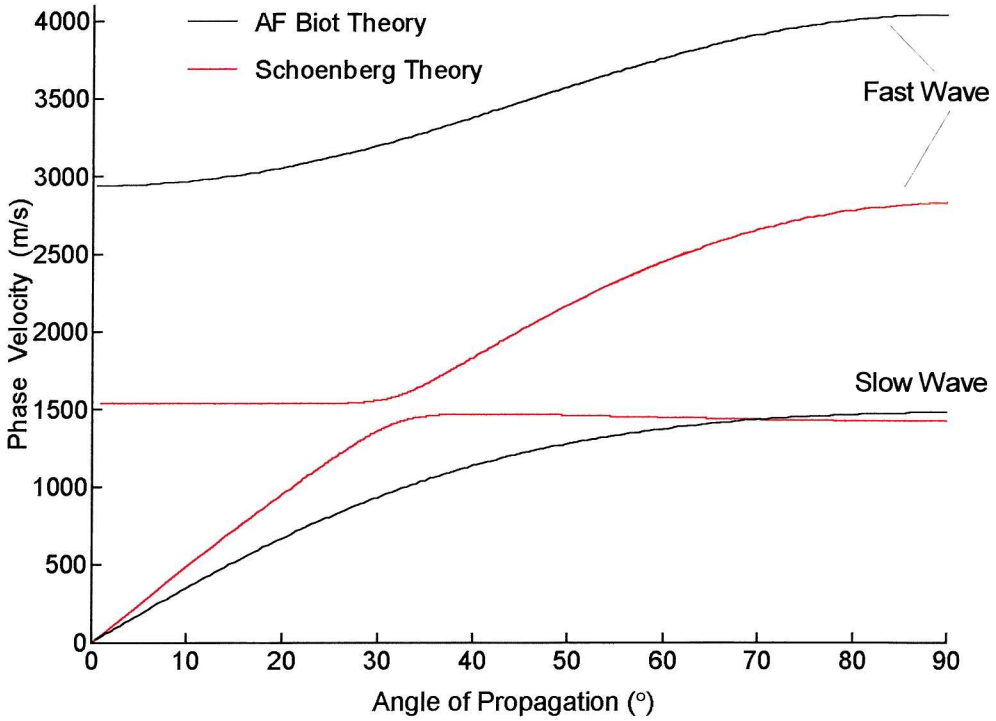

Figure 6.4 - Phase velocities of fast and slow waves versus angle of propagation predicted by the AF Biot and Schoenberg models. 0° is taken as perpendicular to the layers.

6.4 Discussion

Of the methods investigated in this chapter for incorporating anisotropy into Biot's theory, the TI Biot model, concerning frame, is certainly the more rigorous theoretically. However, the AF model, which incorporates the angular tortuosity, gives better agreement with Schoenberg's model in terms of the slow wave velocity. Total equivalence between the two theories may never be achieved, because Biot's theory fundamentally assumes that fluid and solid phases are interpenetrating and continuous. Strictly, an infinitely extending stratified geometry has no continuous phase, except at that direction parallel to the plates. In addition, mechanical moduli cannot be defined for infinite layers with no boundaries, which limits agreement between the two approaches.

Whilst this chapter has presented a theoretical study aimed at bridging the gap between the two theories, the relevance to ultrasonic propagation in cancellous bone should also be discussed. As was previously concluded, the parallel plate structure is an unrealistic idealisation of the cancellous structure, since, bone and marrow phase are interpenetrating in all orientations. Furthermore, as the experiments of section 4.3 show, the properties and dynamics of the pore fluid are important for propagation. In these respects, Biot's theory provides a "truer" model of propagation than Schoenberg, and anisotropic modification is necessary to find the "ultimate" model.

Figure 6.5 summarises all the propagation models considered in this thesis. In addition, the two amendments of sections 6.3 and 6.4 are incorporated together in a third modified Biot model, denoted as the TIAF Biot model (transversely isotropic - anisotropic fluid model). Devising this final model is easily achieved, using the angular tortuosity of equation (6.9) in the expression for ρ_{12} of equation (2.8) in coefficients of Table 6.3. For comparison, the data previously plotted in figure 5.8 against apparent angle of incidence, is replotted here versus angle of propagation. (Error bars are not shown, since, as explained in section 5.5.3, uncertainties are only valid for data plotted versus apparent angle of incidence.)

The combined TIAF modification to the Biot model does not significantly improve agreement to the predictions of Schoenberg. However, the magnitude of the fast wave is consistently in the order of 1500 m/s greater than the Schoenberg

fast wave at all angles: that is, it is faithful to the angular curvature. The TIAF model slow wave velocity gives a poorer match to that of Schoenberg than that provided by the AF Biot model.

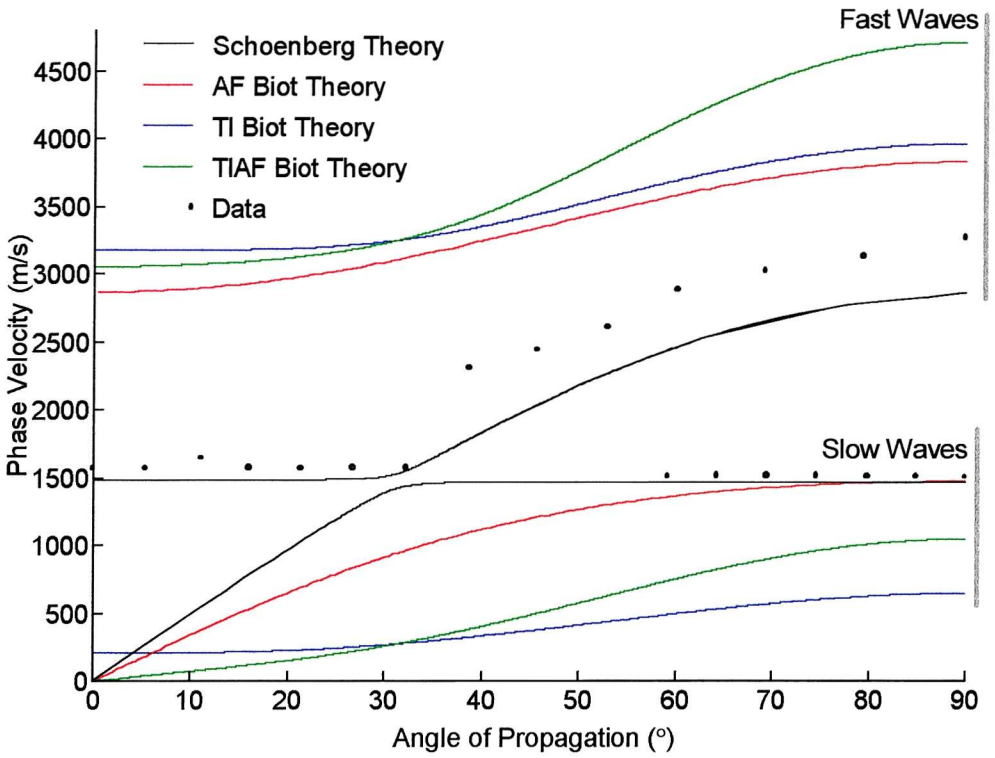

Figure 6.5 - Phase velocities of fast and slow waves versus angle of propagation predicted by the AF, TI and TIAF Biot and Schoenberg models. Data from Chapter 5 is shown. 0° is taken perpendicular to layers.

In conclusion, the unmodified Biot's theory provides a conceptually sophisticated model, which is able to predict the presence of fast and slow compressional waves, and model the phase velocities for propagation in the trabecular direction. This direction dependence phase velocities of the two waves at other angles to trabecular alignment may be modelled by Schoenberg's stratified theory. Introducing anisotropy into Biot's theory does not significantly improve its ability to model wave properties at non-aligned angles. Therefore, whilst Biot is able to account for many subtle effects, Schoenberg's theory is likely to be of greater practical use. The following chapter discusses the usefulness of the models considered throughout this work, and the relevance of the findings to clinical analysis *in vivo*.

Chapter Seven
Discussion and Future Work

7.1 Conclusions of the Present Study

This thesis has dealt with the theoretical modelling of ultrasonic propagation in cancellous bone. The conclusions that were drawn from this work were:

- Fast and slow compressional waves were observed in bovine cancellous bone *in vitro*;
- The measured phase velocities of fast and slow waves are consistent with predictions from Biot's theory, for propagation in the trabecular direction;
- The measured fast and slow wave phase velocities at any angle to the trabecular alignment may be modelled using Schoenberg's theory for propagation in periodically alternating fluid-solid layers;
- Theoretically, the interstitial fluid plays an important role in determining the nature of propagation at certain frequencies, and thus their effect should be noted for ultrasonic frequencies;
- Anisotropy may be introduced into Biot's theory through the definition of a transversely isotropic frame, or through the use of an angular tortuosity.

A list of issues were raised in section 1.6.1, to be tackled throughout the thesis. The first point concerned whether a useful theoretical model may be found to describe propagation. A useful theory may be defined in this context, as one having parameters which may be adequately determined, and from which information about bone condition may be extracted from ultrasonic measurements by inversion[1]. Of the theories considered throughout this thesis, the Schoenberg theory has the potential to be the most useful. This will be discussed later in section 7.3.3.

The second topic tackled throughout the thesis related to the effect of frequency on propagation. It has been learnt that the nature of propagation in a porous solid at a particular frequency is determined by the properties of the saturating fluid. Theoretical and initial practical evidence here suggests that the incident frequency may influence propagation in cancellous bone owing to the frequency-dependent dynamics of the interstitial fluid and the slow wave frequency window of section 3.3.2. Possible frequency-dependent effects for in vivo assessment will be discussed in section 7.3.2.

In response to the third issue, the importance of the cancellous structure is evident in the study of Chapter 5, and will be discussed in greater detail in section 7.2.1. Finally, suggestions are made regarding the improvement of QUS technology and implications for this work on current systems in section 7.3.3.

[1] *inversion* being the process of using a measured parameter to infer the value of the required parameter through an equation.

7.2 Ideas for Future Theoretical Studies

7.2.1 Modelling Structural Deterioration

To date, the only acknowledged mechanism by which the structure of cancellous bone affects ultrasonic measurements is through scattering (Tavakoli and Evans 1992). However, the present study has provided further theoretical description of mechanisms through which the cancellous architecture may influence propagation. In particular, analysis of the Schoenberg model in Chapter 5, and of the AF Biot model of section 6.3, revealed that the direction dependence of wave properties may be partially attributed to the motion of the pore fluid, and to dynamic coupling between fluid and solid. Indeed, inertial coupling, and the related tortuosity parameter, are factors firmly related to structure. This is most evident in the predictions of the AF Biot model, where the introduction of the angular tortuosity term of equation (6.9) leads to the prediction of an anisotropic response. In addition, the geometry of the calcified matrix is likely to influence its mechanical properties. Appreciation of such mechanisms may assist understanding the way in which changes in the cancellous structure with the onset of osteoporosis affect wave properties.

The structural deterioration of cancellous bone with the onset of osteoporosis was envisaged by Hosokawa *et al.* (1997) in the way shown in figure 7.1. In healthy bone, the two dimensional structure is highly anisotropic, forming oriented plates. These gradually erode to a rod-like morphology, as the trabeculae disintegrate and pore spacing increases. At high porosities, anisotropy is lost, and the structure tends towards isotropy.

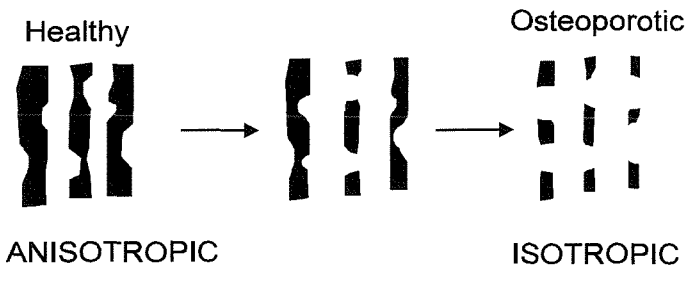

Figure 7.1 - Schematic of the deterioration of the cancellous structure with the progression of osteoporosis (after Hosokawa *et al.* 1997)

The geometric transition shown in figure 7.1 may be incorporated into the structural definition of propagation theories to model wave properties with pathological changes. Schoenberg's theory does not permit a change in the geometry of parallel plates, other than the widening of the fluid layer through increased porosity. However, the means by which the structure is defined in Biot's theory lends itself to this type of investigation. Chapter 6 discussed how the anisotropy of a porous matrix originates from two elements: the compressibility of the frame and the motion of the pore fluid. Both elements, rigorously defined in Biot, would be affected by the erosion of the structure in figure 7.1.

First, using figure 7.1 as a basis for structural erosion, the mechanical properties of such a system may be analysed. For example, in healthy bone, the Young's moduli in orthogonal direction will have significantly differing values. The erosion model suggests that their values will become closer as the structure approaches isotropy in osteoporotic bone. Thus, the ratio of Young's moduli in orthogonal axes will tend to unity with erosion.

The development of the TI Biot model in section 6.2 showed that the elastic coefficients, A, N and M are related in orthogonal directions to F, L and Q, respectively, by parameters $\mathbf{f}$, $\mathbf{l}$ and $\mathbf{m}$. These ratios essentially represent the degree of anisotropy of the porous medium, since $\mathbf{f} = \mathbf{l} = \mathbf{m} = 1$ for an isotropic medium. Therefore, finding independent expressions for these ratios, reflecting structural deterioration, would enable Biot's theory to model propagation through a realistically eroding matrix. Such parameters may be functions of porosity, density, or even a biomedical indication of bone loss.

Second, the motion of the pore fluid will be influenced by the transition in figure 7.1. As with the AF Biot model of section 6.3, the fluid dynamics may be represented by an expression for tortuosity to model the erosion. This may be in terms of, porosity, density, or biomedical indication, which best reflects the erosion. This tortuosity may be incorporated in Biot's theory to model propagation in the eroding matrix.

7.2.2 The Modelling of Scattering

Scattering, and its effect on wave properties, are generally not included in porous media propagation theories, such as the Biot and Schoenberg models. Recently, evidence has accumulated, which supports the novel hypothesis that the cancellous structure acts as a diffraction grating. A diffraction grating is a periodic lattice which produces a pattern of interfering forward scattered waves; the periodicity of which reflects the structural dimensions (pore, or strut widths) of the grating itself (Leighton 1994).

Previously, the present author (Hubbuck 1995), investigated propagation around 1 MHz through a bone phantom of a three-dimensional lattice of epoxy strands. Peaks were observed in the attenuation spectrum, the frequency of which shifted as the lattice was rotated in the field. It was proposed that the phantom acted as a diffraction grating, producing a pattern of forward scattered waves. As the perceived grating spacing altered with the rotation of the lattice, the frequency producing a particular forward scattered intensity pattern would also shift. This may correspond to the shifting peak in attenuation with rotation.

Kitamura *et al.* (1996) modelled forward scattering by considering cancellous bone as a diffraction grating of regularly spaced cylindrical rods. Fraunhofer diffraction patterns were predicted for forward scattered waves and were compared with measurements from synthetic and cancellous samples, giving reasonable agreement, modelling an arrangement similar to that in figure 7.2. Figure 7.3 (a) shows the predicted intensity diffraction pattern for a grating of cancellous bone. The intensity is normalised, where unity is the value of the intensity without the presence of the grating.

Independently, unpublished results, from a parallel experimental study co-supervised by the present author, support the diffraction pattern forward scattering idea (Edwards 1998). Using the system of figure 7.2, fluctuations in measured attenuation of ultrasonic waves at 1 MHz in bovine specimens, were found when the receiver was rotated. Figure 7.3 (b) shows the variation in attenuation[2] over angle measured by Edwards, where the scale indicates the difference in attenuation

[2] taken for a temporal window covering *both* fast and slow wave arrivals for a no-specimen reference pulse.

compared with that at 0°. Figure 7.3 (a) and (b) are plotted on a common angular scale to indicate the mechanisms by which the presence of a diffraction pattern may affect the spatial variation in attenuation.

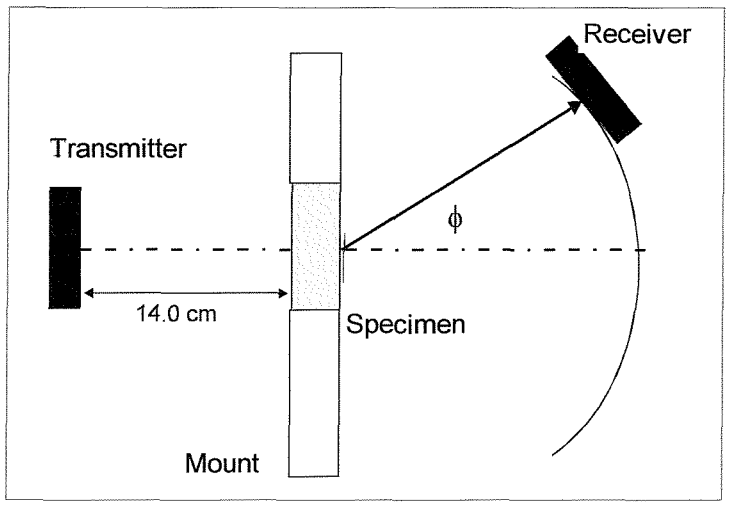

Figure 7.2 - Experimental configuration utilised by Kitamura *et al.* (1996) and Edwards (1998).

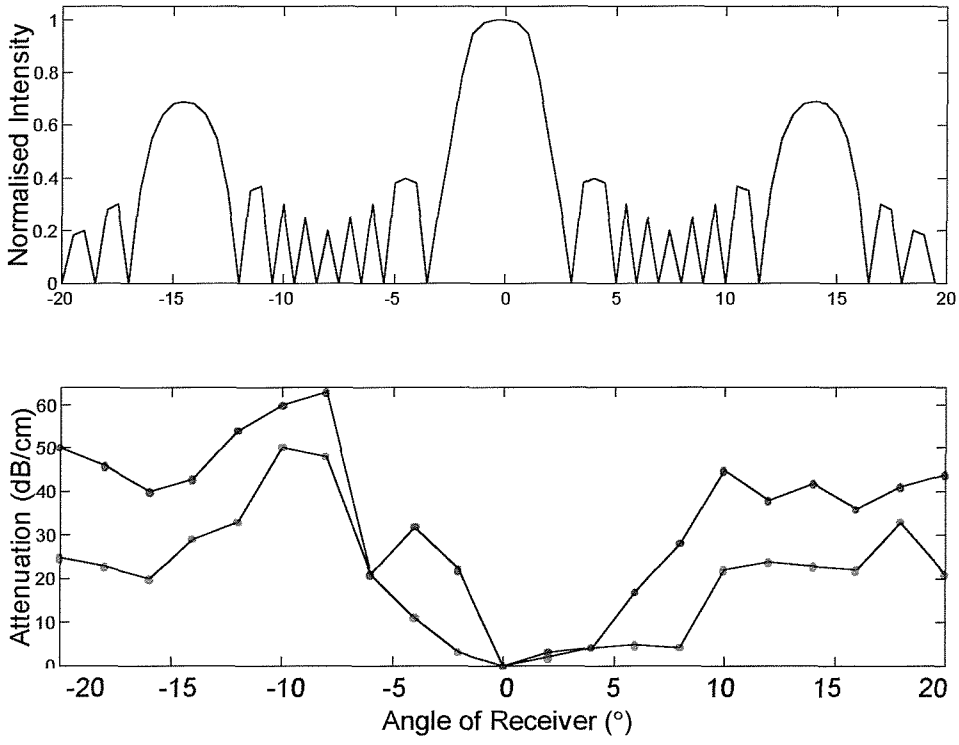

Figure 7.3 - (a) The diffraction pattern predicted by Kitamura *et al.* (1996); (b) the fluctuations in attenuation, measured by Edwards (1998). Data points (◦ &◦) are from two arbitrary samples. 0° corresponds to the direction of trabecular alignment.

With the grating present, the predicted intensity in figure 7.3 (a) is 0° is normalised to unity and the attenuation in figure 7.3 (b) is normalised to 0 dB at 0°. Between angles 3° and 12° (and -3° to -12°), the predicted normalised intensity drops, and therefore attenuation, with respect to that at 0°, would be expected to increase. This is supported by the data in figure 7.3 (b), which shows an increase in attenuation, particularly clear at angles from -5° to -12°. A peak in predicted intensity is again seen between 12° and 17° (and -12° to -17°), which again corresponds to a reduction in attenuation at these angles. Therefore, comparison of Edward's data with Kitamura's predictions provides some evidence supporting the idea that cancellous bone acts as a diffraction grating.

The significance of this results may be seen by considering the factors governing the spatial dimensions of the diffraction pattern. For a given frequency, the periodicity of the intensity pattern emerging from a sample of cancellous bone will depend on the mean trabecular spacing and thickness. Therefore, accurate measurement of its periodicity may provide information about the cancellous structure, and bone health. Future theoretical investigation would benefit from combining direction-dependent effects in the stratified model with forward scattering from the diffraction grating idea. Both may be based on the structure of a regular matrix, the dimensions of which may reflect bone health.

7.3 Implications of Current Work for QUS Assessment

7.3.1 Introduction

The findings of this thesis may have implications, not only for the interpretation of the results of previous *in vitro* studies and current clinical assessment, but also for the development of future systems. Topics of particular interest concern the possibility of observing fast and slow waves *in vivo*, which has not been reported in the literature to date[3], and exploitation of the direction dependence of wave properties as an indicator of bone health. These issues are discussed in the following sections.

7.3.2 The Observation of Fast and Slow Waves *In Vivo*

It is generally assumed that clinical ultrasonic measurements, such as QUS, only record one wave in bone. To rephrase this, no evidence exists for the presence of two waves in bone *in vivo*. Successful observation of the two compressional modes of Biot's theory *in vivo* requires consideration of those aspects which may influence propagation under such conditions. Some of these, such as the effect of fluid and structure, have been examined during the *in vitro* investigations of this thesis.

The *in vivo* condition differs in a number of ways from the *in vitro* case studied here. First, the difference in ambient temperature *in vivo* will alter the viscosity of marrow, and thus modify viscous coupling and absorption. Next, anatomical factors, such as the presence of a cortex and trabecular orientation as accessible sites, is likely to influence the propagation of two waves. Factors such as the flow of blood and the presence of soft tissue, may alter wave properties, but would require further modelling. A few of these issues will now be considered.

(a) Frequency Range

[3] This statement excludes the results of a study in Hosokawa's doctoral thesis (1997), where two waves were reported in the radius of osteoporotic patients. However, to the present author's knowledge, this work has not subsequently appeared as a journal paper, nor have the waves been independently identified or verified.

First, exercising what has been learnt about the influence of frequency on propagation in porous media, it is possible to speculate on whether fast and slow waves would be observed in current Quantitative Ultrasound (QUS).

As discussed in section 2.2.3, two waves theoretically propagate above the critical frequency, ω_{crit} of equation (2.14). Investigations there showed that, since critical bandwidths for marrow-saturated healthy and osteoporotic bone at 37°C were 156 - 341 Hz and 48 - 148 Hz, respectively (Table 2.2), fast and slow waves will propagate at frequencies in the QUS range. However, the practical and more useful limit, the viscous frequency, $\omega_{viscous}$, of equation (2.23), above this two waves will be easily observed was found to be 2.1 ± 0.7 MHz for healthy bone and 0.9 ± 0.5 MHz for osteoporotic bone (Table 3.1). Figure 7.4 shows these limits, with respect to the frequency range currently used QUS.

Figure 7.4 shows that the viscous bandwidth for osteoporotic bone extends over frequencies lower than that covered by healthy bone. For the latter, this bandwidth is significantly above the BUA range, whilst the bandwidth for osteoporotic bone extends into the BUA range. Strictly, this suggests that only one wave may be observed in healthy bone, whilst two may be observed in severely osteoporotic bone at frequencies in the upper BUA range. If this is indeed the case, such a change in the waves being sensed at the receiver, may contribute to the change the gradient of the attenuation spectrum (that is, the BUA value), during the progression of osteoporosis.

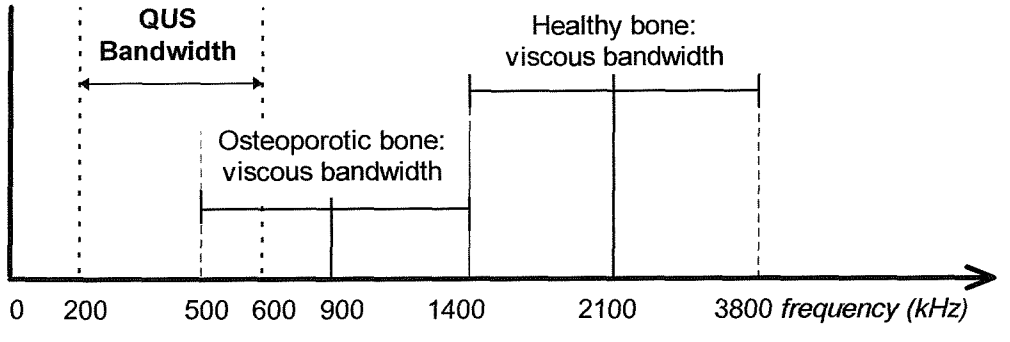

Figure 7.4 - Frequency limits for above which fast and slow waves may be observed, and the BUA range.

(b) The Effect of Structure

The QUS technique performs transmission measurements through the os calcis along the medio-lateral axis, that is, width-ways across the foot. The trabeculae in the heel are approximately aligned in the proximo-distal axis (length-ways), and hence perpendicular to the direction of propagation. With reference to the stratified model, such an arrangement corresponds to the angle of 0°, where only the fast wave propagates. Hence, the wave observed *in vivo* may be the fast wave at this orientation.

If the stratified model is taken as a reliable approximation to propagation in os calcis, it may be used to explain the characteristics of propagation through this site. For example, the velocity through the os calcis *in vivo* at frequencies in the BUA range, has been found to be around 1530 m/s (Truscott *et al.* 1996). This is surprisingly low compared with the velocity in cortical bone (3000 m/s), and closer to the speed in marrow (1450 m/s). However, the stratified theory demonstrates the fast wave velocity is least for propagation perpendicular to the trabecular direction. Indeed, predictions suggested a velocity of around 1500 m/s at this orientation. Hence, not only can the stratified model offer an explanation for the observation of only one mode *in vivo*, but it may also explain why the velocity of that mode is relatively low.

(c) The Presence of the Cortex

Cancellous bone is surrounded by a cortical shell, which constitutes a sealed boundary to the internal porous bone. As mentioned in section 3.3.2, wave propagation, and the efficiency with which the slow wave may be generated, are affected by the presence of such a boundary. The slow wave will not completely disappear at the cortex, but it is unlikely that a high amplitude slow wave, of the type observed in figure 4.1, would be observed *in vivo*, owing to a poor impedance mismatch between the calcified boundary and the marrow.

Studies on the effect of a cortex *in vitro* have been limited, but those which have been performed suggest a shell may not inhibit the production of slow wave at certain angles of propagation (Hosokawa 1997, Edwards 1998).

(d) The Effect of Osteoporosis

Cancellous bone supports slow waves effectively *in vitro*, since an open-pore boundary exists and the structure is highly permeable. Since the cancellous architecture deteriorates during osteoporosis, slow waves may propagate more effectively in the more permeable diseased bone. Hosokawa *et al.* (1997) showed that, at porosities of over 80 %, only one mode, believed to be the fast wave, was observed, the velocity of which decreased significantly to around 1500 m/s, close to that in water. Propagation under such conditions is likely to be dominated by motion of the fluid, and may not support a fast wave. Biot's theory was shown to break down at high porosities, which may occur because inertial coupling, which depends on a large surface area to couple the fluid and solid motion, will be no longer effective at high porosities.

7.3.3 Future Work: Improving QUS

As described in section 1.5.4, current QUS systems, and, in particular, BUA, have an empirical basis and do not directly provide information about physical factors of bone, such as density or porosity. The future success of ultrasonic bone assessment may benefit from the development of systems based on a direct physical relation between ultrasonic parameters and those indicating bone strength. A model designated as the basis of a novel QUS system should relate ultrasonic wave properties to the strength-determining characteristics in a straightforward way. Regarding the models investigated throughout this thesis, Biot's theory demands knowlegde of too many input parameters to be of notable value. However, the simpler Schoenberg model may be used to evaluate bone properties from measurements of velocity. The following example demonstrates one method which may be used to provide information about bone condition from direction dependent ultrasonic data and use of the Schoenberg model.

Figure 7.5 shows the fast wave phase velocity versus angle of propagation, as predicted by Schoenberg's theory for two porosities (healthy, 70 %, and diseased, 95 %). The change in porosity influences the magnitude of the fast wave

velocity, as well as a subtle alteration in curvature for the same angular range. For example, examining the change in fast wave velocities over the angular range[4] 0 - 40°, it may be seen that, for a porosity of 70 %, the fast wave velocity changes by around 250 m/s (16 %), whilst for the higher porosity, the velocity change is 300 m/s (20 %). Therefore, the change in ultrasonic velocity over a fixed angular range, may be directly related to a unique value of porosity through the equations of Schoenberg. Similar relations may be established for the measurement of bone density.

The following point should also be noted. In the predictions of figure 7.5, increased porosity only affects Schoenberg layered geometry by a thinning of the plates for the same spatial period. However, if, as suggested in figure 7.1, the layers in the structure of real bone becomes isotropic with erosion, the change in curvature with increasing porosity from real ultrasonic data may be even more marked. Such observations could be the basis for a future model-based measurement system.

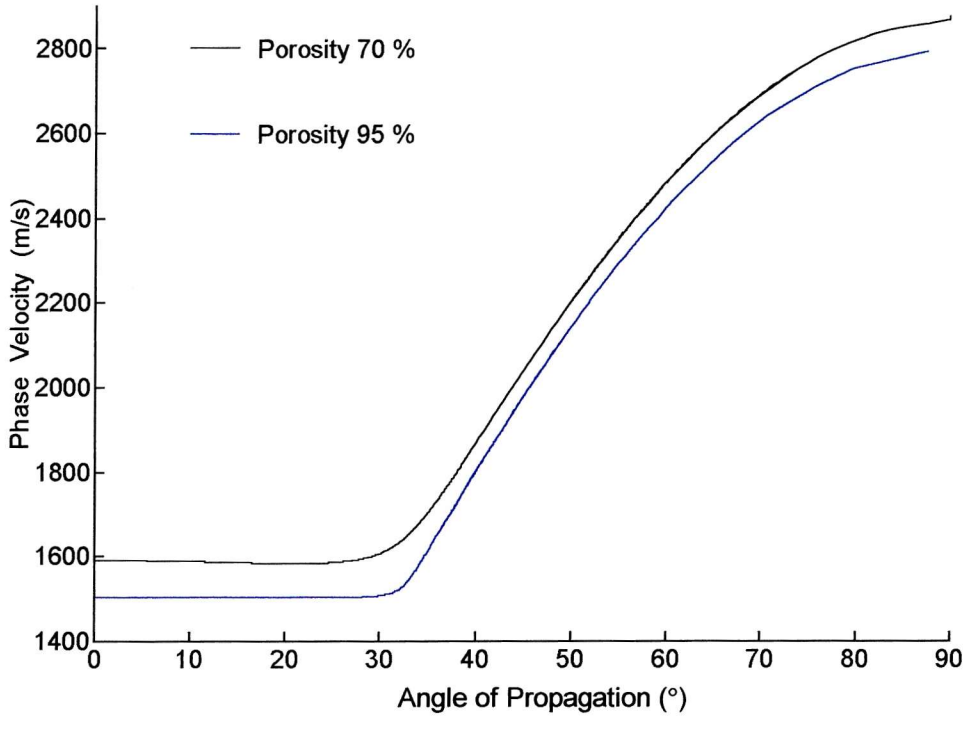

Figure 7.5 - Changes in stratified model with increasing porosity, from 70 to 95%.

[4] Recall that measurements are currently made at 0°, so it is assumed physically possible to measure angles up to 40°.

An investigation should be carried out into how the change in velocity with orientation may be utilised to infer the condition of bone *in vitro* and *in vivo*. The change in ultrasonic velocity measured over an angular range around a skeletal site containing well-oriented cancellous bone could be used to estimate the porosity from Schoenberg's theory.

The potential role and subsequent success of a model-based bone assessment technique relies on its ability to fulfil a number of requirements. First, any system should provide information about fracture risk from an ultrasonically derived parameter which is medically beneficial. Research should establish the clinical usefulness of a porosity index derived from Schoenberg's model.

Second, section 1.4.2 discussed how the role of a clinical assessment technique is dependent on its precision, usually defined as a coefficient of variance (= {std / mean}), with respect to the population distribution: For screening measurements, the precision should be of a level to infer bone condition from one test. To detect a change in bone status over time, the uncertainty should be significantly less than any difference it is trying to distinguish. Ultimately, the precision of a model-based system will defined its clinical role. It was noted in section 1.4.2 that the coefficient of variance of a bone densitometry system should be better than 2 % for screening, and better than 1% for monitoring the response to treatment (Reid and Stewart 1998). However, these coefficients are relative to measurement of bone mineral density, and equivalent coefficients for a system measuring Schoenberg-derived porosity need to be obtained before the role of the system can be identified.

Since a Schoenberg-based system will require measurement of ultrasonic velocity, it is worth considering how this parameter changes with time, for the purposes of longitudinal measurements. The speed of sound (SOS), measured in one direction, has been observed to change by 1.4 % over a 20 years age range (Truscott *et al.* 1996), which is comparable to the coefficients of variance for such measurements. therefore, it will be vital for any future system to improve on this performance to be clinically useful. It is suggested here that combining velocity data taken from different angles may provide a more sensitive measure, and, more importantly, one that changes significantly with structural changes, than measurements of SOS in one direction alone.

The success of such a model-based system would mark a breakthrough in the utilisation of ultrasound in clinical bone assessment. The ultimate aim of current research programme is to find a technology that is cheap, easy-to-use, reliable, accurate, and, eventually, widely available. When this is so, a screening programme becomes viable. Not only will osteoporosis sufferers be identified and be available for early treatment, but reassurance can be given to healthy individuals potentially at risk, improving the quality of life in both groups. An additional bonus for health care arises from the benefit to budgets that will accrue when the existing technology is made reliable, and by a reduction in osteoporosis-related fractures. This thesis has attempted to contribute to theoretical understanding which may lead to such a development.

Appendix I

Transducer Characterisation & Acoustic Field Properties

Two 1 MHz-resonant 2.5 cm-diameter transducers were calibrated by an NPL Beam Calibration Unit, based at Southampton General Hospital. The system evaluates key parameters of the function of the transducer: maximum and minimum pressure, beam width, temporally averaged intensity, and total power. The transducer being tested was submerged in a water-filled cylinder (figure A1). It was coaxially aligned with the centre axis of the cylinder, so that its beam was directed vertical downwards, above the membrane receiving hydrophone. The transmitter's location was measured in three dimensions. A pulse, centre frequency 1 MHz, 800 mV and amplified 50 dB, was generated, and the transmitter's horizontal position was altered until the output signal was a maximum. The processing unit calculated the field parameters from the output, and the results are given in Table A1.

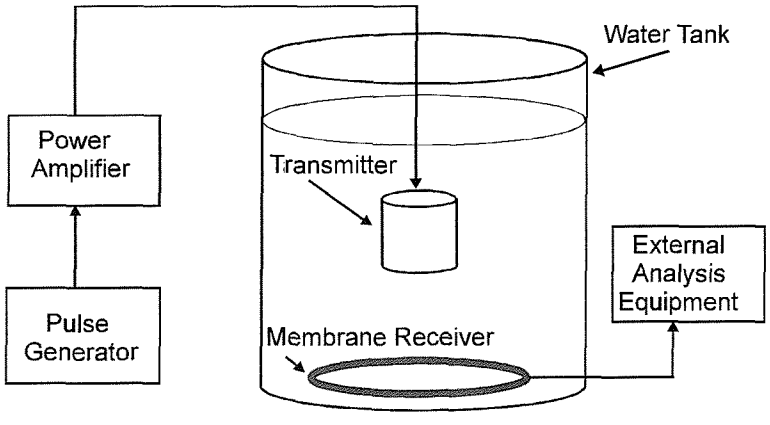

Figure A1 - Schematic diagram of NPL calibration equipment.

Table A1 - Properties of Projected Field for a 1 MHz pulse

On-axis distance *mm*	**P+** *kPa*	**P-** *kPa*	**Beam width** *mm*	**Pulse duration** *s*	$\mathbf{I_{spta}}$ W/cm^2	**Total power** *W*
80	28.1	-8.59	12.0	5.04	6.53	3.56
90	36.7	-31.2	12.0	2.00	13.6	9.37
100	46.1	-32.8	12.0	2.17	14.7	8.80
110	47.7	-32.0	12.0	3.67	14.1	8.79
120	48.4	-32.2	12.0	2.42	14.6	9.19

Appendix II

Validating Experimental Method

A2.1 Validating the Refraction Compensation Algorithm

Section 5.3 outlined an algorithm for evaluating the phase velocity of a refracted wave, which accounts for path lengthening at non-normal angles of incidence. This routine was programmed in MatLab and, to verify its operation, was tested with data from a homogeneous test object. It was expected that the phase velocity of a wave through an isotropic sample is at all angles of incidence and that calculated speeds may be compared with established values for the medium. The code was tested, using homogeneous test object of acrylic and the experimental apparatus described in section 3.5.

The phase velocity with angle of propagation in the acrylic object is plotted in figure A2, subject to a deviation of 6.0 %, from repositioning. It may be seen that the measured phase velocity is approximately constant with angle, that is, the mean value is 2819 m/s, subject to a standard deviation of 58 m/s, or 2.0 %. It is well known that, as with light, acoustic waves penetrating a homogenous object at non-normal angles of incidence, will encounter a critical angle, where total internal reflection occurs. Using the measured mean velocity and Snell's Law (Leighton 1994), the critical angle for acrylic was 31.6°. Hence, the data in figure A2 is valid up to angles of 30°.

Since the measured velocities are approximately equal with angle, it may be concluded that this programme is suitable for use in the experimental analysis of Chapter 5.

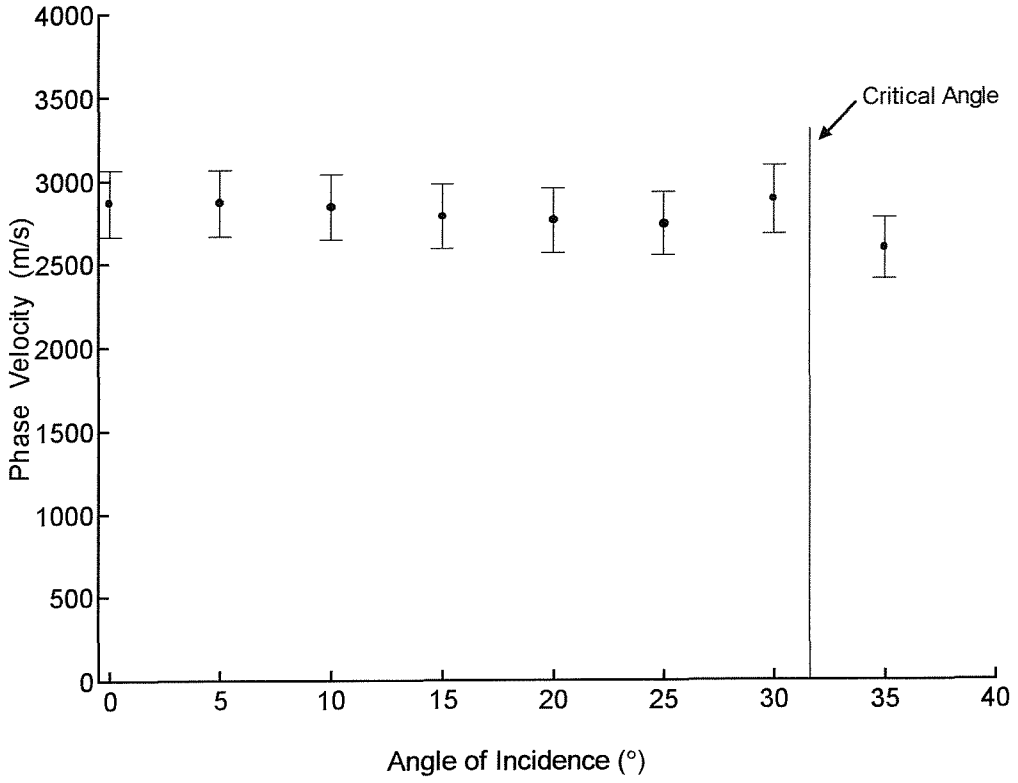

Figure A2 - Phase velocity versus angle of incidence of a pulse through an acrylic test object.

A2.2 Validating the Evaluation of the Schoenberg Equations

Section 5.3 discussed the prediction of phase velocities by Schoenberg's theory for waves in layers. Equations (5.1 - 5.4) were written in MatLab, and to check the operation of this code, predicted values were compared with those from previous authors, such as Plona *et al.* (1987), who applied Schoenberg's theory to Plexiglas layers filled with water.

Plona *et al.* used an alternative graphical method for portraying wave properties; namely the *slowness surface*. The slowness surface is a polar plot of the components of the slowness vector, **s**, and it is an established and convenient way to depict wave direction and energy flow in anisotropic media. In this case, the component of slowness perpendicular to the layers. s_3, is plotted versus that component parallel to the layers, s_1, found from equation (5.1). For porous media, this plot displays two contours for fast and slow waves.

The co-ordinates of points (s_1, s_3) along the predicted slowness surface were extracted from figure 2 in Plona's paper, by enhancing the image. These were then plotted on figure A3, along with the predictions from the MatLab code, using the values in Table A2 for Plona's system. The data was normalised for fluid speed, that is, *Parallel Slowness* = $V_f.s_1$, and *Perpendicular Slowness* = $V_f.s_3$. The figure shows significant correspondence between the two curves. It may therefore be concluded that the MatLab code operated correctly.

Table A2 Parameters for a layered system for Plexiglas and water, from Plona *et al.* (1987).

Material	Compressional Speed	Shear Speed	Density
Water	1490 m/s	n/a	1000 kg/m^3
Plexiglas	2700 m/s	1380 m/s	1200 kg/m^2

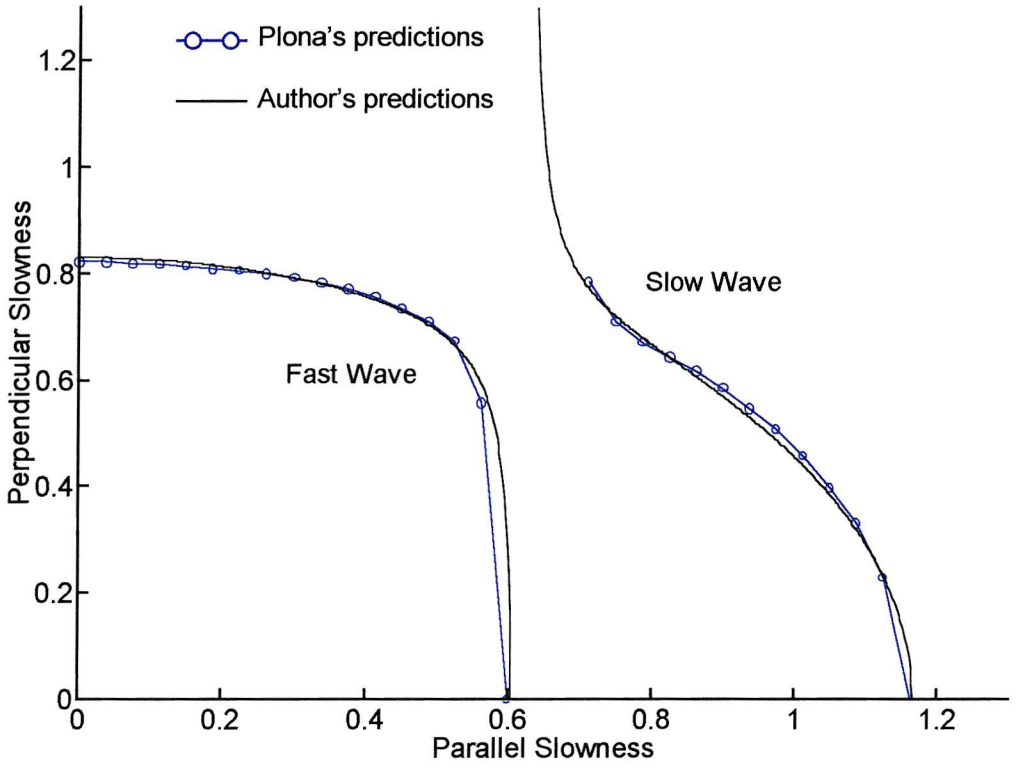

Figure A3 - Slowness surfaces of fast and slow waves for a system of Plexiglas-water layers, showing predictions by the authors, and those taken from Plona *et al.* (1987).

Appendix III
The Simplex Method for Optimisation

A3.1 Optimisation and the Simplex Method

To be useful scientifically, a theoretical model must be tested against observation. Adequate comparison requires quantitative observation of the test system and mathematical procedures for specifying the model. The input parameters of theoretical models relate to the physical properties of the system. Such variables may be accurately known, enabling a straightforward comparison between experiment and theory. However, often, the input variables are undetermined, or determined to an insufficient degree, and the behaviour of the model must be estimated. This appendix discusses the estimation of model response.

If the model input parameters are known with some uncertainty, the theoretical predictions may take a range of values. The extreme values of the predictions indicate the degree of inherent uncertainty, found from the appropriate combination of input values. If the experimental data lies within these bounds, it may be said that no discrepancy between the system and the model has been observed, at that precision. Finding the combination of inputs that give the extreme values can be tackled automatically by computer algorithms that perform optimisation.

Optimisation implies either minimising or maximising a 'cost' function, $h(x)$. However, since the maximum of $h(x)$ occurs at the same place as the minimum of $-h(x)$, it is possible to consider only minimisation. To find the maximum and minimum bounds of a theory, the cost function, $f(x)$, is simply the output of the model itself. There are many numerical optimisation methods, including classic Least Mean Squares, Chi-squared and Newton's method (Kincaid and Cheney 1990). Some find the point at which derivatives are zero, whilst others search for the gradient of steepest descent. Such methods adjust one input at a time to minimise the cost function, but are slow for complex problems. More sophisticated methods, such as genetic algorithms and simulated annealing (Kirkpatrick *et al.* 1983), change many

variables at once (Kincaid and Cheney 1990), and allow inputs to be constrained within set limits. An important class of optimisation problems is that where the function and the constraints are linear. In such cases, the region containing the minimum is bounded by straight lines or planes.

The Simplex method uses linear constraints to search a polyhedron (or 'simplex') with $n+1$ corners in n-dimensions. The search starts at one corner and proceeds successively to other corners, simultaneously monitoring that the value of the cost function is decreasing all the time. This progresses until the minimum is found, with respect to some tolerance. The Simplex method is computed using the Nelder-Mead algorithm (Kincaid and Cheney 1990), programmed in MatLab.

A3.2 Establishing Linearity

Before using the Simplex method to find the bounds of a theory, it is necessary to establish that the constraints and the cost function are linear. For the theories considered here, all inputs are limited in the numerical value they can take. Therefore, the constraints are purely numerical and, so, linear. Next, it must be established whether the cost function (the equation for velocity) is linear.

Linearity of an equation may be easily established. If the value of an input parameter, I_1 is varied within its limits, it causes a change in the output, O, of ($\Delta O'$). Similarly, a variation in the value of input, I_2 (say, ΔI_2) produces ($\Delta O''$); (ΔI_3) produces ($\Delta O'''$); et cetera. If the system is linear, when all input variables are changed simultaneously by the given amount, the independent changes in velocity will linearly combine to produce a total change of $(\Delta O' + \Delta O'' + \Delta O''' + ...)$.

If linearity is established, the function may be optimised using the Simplex method. MatLab command *fmins*('*velocity*', [x]) performs a multivariable simplex minimisation on the function $h(x) = velocity$, which contains the model equations. The vector, x, contains arbitrary starting input values. Once the minimum is reached, the final input values are recorded. The procedure is repeated to find the maximum, by

optimising the function $-h(x) = -velocity$. The maximum and minimum velocities are then found by inserting the final input values into the model.

A3.3 Evaluating Uncertainties in Biot's Theory

The values for a model of bovine bone, saturated with marrow at 20°C, where the pore size and porosity were independently established, were listed in Table 4.2, where the values for the properties of bone and marrow are taken from literature. Five *Independent and Variable* parameters were identified, whose values had a given range (porosity, fluid and solid densities, Young's modulus and pore size). The variation of these parameters within such ranges contribute to the optimisation.

Before performing the optimisation, it is necessary to determine whether the model is linear, that is, whether equation (2.9) behaves in a linear manner for the particular medium being considered. Fast and slow wave phase velocities were plotted against the five inputs, over permitted limits from Table 4.2 (figure A4 (a - e)). In all figures, velocities vary approximately linearly in the limits. Therefore, those input values which independently minimise the velocity may be found. For example, in figure A4 (a), the velocities clearly reach minima at the upper permitted limit of the porosity. It follows that velocities are maximised for the lower porosity value. In the remaining graphs, velocities also reach minimum values either at the upper or lower bound of permitted input limits.

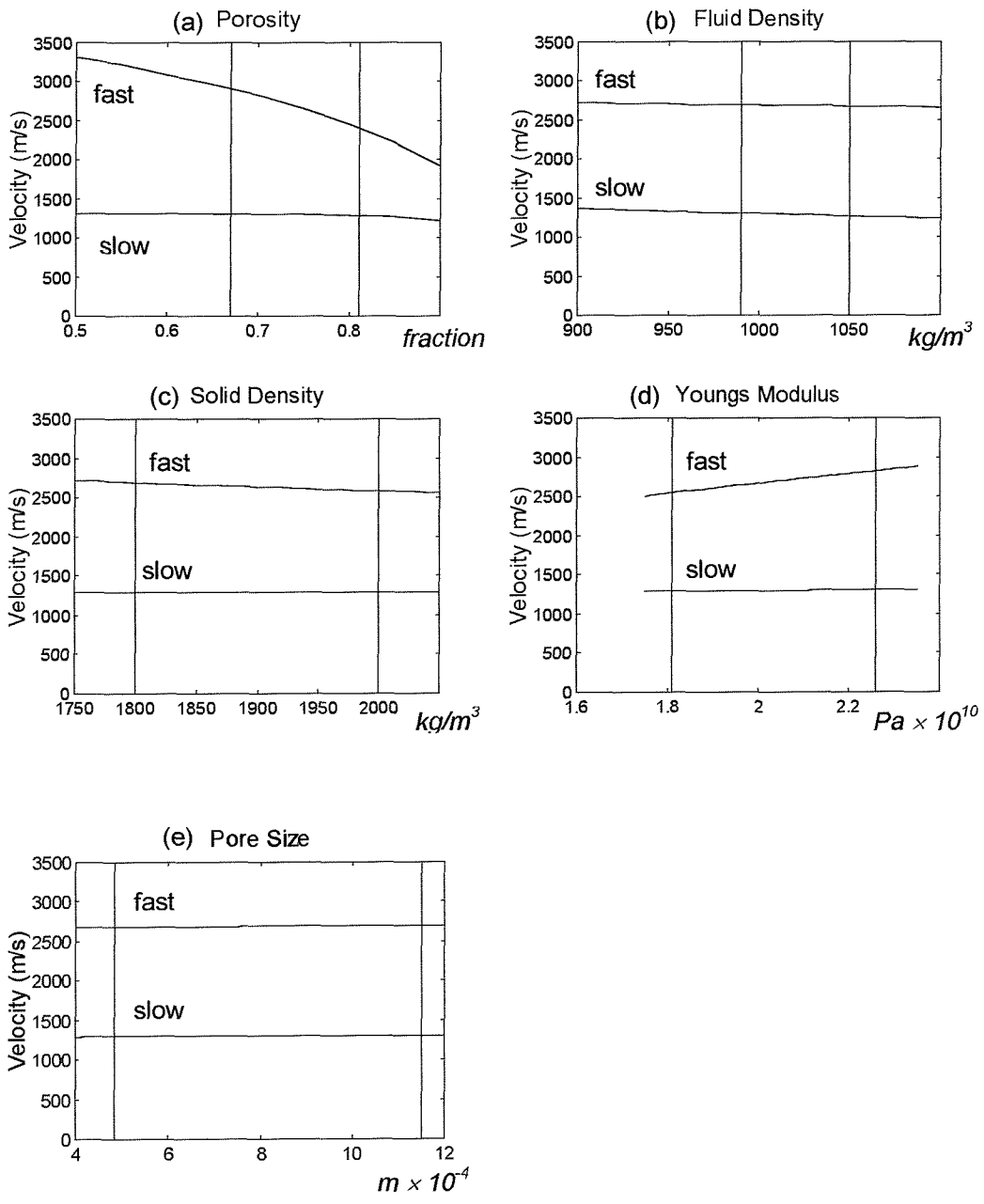

Figure A4 - Phase velocities of fast and slow waves predicted by Biot's theory versus (a) porosity; (b) fluid density; (c) solid density; (d) Young's modulus; and (e) pore size.

Biot's theory will behave linearly in the conditions of interest, if the sum of velocity changes, due to independent input variations, equals the total change in velocity when inputs are changed, by the same amounts, simultaneously. Velocities are subject to a random error of ± 9 m/s, and a quantisation error of ± 10 m/s, giving a quadrature error of ± 22 m/s. Table A3 shows independent changes in velocities, from figure A4 (a - e), when each input is varied within its range, which, when summed, result in a change of 440 m/s for the fast wave and 30 % for the slow wave. The change when all parameters are adjusted simultaneously is 391 m/s and 30 m/s, repectively. Whilst comparison of these two results for each wave does not appear to indicate strong linear behaviour, they are in agreement to within the errors, and thus adequate for the purposes of optimisation using the Simplex method.

Using the MatLab command *fmins*('*velocity*', [*x*]), the function *velocity*, was optimised, using various starting vectors, to ensure the global minimum was found. The routine, *velocity*, is equation (2.9) and relevant definitions, for the fast wave velocity. The process was repeated for maximum value. The final input values were substituted into *velocity* to predict the fast wave velocity extremes, as well as those bounds for slow wave velocity and absorption. The results are shown in figures 2.5, 2.6, 4.4, 4.5, 4.7 and 4.10.

Table A3 Fast and slow wave velocity changes to individual and combined changes in input parameters to a Biot model

Parameter	**Range**		**Change in velocity (m/s)**	
	1st value	**2nd value**	V_{fast}	V_{slow}
Porosity, β	0.74	0.81	265	10
Solid density (kg/m^3)	1900	2000	40	0
Fluid density (kg/m^3)	1000	1050	10	20
Young's modulus (GPa)	20.35	22.6	125	0
pore size (μm)	815	1150	0	0
	Summed changes		**440**	**30**
	Combined changes		**391**	**50**

A3.4 Uncertainties in Schoenberg's Theory

The second model compared with experiment in this work is Schoenberg's theory. Since the input properties of bone and marrow are again inadequately specified, optimisation may be used to find the theoretical bounds. Schoenberg's theory uses fewer input variables than Biot's theory, and these are listed in Table A4. All parameters, except for the fluid speed, are *Independent and Variable*, and may be varied to find the combination of inputs that optimises the cost function.

First, it should be noted that Schoenberg's theory predicts phase velocities that change with angle. It is conceivable that, rather than shifting by an absolute amount, the curves may change shape when inputs are altered. The maximum value at one angle may arise from a different set of input values from the maximum value at a second angle. Therefore, one simple approach is to optimise the function at each angle separately. This will give the bounds for each angle, which may be interpolated to give a smooth curve over the whole angular range.

It is then necessary to establish whether the cost function and the constraints are linear. As with Biot's theory, the constraints are purely numerical, and therefore linear. The cost function is the equation giving the phase velocity from the inverse of the modulus of the slowness vector from Schoenberg's theory (equations (5.1 - 4)). This approach requires checking the linearity of the equation over 0° to 90°. Figure A5 shows plots of phase velocity versus angle when the input parameters (porosity, fluid and solid density, solid compressional and shear speeds) are varied within their ranges given in Table A4.

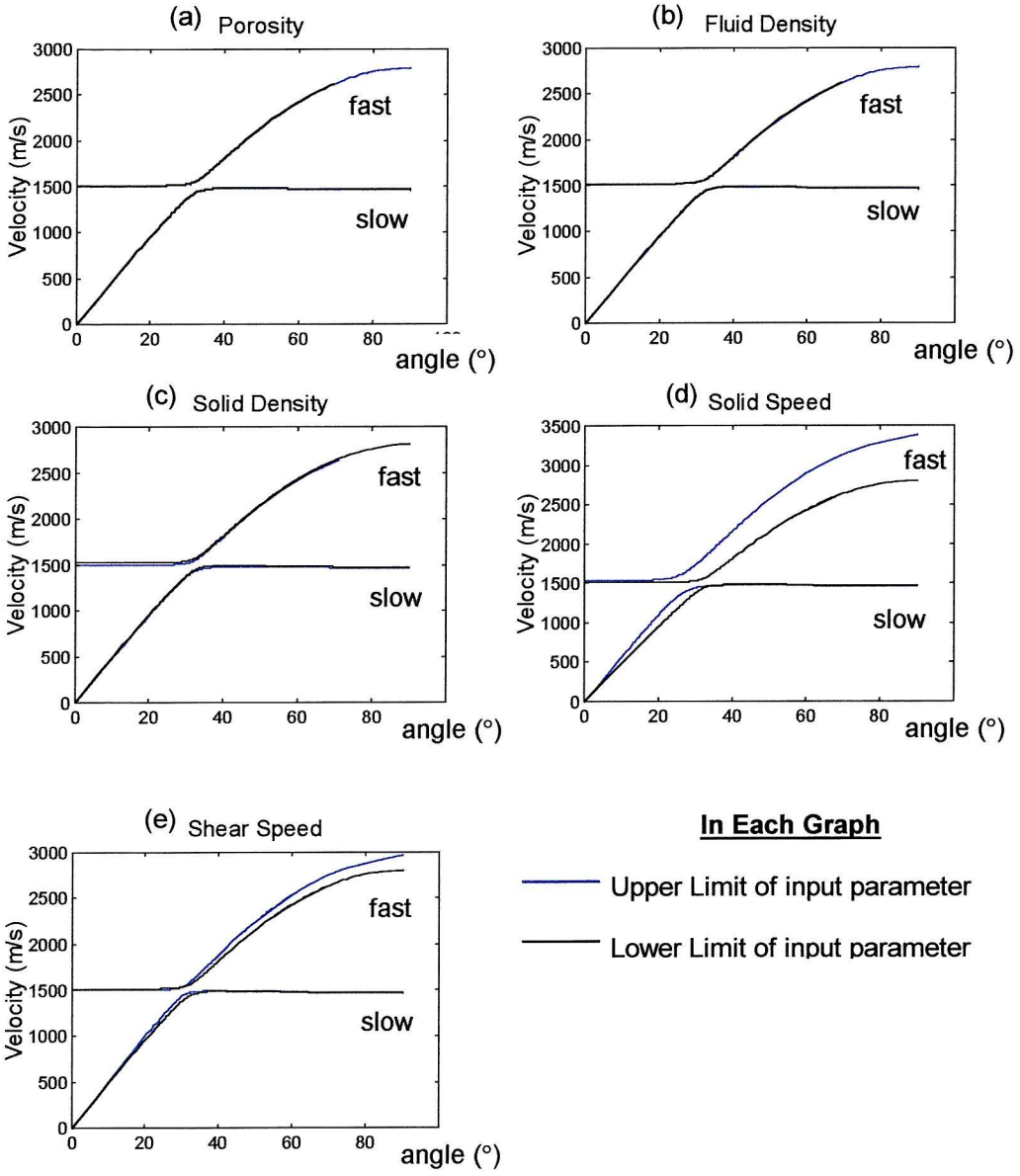

Figure A5 - Phase velocities of fast and slow waves predicted by Schoenberg versus angle of propagation, for changes in: (a) porosity, (b) solid density; (c) fluid density; (d) solid compressional speed and (e) shear speed. Changes in input parameters are given in Table A4.

Schoenberg's theory will behave linearly under the conditions of interest, if the sum of velocity changes due to independent input variations equals the total change in velocity when all inputs are changed simultaneously. Table A4 shows independent changes in velocities when each input is varied within its range, from figure A5 (a - e), at 0°, 30°, 60° and 90°, and the summed and combined changes. Whilst there is an error of 10 - 15 % for each condition in the resulting velocities between independently and simultaneously adjusted inputs, and therefore no distinct linear behaviour, the two results are in agreement to within the quantisation and random errors for determining such changes graphically. Therefore, the function behaves sufficiently linearly in these conditions to enable Schoenberg's equations to be optimised using the Simplex method.

The function, $h(x) = velocity$, containing the equations of Schoenberg's theory, was optimised to ensure the global minimum was found. The process was repeated for $h(x) = -velocity$, to find the maximum value. The final input values were substituted into *velocity* to predict the fast and slow wave velocity extremes with angle of propagation. The results are shown in figure 5.9.

Table A4 Changes in velocity of fast and slow waves at various angles, to individual and combined changes in input parameters to Schoenberg model.

Parameter	Range		Change in V_{fast} (m/s)				Change in V_{slow} (m/s)			
	1st	2nd	0°	30°	60°	90°	0°	30°	60°	90°
Porosity (fraction)	0.804	0.874	0*	0	0	0	0	0	0	0
Solid density (kg/m^3)	1800	2000	30	18	0	0	0	0	0	0
Fluid density (kg/m^3)	992	1047	12	0	0	0	0	0	0	0
Solid speed (m/s)	3100	3200	24	201	406	505	0	83	0	0
Shear speed (m/s)	1650	1800	0	0	112	166	0	60	0	0
	Summed changes		**66**	**219**	**518**	**671**	**0**	**143**	**0**	**0**
	Combined changes		**58**	**190**	**430**	**595**	**0**	**120**	**0**	**0**

* change not detected by resolution of analysis method.

Glossary

absorption	the loss of acoustic wave energy through viscous friction
attenuation	the process by which the intensity of an ultrasonic beam is reduced by a combination of absorption and scattering
azimuth	the axis orthogonal to isotropic planes
cancellous bone	bone consisting of a matrix of trabeculae
coefficient of variance	statistical index of a random distribution, equalling the ratio of the standard deviation to the mean
compressional wave	acoustic disturbance where the displacement of particles is in the same direction as propagation
cortical bone	dense bone pertaining to the nature of a cortex
density	unless otherwise specified, this term refers to the macroscopic, or volume density of cancellous bone, rather than that of an individual trabecula.
diffraction	the interference of waves from parts of a finite-sized emitter, resulting in a spatially varying field
diffraction grating	a periodic array of scatterers capable of producing a pattern of diffracted energy
dispersion	the process where different frequency components of a complex ultrasonic wave progress at different speeds
empirical signal loss	reduction in measured intensity by absorption, scattering, and artefacts such as phase cancellation and diffraction
epiphysis	the bulbous end of a long bone
evanescent wave	disturbance which decays as $exp(\lambda x)$ (as opposed to $exp(j\lambda x)$) from a source.
High Frequency Region	that bandwidth (Biot 1956), where two compressional waves propagate, the lower limit of which is $\omega_{crit} = 2\eta/\rho r^2$, where the viscous skin depth equals the pore radius.
in vitro	in an artificial environment
in vivo	within the living body
inertial coupling	the process where a fluid mass is accelerated by an adjacent solid.

isotropy	the feature where a medium has the same properties in all axes.
geometrical dispersion	the effect where the propagation mechanism depends on the ratio of the wavelength, λ, to the sample size, d: Bar waves occur for $(\lambda/d)<<1$; bulk waves occur for $(\lambda/d)<<1$.
long wavelength regime	the bandwidth where the wavelength is much greater than the size of discontinuities in a porous medium.
Low Frequency Region	that bandwidth where only the fast wave propagates; the upper limit of which is, $\omega_{crit} = 2\eta/\rho r^2$, where the viscous skin depth equals the pore radius.
optimisation	mathematical process for finding the solution to a multivariable problem best satisfying given criteria
os calcis, calcaneum	the heel bone
permeability	the property characterising the capability of a medium of being penetrated by, or allowing the passage of, fluids.
phantom	a synthetic object used to simulate biological conditions.
phase velocity	the velocity with which components of the same phase in propagate a complex wave
precision	*engineering:* the resolution to which a measurement may be made (scale gradations, decimal places, etc.) *diagnostics*: the coefficient of variance of a measurement of a clinical technique. The latter is used here.
speed of sound, SOS, group velocity	the speed with which the energy of a wave travels, found from the transit time of a wave over a known distance.
tortuosity	term describing the twisting of pores, as the ratio of a winding path length through a pore joining *A* to *B*, to the straight length, *A* to *B*.
trabecula	a calcified strand in cancellous bone
transversely isotropic	the property where the characteristics of a medium are isotropic in all directions at right angles to the azimuth
viscous coupling	the process where a fluid moves with the acceleration of an adjacent solid owing to viscous friction
vorticity	vector field describing the rotation of fluid particles, which relates the flow of adjacent layers
wavefront	a surface connecting points of the same phase

References

Abendschein W, Hyatt GW, Ultrasonic and Selected Physical Properties of Bone, Clin Orthop and Related Research, 69: 294-301 (1970).

Allard JF, Champoux Y, New Empirical Equations for Sound Propagation in Rigid Frame Fibrous Materials, J Acoust Soc Am, 91(6): 3346-53 (1992).

Alvarez-Arenas TEG, De Sarabia ER-F, De Espinosa-Feijo FRM, Observation of a Very Slow Ultrasonic Bulk Compressional Wave in an Inhomogeneous Porous Material, Ultrasonics, 32(2): 131-40 (1994).

Alves JM, Ryaby JT, Kaufman JJ, Magee FP, Siffert RS, Influence of Marrow on Ultrasonic Velocity and Attenuation in Bovine Bone, Calcif Tissue Int, 58: 362-7 (1996).

Anast GT, Fields T, Siegel IM, Ultrasonic technique for the evaluation of bone fractures, Am J Phys Med, 37: 157-9 (1958).

Antich PP, Ultrasound Study of Bone *In Vitro*, Calcif Tissue Int, 53(Suppl 1:) S157-S161 (1993).

Asaba H, Ohdaira E, Masuzawa N, Ide M, Fundamental Study to Develop Bone-Mimicking Phantom, Jpn J Appl Phys, Pt 1, 38(5B): 3412-3 (1999).

Ashman RB, Cowin SC, Van Buskirk, Rice JC, A Continuous Wave Technique for the Measurement of Elastic Properties of Cortical Bone, J Biomech, 17(5): 349-61 (1984).

Ashman RB, Rho JY, Elastic Modulus of Trabecular Bone Material, J Biomech, 21(3): 177-81 (1988).

Attenborough K, Acoustical Characterisation of Rigid Frame Absorbent and Granular Materials, J Acoust Soc Am, 73: 785-99 (1983).

Attenborough K, On the Acoustic Slow Wave in Air-Filled Granular Media, J Acoust Soc Am, 81(1): 93-103 (1987).

Bamber JC, Chapter 141: Acoustical Characterisation of Biological Media, Encyclopaedia of Acoustics, ed. Crocker M, John Wiley & Sons, London (1997).

Beaupre GS, Hayes WC, Finite Element Analysis of a 3-D Open-Celled Model for Trabecular Bone, J Biomed Eng, 107: 249-56 (1985).

Beaver WL, Sonic Nearfields of a Pulsed Piston Radiator, J Acoust Soc Am, 56(4): 1043-8 (1974).

Berryman JG, Confirmation of Biot's Theory, Appl Phys Lett, 37: 382-4 (1980).

Biot MA, Theory of Propagation of Elastic Waves in a Fluid Saturated Porous Solid I. Low Frequency Range, J Acoust Soc Am, 28(2): 168-78 (1956a).

Biot MA, Theory of Propagation of Elastic Waves in a Fluid Saturated Porous Solid II. High Frequency Range, J Acoust Soc Am, 28(2): 179-91 (1956b).

Biot MA, Willis DG, The Elastic Coefficients of the Theory of Consolidation, J Appl Mech (Trans ASME), 24: 594-601 (1957).

Biot MA, Generalised Theory of Acoustic Propagation in Porous Dissipative Media, J Acoust Soc Am, 34(9): 1254-64 (1962).

Bourbie T, Coussy O, Zinszner B, Chapter 2: Wave Propagation in Saturated Porous Media, Acoustics of Porous Media, Gulf Publishing Company, Editions Technip, Paris (1987).

Brekhovskikh LM, Chapter 5, Waves in Layered Media, Academic Press Inc, Oval Road, London (1981).

Bryant JD, David T, Gaskell PH, King S, Lond G, Rheology of Bovine Marrow, Proc Instn Mech Eng, 203: 771-5 (1989).

Carter DR, Hayes WC, Compressive Behaviour of Bone as a Two-Phase Porous Structure, J Bone & Joint Surgery, 59-A(7): 954-62 (1977).

Champoux Y, Stinson MR, On Acoustical Models for Sound Propagation in Rigid Frame Porous Media and the Influence of Shape Factors, J Acoust Soc Am, 92(2), Pt1: 1120-31 (1992).

Chandler RN, Johnson DL, The Equivalence of Quaisistatic Flow in Fluid-Saturated Porous Media and Biot's Slow Wave in the Limit of Zero Frequency, J Appl Phys, 52(5): 3391-5 (1981).

Chivers R, Measurement of Ultrasonic Attenuation in Inhomogeneous Media, Acustica, 74: 8-15 (1991).

Clarke AJ, Evans JA, Truscott JG, Milner R, Smith MA, A Phantom for Quantitative Ultrasound of Trabecular Bone, Phys Med Biol, 39: 1677-87 (1994).

Consensus Development Conference, Diagnosis, Prophylaxis, and Treatment of Osteoporosis, Am J Med, 94, 646-50 (1993).

Cooper C, Osteoporosis - An Epidemiological Perspective: A Review, J Royal Soc Med, 82: 753-57 (1989).

Currey J, Comparative Mechanical Properties and Histology of Bone, Amer Zool, 24: 5-12 (1984).

Croucher PI, Garrahan NJ, Compston JE, Structural Mechanisms of Trabecular Bone Loss in Primary Osteoporosis: Specific Disease Mechanism or Early Ageing? Bone & Mineral, 25: 111-21 (1994).

Daily JW, Harleman DRF, Chapter 6: Fluid Dynamics, Addison-Wesley Company, Massachusetts, USA (1966).

Duck FA, Chapter 5: Elastic Moduli of Bone and Teeth, Physical properties of Tissue: A Comprehensive Reference Book, Academic Press, University Press, Cambridge, GB (1990).

Dunn F, O'Brien WD (ed.), Chapter 34: Ultrasonic Biophysics, Hutchinson & Ross Inc, Pennsylvania (1965).

Edwards J, Study of the Propagation of Ultrasound through Trabecula Bone: Bridging the Gap Between *in vitro* and *in vivo* BUA Measurements, Southampton University MSc Thesis (1998).

European Foundation for Osteoporosis & Bone Disease, News, 5(2):1 (1998).

Evans JA, Tavakoli MB, Ultrasonic Attenuation and Velocity in Bone, Phys Med Biol, 35(10): 1387-96 (1990).

Evans JA, Strelitzki R, Clarke AJ, Truscott JG, Ultrasound Bone Measurements - Difference Between Manufacturers: Why and When? Proc: Bath Conference on Osteoporosis & Bone Mineral Measurement, 55 (1996).

Fry FJ, Barger JE, Acoustical Properties of Human Skull Bone, J Acoust Soc Am, 63: 1576-90 (1978).

Geertsma J, Smit DC, Some Aspects of Elastic Wave Propagation in Fluid-Saturated Porous Solids, Geophysics 26: 169 (1961).

Gibson LJ, The Mechanical Behaviour of Cancellous Bone, J Biomech, 18: 317-28 (1985).

Gibson LJ, Ashby M, Chapter 11: Cancellous Bone, Cellular Solids: Structure and Properties, Pergamon Press, Oxford, England (1988).

Gluer CC, Wu CY, Genant H, Broadband Ultrasonic Attenuation Signals Depend on Trabecular Orientation: an *In Vitro* Study, Osteop Int, 3: 185-91 (1993).

Greenspan SL, Bouxsein ML, Melton ME, Kolodny AH, Clair JH, DeLucca PT, *et al.*, Precision and Discriminatory Ability of Calcaneal Bone Assessment Technologies, J Bone Mineral Research 12(8): 1303-13 (1997).

Hammond JK, Peardon LG, Cepstral Analysis and its Applications, Time Series Analysis course notes, ISVR (1994).

Hampton L, Section 1, Physics of Sound in Marine Sediments, Plenum Press, Lower John Street, London (1974).

Hans D, Dargent-Molina P, Schott AM, Ultrasonographic Heel Measurements to Predict Hip Fracture in Elderly Women: the EPIDOS prospective study, Lancet, 348: 511-4 (1996).

Hill CR, Chivers R, Huggins RW, Nicholas D, Chapter 7: Scattering by Human Tissue, Ultrasound - Applications in Medicine and Biology III, ed. Fry FJ, Elsevier Scientific, Amsterdam (1978).

Hodgskinson R, Njeh CF, Whitehead MA, Langton CM, The Non-Linear Relationship Between BUA and Porosity in Cancellous Bone, Phys Med Biol, 41: 2411-20 (1996).

Hosokawa A, Otani T, Ultrasonic Wave Propagation in Bovine Cancellous Bone, J Acoust Soc Am, 101(1): 558-62 (1997).

Hosokawa A, Otani T, Suzaki T, Kubo Y, Takai S, Influences of Trabecular Structure on Ultrasonic Propagation in Bovine Cancellous Bone, Jpn J Appl Phys, 36: 3233-7, Pt 1, No 5B (1997).

Hosokawa A, A Study on the Propagation Phenomenon of Ultrasonic Waves in Cancellous Bone, Doshisha University PhD Thesis, Japan (1997).

Hrazdira I, Chapter 34: Direct and Indirect Effects of Ultrasound on Bone Marrow Cell Suspensions, Ultrasonic Biophysics, ed. Dunn F, O'Brien,WD, Dowden, Hutchinson & Ross Inc, Pennsylvania (1965).

Hubbuck ER, Use of an Ultrasonic Technique for the Identification of Microanatomical Bone Structure Dimensions, Southampton University MSc Thesis (1995).

Hubbuck ER, Leighton TG, White PR, Petley GW, A Theoretical Study of Factors Affecting the Biot Slow Wave in Cancellous Bone, ISVR Technical Report No 271 (1998).

Hunt KD, Dean O'Loughlin V, Fitting DW, Adler L, Ultrasonic Determination of Elastic Modulus of Human Cortical Bone, Med Biol Eng Computing 51-6 (1998).

Jaeger JC, Section 13, Elasticity, Fracture and Flow, John Wiley & Sons, New York (1964).

Johnson DL, Plona TJ, Acoustic Slow Waves and the Consolidation Transition, J Acoust Soc Am, 72(2): 556-65 (1982).

Johnson DL, Koplik J, Dashen R, Theory of Dynamic Permeability & Tortuosity in Fluid-saturated Porous Media, Fluid Dynamics, 176: 379-402 (1987).

Johnson DL, Plona TJ, Kojima H, Probing Porous Media with First and Second Sound. II. Acoustic Properties of Water-Saturated Porous Media, J Appl Phys, 76(1): 115-25 (1994).

Kincaid DR, Cheney EW, Chapter 4: Numerical Analysis, Brookes-Coles Publishing, California (1990).

Kinsler LE, Frey AR, Coppens AB, Sanders JV, Fundamentals of Acoustics, Third Editions, John Wiley & Sons, Canada (1982).

Kirkpatrick S, Gelatt CD, Vecchi MP, Optimisation by Simulated Annealing, Science 220 (4598): 671 (1983).

Kitamura K, Pan HT, Ueha S, Kimura S, Ohtomo S, Ultrasonic Scattering Study of Cancellous Bone for Osteoporosis Diagnosis, Jpn J Appl Phys, Pt 1, 35(5B): 3156-62 (1996).

Kleerekoper M, Villanueva AR, Stanciu J, Rao DS, Parfitt AM, The Role of Three-Dimensional Trabecular Microstructure in the Pathogenesis of Vertebral Compression Fractures, Calcif Tissue Int, 37: 594-7 (1985).

Lakes RS, Yoon HS, Katz JL, Slow Compressional Wave Propagation in Wet Human and Bovine Cortical Bone, Science, 220: 513-5 (1983).

Lang SB, Ultrasonic Methods for Measuring Elastic Coefficients of Bone on Fresh and Dried Bovine Bones, IEEE Trans Biomed Eng, BME-17: 101-5 (1970).

Langton CM, Palmer SB, Porter RW, The Measurement of Broadband Ultrasonic Attenuation in Cancellous Bone, Engineering in Medicine, 13(2): 89-91 (1984).

Langton CM, Ali AV, Riggs CM, Evans GP, Bonfield W, A Contact Method of the Assessment of Ultrasonic Velocity and Broadband Attenuation in Cortical and Cancellous Bone, Clin Phys Physiol Meas, 11: 243-9 (1990).

Langton CM, Ballard PA, Bennet DK, Purdie DW, Maximising the Cost Effectiveness of BMD Referral for DXA using Ultrasound as a Selective Population Pre-screen, Technology in Healthcare, 5 (1997).

Laugier P, Giat P, Berger G, Bone Characterisation with Ultrasound: State of the Art and New Proposals, Clinical Rheumatology, 13(S1): 22-32 (1994).

Lauriks W, Thoen J, Van Asbroek I, Lowet G, Van der perre G, Propagation of Ultrasonic Pulses through Trabecular Bone, J de Physique IV, C5:1255-8, (1994).

Lawrence DEP, Don CG, Impulse measurements of impedance and propagation constant compared to rigid-frame and dual-wave predictions for foam, J Acoust Soc Am, 97(3): 1477-85 (1996).

Lee CC, Lahham M, Martin BG, Experimental Verification of the Kramers-Kronig Relationship for Acoustic Waves, IEEE Trans Ultrasonics, Ferroelectrics and Frequency Control, 37(4): 286-94 (1990).

Lees B, Stevenson JC, Preliminary Evaluation of a New Ultrasound Bone Densitometer, Calcif Tissue Int, 53: 149-52 (1993).

Leighton TG, The Acoustic Bubble, Academic Press, London (1994).

Lesspessailles E, Jacquet G, Harba R, Jennane R, Loussot T, Viala JF, Benhamou CL, Anisotropic Measurements Obtained by Fractal Analysis of Trabecular Bone at the Calcaneus and Radius, Revue du Rhumatisme, 63(5): 337-43 (1996).

Marcus PM, Carstensen EL, Problems with Absorption Measurements of Inhomogeneous Solids, J Acoust Soc Am, 58: 1334-5 (1975).

McFadyean, Chapter 1, Osteology and Arthrology of the Domesticated Animal, ed. Hughes HV, Dransfield JW, Bailliere, Tindall & Cox, London (1953).

McKelvie ML, Palmer SB, The Interaction of Ultrasound with Cancellous Bone, Proc. Ultrasonic Studies of Bone IOP Short Meeting (1987).

McKelvie ML, Palmer SB, The Interaction of Ultrasound with Cancellous Bone, Phys Med Biol, 36(10): 1331-40 (1991).

Mellish RWE, Garrahan NJ, Compston JE, Age-Related Changes in Trabecular Width and Spacing in Human Iliac Crest Biopsies, Bone & Mineral, 6: 331-8 (1989).

Miller PD, Bonnick SL, Rosen CJ, Consensus of an International Panel on the Clinical Ultility of Bone Mass Measurements in the Detection of Low Bone Mass in the Adult Population, Calcif Tissue Int 58:207-14 (1996).

National Osteoporosis Society, Osteoporosis: The Silent Epidemic (1998a).

National Osteoporosis Society, The Use of Quantitative Ultrasound in the Management of Osteoporosis in Primary or Secondary Care, Position Statement as of 30th June 1998b.

Nicholson PHF, Haddaway MJ, Davie MWJ, The Dependence of Ultrasonic Properties on Orientation in Human Vertebrae, Phys Med Biol, 39: 1013-24 (1994).

Nicholson PHF, Lowet G, Langton CM, Dequeker J, Van der Perre G, A Comparison of Time-Domain and Frequency-Domain Approaches to Ultrasonic Velocity Measurement in Trabecular Bone, Phys Med Biol, 41: 2421-35 (1996).

Njeh CF, Hodskinson R, Currey JD, Langton CM, Orthogonal Relationships and Material Properties of Bovine Cancellous Bone, ABS Med Eng Phys, 18(5): 373-81 (1996).

Oppenheim AV, Schafer RW, Digital Signal Processing, Prentice Hall, London (1975).

Papadakis EP, Ultrasonic Diffraction Loss and Phase Change in Anisotropic Materials, J Acoust Soc Am, 40: 863-76 (1966).

Petley GW, Hames TJK, Cooper C, Langton CM, Cawley MID, Comparison between BUA and SPA of the Os Calcis, Proc Int Symposium on Osteoporosis, 408-9, ed. Christiansen C, Johnsen, JS, Riis BJ, Denmark, (1987).

Petley GW, The Use of Ultrasonic Transmission Measurement for the Assessment of Properties of Bone in Normal and Diseased States, Southampton University PhD Thesis (1994).

Plona TJ, Johnson DL, Experimental Study of Two Bulk Compressional Modes in Water-Saturated Porous Structures, Ultrasonics Symposium, IEEE, 868-72 (1980).

Plona TJ, Winkler KW, Schoenberg M, Acoustic Waves in Alternating Fluid Solid Layers, J Acoust Soc Am, 81(5): 1227-34 (1987).

Reid DM, Stewart A, Quantitative ultrasound - Clinical Utility, Proc 5th Bath Conference on Osteoporosis and Bone Mineral Measurement, ed. Ring EFJ, Elvins DM, Bhalla AK, British Institute of Radiology (1998).

Rich C, Klinik E, Smith R, Graham B, Measurement of Bone Mass from Ultrasonic Transmission Time, Proc Soc Exp Bio Med, 123: 282-5 (1966).

Rho JY, Ultrasonic Characterisation in Determining Elastic Modulus of Trabecular Bone Material, Med Biol Eng Computing, 57-9 (1998).

Royal College of Physicians, Summary of Guidelines for Osteoporosis Care, Department of Health (1999).

Rytov SM, The Acoustic Properties of a Thin-Layered Medium, Sov Phys Acoust, 2(1):71-83 (1956).

Sachse W, Pao Y-H, On the Determination of Phase and Group Velocities of Dispersive Waves in Solids, J Appl Phys, 49(8): 4320-7 (1978).

Schoenberg M, Wave Propagation in Alternating Solid and Fluid Layers, Wave Motion, 6: 303 (1984).

Schoenberg M, Sen PN, Properties of a Periodically Stratified Acoustic Half-Space and its Relation to a Biot Fluid, J Acoust Soc Am, 73(1): 61-7 (1983).

Schwartz L, Plona TJ, Ultrasonic Propagation in Close-Packed Disordered Suspensions, J Appl Phys, 55(11): 3971-7 (1984).

Seki H, Granato A, Truell R, Diffraction Effects in the Ultrasonic Field of Piston Source and their Importance in the Accurate Measurement of Attenuation, J Acoust Soc Am, 38: 230-8 (1956).

Selle WA, Jurist JM, Acoustical Detection of Senile Osteoporosis, Proc Soc Exp Med, 121:150 (1966).

Sharma MD, Gogna ML, Wave Propagation in Anisotropic Liquid-Saturated Porous Solids, J Acoust Soc Am, 90(2) Pt1: 1068-73 (1991).

Sherman FS, Viscous Flow, McGraw-Hill Publishing Company, London (1990).

Smith RE, Ultrasonic Elastic Constants of Carbon Fibres and their Composites, J Appl Phys, 43(6): 2555-61 (1972).

Smith DM, Khairi MRA, Johnston CC, The Loss of Bone Mineral with Ageing and its Relationship to Risk of Fracture, J Clin Invest 56: 311-8 (1975).

Smith SW, Phillips DJ, Von Ramm OT, Thurstone FL, Some Advances in Acoustic Imaging through the Skull, Ultrasonic tissue characterisation II, Nat Bureau Standards Spec Publ, 525: 209-17, ed. M Linzer, Washgt'n DC US Government Printing Office (1979).

Stewart A, Reid DM, Risk factors, quantitative ultrasound or a combination of both - which is the most sensitive and specific for osteoporosis? Proc 5th Bath Conference on Osteoporosis and Bone Mineral Measurement, ed. Ring EFJ, Elvins DM, Bhalla AK, British Institute of Radiology (1998).

Stoll RD, Bryan GM, Wave Attenuation in Saturated Sediments, J Acoust Soc Am, 47: 1440-7 (1970).

Strelitzki R, Clarke AJ, Evans JA, The Measurement of the Velocity of Ultrasonic in Fixed Trabecular Bone Using Broadband Pulses and Single-Frequency Tone Bursts, Phys Med Biol, 41:743-53 (1996).

Strelitzki R, Evans JA, On the Measurement of Velocity of Ultrasound in the Os Calcis using Short Pulses, Eur J Ultrasound, 4: 205-13 (1996).

Strelitzki R, Nicholson PHF, Evans JA, Low-frequency Ultrasonic Velocity Measurements in Human Calcaneal Trabecular Bone, Physiol Meas, 18: 119-27 (1997a).

Strelitzki R, Evans JA, Clarke AJ, The Influence of Porosity and Pore Size on the Ultrasonic Properties of Bone Investigated using a Phantom Material, Osteoporosis Int, 7(4): 370-5 (1997b).

Strelitzki R, Evans JA, Diffraction and Interface Losses in Broadband Ultrasonic Attenuation Measurements of the Calcaneum, Physiol Meas, 19: 197-204 (1998).

Strelitzki R, Metcalfe SC, Nicholson PHF, Evans JA, Paech V, On the Ultrasonic Attenuation and its Frequency Dependence in the Os Calcis Assessed with a Multielement Receiver, Ultrasound Med Biol, 25(1): 133-41 (1999).

Stremler FG, Chapter 2, Introduction to Communication Systems, Addison-Wesley Publishing Company, Wokingham UK (1990).

Tavakoli MB, Evans JA, The Effect of Bone Structure on Ultrasonic Attenuation and Velocity, Ultrasonics, 30(6): 389-95 (1992).

Theismann H, Pfander F, Uber die Durchlassigkeit des Knochens fur Ultraschall, Strahlentherapie, 80: 607-10 (1949).

Thurston RN, Elastic Waves in Rods and Clad Rods, J Acoust Soc Am, 64(1):1-31 (1978).

Trim DW, Calculus & Analytic Geometry, Addison-Wesley, USA (1983).

Truscott JG, Lightly D, Smith A, Smith MA, Reference Ranges for Speed of Sound and Broadband Ultrasonic Attenuation Measured with a Lunar Achilles in 949 Caucasian Women, Proc 4th Bath Conference on Osteoporosis & Bone Mineral Measurement (1996).

Turner CH, Cowin SC, Dependence of Elastic Constants of an Anisotropic Porous Material upon Porosity and Fabric, J Mat Sci, 22: 3178-3184 (1987).

Watkinson KM, Studies of Texture and Elastic Constants of Oriented Polyethylene, Surrey University PhD Thesis (1977).

Wells PNT, Chapter2, Biomedical Ultrasonics, Academic Press, (1977).

Williams JL, Lewis JL, Properties and an Anisotropic Model of Cancellous Bone from the Proximal Tibial Epiphysis, J Biomech Eng 104: 50-6 (1982).

Williams JL, Ultrasonic Wave Propagation in Cancellous and Cortical Bone: Predictions of Some Experimental Results by Biot's Theory, J Acoust Soc Am, 91(2): 1106-12 (1992).

Williams JL, Grimm MJ, Wehrli FW, Foster KR, Chung H-W, Prediction of Frequency and Pore-Size Dependent Attenuation of Ultrasound in Trabecular Bone using Biot's Theory, Mechanics of Poroelastic Media, 263-71 (1996).

Wu JR, Cubberly F, Measurement of Velocity and Attenuation of Shear Waves in Bovine Compact Bone using Ultrasonic Spectroscopy, Ultrasound Med Biol, 23(1): 129-34 (1997).

Xu W, Kaufman JJ, Diffraction Correction Methods for Insertion Ultrasound Attenuation Estimation, IEEE Trans Biomed Eng, 40(6): 563-70 (1993).

Yamada H, Chapter 11, Strength of Biological Materials, Williams & Wilkis Company, Baltimore (1970).

Yoon HS, Katz JL, Ultrasonic Wave Propagation in Human Cortical Bone I, Theoretical Considerations for Hexagonal Symmetry, J Biomech, 19: 407-12 (1976).

Zwikker C, Kosten CW, Chapter 1, Sound Absorbing Materials, Elsevier Publishing Company (1949).

Bibliography

Bourbie T, Coussy O, Zinszner B, Acoustics of Porous Media, Gulf Publishing Company, Editions Technip, Paris, France (1987).

Brekhovskikh LM, Waves in Layered Media, Academic Press Inc, Oval Road, London, UK (1981).

Crocker MJ (ed.), Encyclopaedia of Acoustics, John Wiley & Sons Incorporated, London, UK (1997).

Daily JW, Harleman DRF, Fluid Dynamics, Addison-Wesley Company, Massachusetts, USA (1966).

Duck FA, Physical Properties of Tissue: A Comprehensive Reference Book, Academic Press, The University Press, Cambridge, UK (1990).

Dunn F, O'Brien WD (ed.), Ultrasonic Biophysics, Hutchinson & Ross Incorporated, Pennsylvania, USA (1965).

Fry FJ (ed.), Ultrasound - Applications in Medicine and Biology III, Elsevier Scientific Publishing Company, Amsterdam, Netherlands (1978).

Gibson LJ, Ashby M, Cellular Solids: Structure & Properties, Pergamon Press, Oxford, UK (1988).

Hampton L, Physics of Sound in Marine Sediments, Plenum Press, Lower John Street, London, UK (1974).

Jaeger JC, Elasticity, Fracture and Flow, John Wiley & Sons Incorporated, New York, USA (1964).

Kincaid DR, Cheney EW, Numerical Analysis, Brookes-Coles Publishing, California, USA (1990).

Kinsler LE, Frey AR, Coppens AB, Sanders JV, Fundamentals of Acoustics, Third Edition, John Wiley & Sons Incorporated, Canada (1982).

Leighton TG, The Acoustic Bubble, Academic Press, London, UK (1994).

McFaydean, Osteology and Arthrology of the Domesticated Animal, ed. Hughes HV, Dransfield JW, Bailliere, Tindall & Cox, London, UK (1953).

Oppenheim AV, Schafer RW, Digital Signal Processing, Prentice Hall, London (1975).

Sherman FS, Viscous Flow, McGraw-Hill Publishing Company, London, UK (1990).

Stremler FG, Introduction to Communication Systems, Addison-Wesley Publishing Company, Wokingham, UK (1990).

Trim DW, Calculus and Analytic Geometry, Addison-Wesley Publishing Company, USA (1983).

Wells PNT, Biomedical Ultrasonics, Academic Press, London, UK (1977).

Yamada H, Strength of Biological Materials, Williams & Wilkis Company, Baltimore, USA (1970).

Zwikker C, Kosten CW, Sound Absorbing Materials, Elsevier Publishing Company, London (1949).